Master's thesis

2019

Diego Sanchez Saldana

NTNU
Norwegian University of
Science and Technology
Faculty of Engineering
Department of Energy and Process Engineering

Master's thesis

Diego Sanchez Saldana

Fabrication of nanoplasmonic sensor device using Electron Beam Lithography (EBL) and optimization performance for submicron particle detection

June 2019

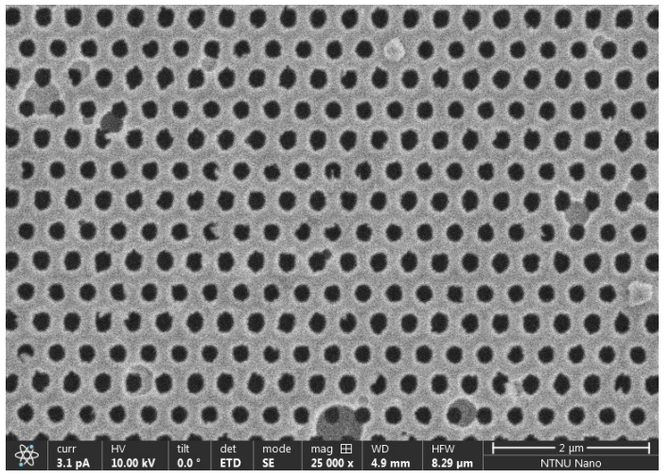

NTNU
Norwegian University of
Science and Technology

NTNU
Norwegian University of
Science and Technology

NTNU

Norwegian University of
Science and Technology

Fabrication of nanoplasmonic sensor device using Electron Beam Lithography (EBL) and optimization performance for submicron particle detection

Diego Sanchez Saldana

Natural Gas Technology
Submission date: June 2019
Supervisor: Carlos Alberto Dorao
Co-supervisor: Jonas M. Ribe

Norwegian University of Science and Technology
Department of Energy and Process Engineering

Acknowledgements

I would first like to thank my thesis supervisor Carlos Alberto Dorao of the Department of Energy and Process Engineering at Norwegian University of Science and Technology NTNU. Prof. Dorao was always available to give me advice about the project and help me out whenever I ran into a trouble spot or had a question about my research or writing. He consistently allowed this paper to be my own work but steered me in the right the direction whenever he thought I needed it.

I would also like to thank the expert who was involved in the validation survey for this research project Jonas M. Ribe. Without his passionate participation and experience advices, the project could not have been successfully carried out.

The Research Council of Norway is acknowledged for the support to the Norwegian Micro- and Nano-Fabrication Facility, NorFab, project number 90315200.

Summary

The detection of nanosized particles is playing a main role in the field of protecting the environment and public health nowadays. Online monitoring is necessary to control pollutants in our environment, due to legislation regulations and the development of new technologies. Environmental monitoring has raised several issues, including the control of CO_2 levels, drinking water quality, and the detection of specific components in waste. Moreover, related to the medical field, the detection of target particles in fluids, such as exosomes in blood which can lead to an early detection of cancer. Exiting methods, such as gas/liquid chromatography-mass spectrometry, inductively coupled plasma mass spectroscopy, and analytical centrifugation, can already perform this detection. These methods, however, require elaborate sample preparation and are costly. One alternative presented in literature is the use of plasmonic nanostructures as a promising sensor device.

The main goal of this work is to optimize a gold nanostructured mesh sensor for surface plasmon resonance (SPR) by testing different geometries and thicknesses of gold deposited, as well as a performance study of different substrates, implementation of microfluidics, surface acoustic waves (SAW) and functionalization of the sensor. The fabrication method is based on Electron Beam Lithography (EBL) combined with electron beam evaporation for thin-film metal deposition, less costly than methods currently provided in the literature. Microfluidics are developed with soft lithography. SAW is made with photolithography and functionalization is carried out with Polyethylene Glycol (PEG). This study developed a Lab-on-a-chip prototype including nanoplasmonic sensor for detection, SAW for mixing optimization improving detection and functionalization for achieving binding effects of target particles together with microfluidic implementation, reducing liquid sample usage.

This work demonstrates use of the nanofabrication method of a device with controllable gold patterned structures to enhance the optical characteristics, use as nanoplasmonic sensors combined with microfluidics, SAW and gold surface functionalization for nanosized particle detection.

Key words – nanoparticles detection, plasmonic sensors, nanofabrication, Electron Beam Lithography, microfluidics, SAW, functionalization.

Contents

Figures

List of tables

1. Introduction

1.1. Motivation and background

The monitoring and detection of nanosized particles plays a major role in the field of public health and environmental issues. The main focus of detection applications includes controlling the concentration levels of pollutants in fluids for environmental analysis [1], and bioanalytical applications, [2] including the early detection of biomarkers for STD [3] and cancer cells [4]. Only in public health, the detection of nanosized particles in water represents the 75% of the total cost for industry, this includes transport, sample collection and analysis. Furthermore, the detection of contaminants in drinking water affect more than 500 million of people around the world [5], which has motivated R&D in the area for an estimation of more than millions of euros for 2030 [6].

Research studies have described different methods for the detection of nanosized particles, e.g. electrochemical detection by 'nano-impact' methods [7], hydrodynamic chromatography [8], nanoparticle–fluorescent polymer 'chemical nose' sensors for proteins [9], colorimetric detection based on DNA oligonucleotides and unmodified gold nanoparticles (DNA/AuNPs) [10], different fluorescence-response sensor [11], and nanoparticle-enhanced microcantilever sensor [12]. These methods, however, require elaborate sample preparation and the detection efficiency is not enough for detecting low concentration of nanosized particles. In turn, nanoplasmonic [13] sensors based on gold nanostructures in combination with microfluidics and SAW seem to be a promising device for nanosized particles detection.

The working mechanism of the nanoplasmonic sensors is based on spectrometric analysis. The presence of nanostructures generates a specific resonance wavelength frequency of the white light for a certain geometry, presenting a peak on the spectrum from the light transmitted by the sensor which is sensible to changes in the dielectric environment of the sensor. Nanoparticles in a fluid can produce changes in how light is transmitted (refractive index changes) when they get attached to the surface of the sensor, thus changing the dielectric environment. This produces a shift in the peak of the spectrum, making it possible to detect nanoparticles in a fluid. Microfluidics, SAW and functionalization are implemented to ensure an optimal performance of the sensor.

This project studies nanoplasmonic sensor optimization performance together with an optimization of the fabrication process. It tests nanostructure

designs, and the study of the microfluidics, SAW and carries out the functionalization implementation. Following these tests, this study results in the attaining of a higher sensitivity of the nanoplasmonic sensor in comparison with conventional commercial sensors [14].

1.2. Objectives

The main goal of this thesis is to optimise nanoplasmonic sensors fabrication recipe and performance, implementation of microfluidics, surface acoustic waves (SAW) and functionalization of the sensor for a better control and stability of the detection performance. Different parameter for the nanofabrication will be discussed. Experiments will be carried out to analyse the performance of the nanoplasmonic devices with different geometric features. Implementation of microfluidics will be tested as well as functionalization of the sensor. Development of a prototype for online nanosized detection will be designed.

Different sub-tasks to be accomplished are:

1. Present a state-of-the-art related with the current nanoplasmonic sensor devices for detecting nanoparticles.

2. Validate and optimize the fabrication recipe together with a characterization of the different nanodevices made in the NTNU Nano Lab.

3. Experimental study and analysis of spectrometric analysis to test the sensor performance and functionalization experiments for nanoparticles binding effect to the sensor.

1.3. Scope of the work

Development of Nanoplasmonic sensor with implementation of microfluidics, SAW and functionalization of the sensor is the main aim of this project. A combination of Electron Beam Lithography (EBL) and e-beam evaporation will be required to achieve an optimal fabrication. Experiments will be carried out experiments with an implementation of microfluidics and functionalization of the sensor.

1.4. Structure

This report is divided in different chapters:

Chapter 2 introduces the definition of the nanoplasmonic sensing and the historical development of the plasmon phenomenon. Also, a theoretical explanation of the plasmon phenomenon is described.

Chapter 3, main working mechanism of the nanoplasmonic detection principle is explained. A state-of-the art of previous works using nanoplasmonic sensors for detection application is presented

Chapter 4, process fabrication for a prototype based on nanoplasmonic sensor, SAW and microfluidics is described separately in detail.

Chapter 5, detailed description of the facility setup used for detection testing is given in this chapter as well as the methods used for spectrometric and fluorescence analysis.

Chapter 6, results and related discussion are presented.

Chapter 7, conclusion and possible further work related with the project is described.

2. Theory background

2.1. SPR Nanoparticles detection history

Surface Plasmon Resonance (SPR) phenomenon take place when light source strikes a thin layer of conductor metal (gold and silver are the most common for nanoplasmonic sensors). Free electrons at the boundary metal layer starts to oscillate. Therefore, this electron oscillation results in extraordinary optical properties due to an enhancement of the electromagnetic field near the surface caused by resonance amplification. Gold and silver are optimal materials due to resonance frequency is found inside the range of visible light, also gold and silver material can be easily functionalized using different ligands, polymers, biomolecules, etc. depending on the application. For example, the use of thiols provides a strong binding affinity to the gold surface [15], which is used in this project for functionalization and bind nanosized particles. Resonance wavelength can varying for different nanostructures on the metal layer, presenting a different wavelength peak on the transmitted spectrum [16].

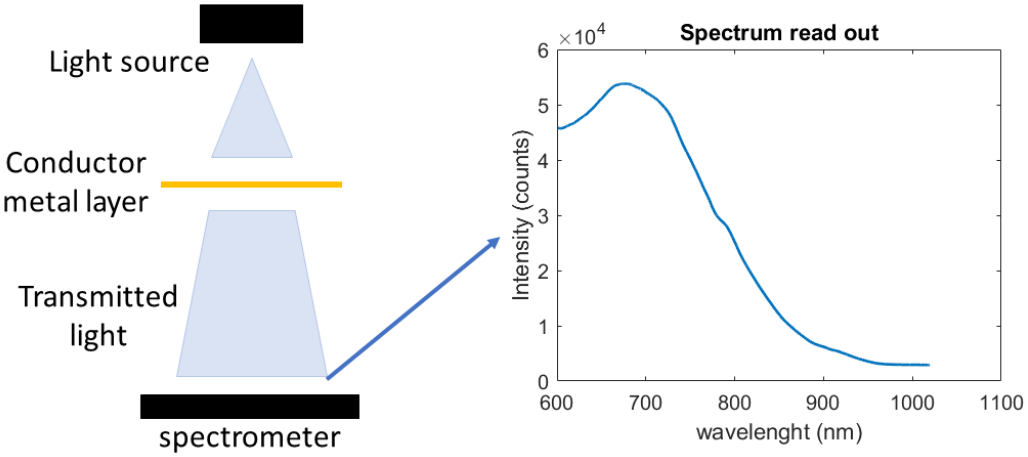

Figure 1- Surface plasmon resonance phenomenon scheme, peak of the resonance wavelenght is recorded in the light transmitted.

This phenomenon was first studied by R.W. Wood [17] in 1902 through experiments. Diffraction grating of the light was testing in different materials where an even distribution of the light was presented. Not clear answer was discovered about how light, gratings and metal materials interact.

Further development of the theory was investigated by L. Rayleigh [18] in 1907 who focused on the resulted transmitted light. The angle of the incident light changes due to partial propagation of the incident initial energy in the form of electric waves along the surface when the grating intervals of the surface are

close to the wavelength of the light. This effect was considered as anomalies and was the initial hypothesis for the plasmons.

Deeper studies with focus on these anomalies were presented by R.W. Wood (1935) [19] and C. H. Palmer (1952) [20] as a confirmation of the anomalies existence related with electric field polarized on the surface for specific conditions, such us gratings with deep grooves.

Publications of Pines and Bohm (1950) [21] describe experiments performed with gases and thin foils where electron energy loss was present, the reason found for this energy loss was the excitation of the plasma created by the conducting electrons of the gas which produced oscillation. This plasma oscillations were named as plasmons. Following years [22] was discovered that this energy loss is propagated on the surface of the sample. Therefore, the presence of any alteration on the surface affects this plasma oscillation. In the seventies, the plasmons field was studied testing thin metal layers and light interaction [23].

On 1970, surface plasmons had increased interest and a better understanding of the surface plasmons optical excitation was developed as a result of light reflection attenuation studies by scientist as Kretschmann [24] and Andreas Otto [25], leading to sensing application. One of the first publication with sensing purposes using surface plasmons was presented by Nylander and Liedberg [26] in 1983 where different substrates were tested for gas concentration detection, metal thin layer were tuned with photolithography. This simple method triggered an enormous interest in the detection of nanoparticles and biosensing field [1][3][4].

Nowadays, the aim to detect biological substances is on the raise, for development of lab-on-a-chip prototypes is required, implementation of microfluidics and functionalization of the sensor to get binding effects of the specific particle targets for detection. A prototype example is shown in Figure 2.

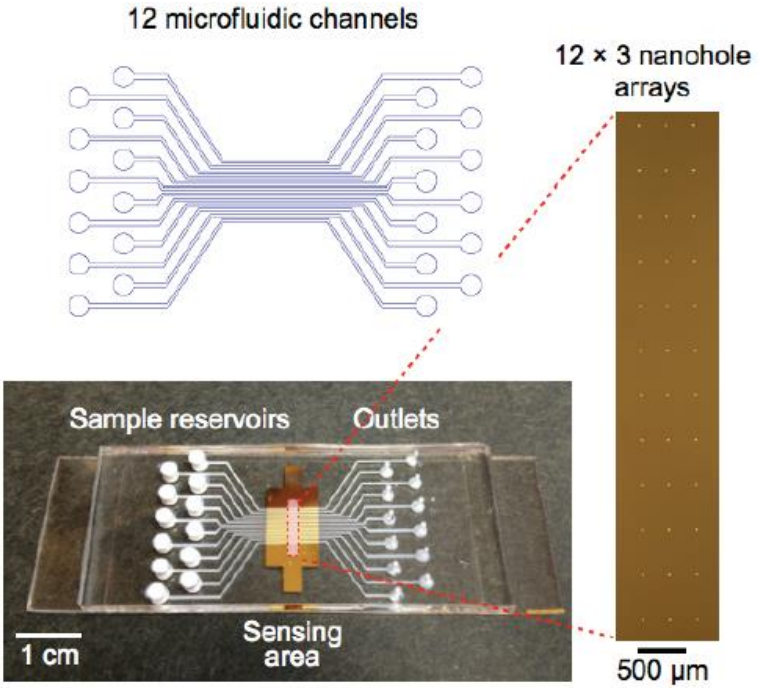

Figure 2 - nPLEX sensor combining nanoplasmonic sensors based on a functionalized nanostructured thin gold layer and implementation of microfluidics for biological sensing [4]

Different parameters for the sensing prototype fabrication must be considered such us optimization of the nanoplasmonic sensors, this includes the substrate used, fabrication method, sensor geometric features (shape, diameter, pitch, array, metal deposit thickness) to get the maximum sensitivity, microfluidics design for reduce sample usage, functionalization technique to detect the specific particle target and optimal device design for testing on the facility setup. This thesis goal is the fabrication of a chip-on-a-lab prototype with nanoplasmonic sensors, microfluidics, SAW, functionalization, together with a performance optimization.

2.2. Theory

2.2.1. Surface plasmon resonance

A theoretical explanation of the phenomenon, surface plasmon resonance, is explained in this section to have a better understanding of nanoplamonic sensors with sensing application.

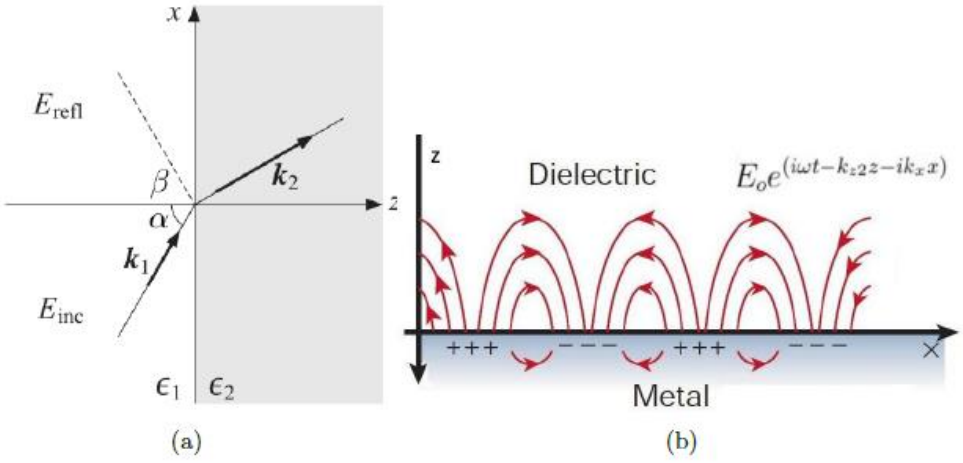

Figure 3 - a) Electric field incident from medium ε_1 into medium ε_2 at angle α. Under the plasmon resonance condition, rather than reflect at angle β, an evanescent wave forms b) and propagates along x plane [27].

In Figure 3, scheme of the light striking a metal surface is shown, here we have a 2D plane where the waves can be propagated, there are two different mediums ε_1 and ε_2. A field parallel component of the wave propagated (K), must be conserved when the light is transmitted from medium ε_1 to the medium ε_2, thus x-component is equal during the propagation, this means [28] :

$$K_{x1} = K_{x2} = K_x$$

Also, the wavelength frequency is constant:

$$\omega_1 = \omega_2 \rightarrow n_1 K_1 = n_2 K_2$$

These two parameters must be fulfilled. Therefore, Expression for z-component of the wave propagated and the interfacial reflection coefficient r_p for p-polarized light parameter can be formulated:

$$K_{z1}^2 = K_o^2 \varepsilon_1 - K_x^2 \ , \ K_{z2}^2 = K_o^2 \varepsilon_2 - K_x^2 \ , \ r_p = \frac{E_i}{E_r}$$

E_i and E_r are two parameters related with the electric fields, the incident E_i and reflected E_r. r_p can be redefined with the angles of the incident (α) and reflected (β) light [29] as well as with the z-component vectors of the wave [30]:

$$r_p = \left| \frac{tan(\alpha - \beta)}{\tan(\alpha + \beta)} \right| e^{i\Psi} = \frac{K_{z2}\varepsilon_1 - K_{z1}\varepsilon_2}{K_{z2}\varepsilon_1 + K_{z1}\varepsilon_2}$$

With this definition of r_p different cases can be remarkable. First case, when the incident (α) and reflected (β) angles are the same, this leads to $r_p = 0$

meaning no p-polarized light is reflected, in this case the angles are named as Brewster angle and it is defined as perfect partial polarization. Second case is when $r_p \gg 0$ which occurs when $K_{z2}\varepsilon_1 = -K_{z1}\varepsilon_2$, known as a resonance condition, in this case wave vectors can be defined as follows:

$$K_x = K_o\sqrt{\frac{\varepsilon_1\varepsilon_2}{\varepsilon_1+\varepsilon_2}}\ ,\ K_{z1} = \frac{K_o\varepsilon_1}{\sqrt{\varepsilon_1+\varepsilon_2}}\ \ ,\ K_{z2} = -\frac{K_o\varepsilon_1}{\sqrt{\varepsilon_1+\varepsilon_2}}$$

To fulfil this definition the wave propagated in the medium 2 (E_2) must follow this expression:

$$E_2 = E_o e^{(i\omega t - K_{z2}z - iK_x x)}$$

E_2 is the evanescent wave which is propagated along the sample surface and hundreds of nanometres through medium ε_2.

Not all materials can reach the resonance state, it is required specific materials under certain conditions. For a medium ε_1 with low dielectric conductivity (lossless medium) such us glass or air, to satisfy the resonance state it is required a slightly lossy material for the medium ε_2 ($\varepsilon_2 < -\varepsilon_1$). Gold and silver are considered slightly lossy materials, they reach resonant state with frequencies inside the visible range only when they are excited with a lossless medium ε_1 e.g. glass or air. Therefore, they are optimal materials for this phenomenon to be present.

Excitation from light is generating a physical effect on the material. When the material comes to a resonances state, the surface electron free of the sample starts to oscillate. Furthermore, when resonance wavelength matches the light striking the surface, this effect is denominated surface plasmon resonance. This effect generates an evanescent wave that is propagated through the material of the medium ε_2, normally 200 nm depth depending on several parameters such us the thickness of the thin layer and the intensity of the incident light (E_o). Perturbations close to the medium ε_2 affects the evanescent wave due to its high sensitivity to changes, for this reason is an optimal phenomenon to detect nanoparticles close to the surface of the sensor [27].

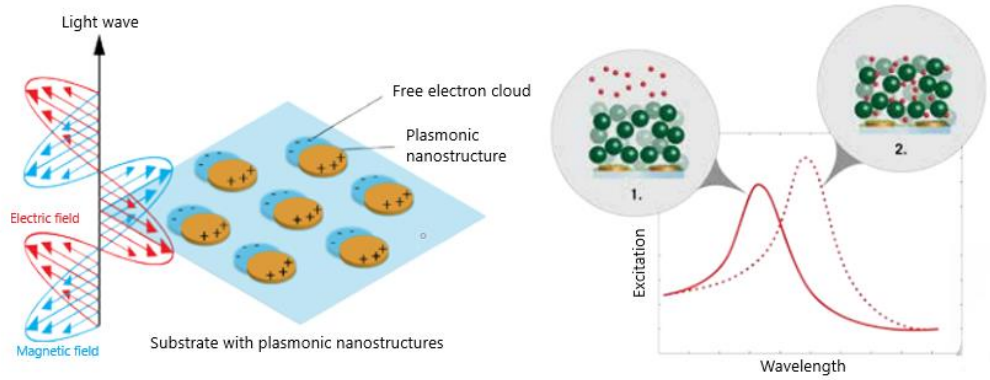

Figure 4 - (Left Image) Scheme of the nanoplasmonic device and the light excitation source. (Right Image) Shift of the spectrum when changing the dielectric environment, in this case adding particles to the existing medium, image courtesy of M. Graetzel et al.[31]

For deeper theoretical explanation of how plasmons in metal films behaves, check [32]

3. Spectrum Shifting effect of the nanoplasmonic sensor

Theory explained in Section 2.2.1 is explained in this chapter as a mechanism for detecting nanosized particles using nanoplasmonic sensors.

Surface plasmon resonance (SPR) phenomenon is a powerful optical detection technique which enables the study label-free biomolecular interactions in real time within a variety of diverse applications such as life science, electrochemistry, gas phase/chemical vapor detection, food and environmental safety and beyond as explained before.

Due to its simplicity, nearly every commercially available SPR instrument uses a detection scheme called the crush mode configuration. In this setup a light source passes through a prism, reflects of the backside of the sensor chip surface and into a detector.

At a certain incident angle known as the resonance angle, light is absorbed by the electrons in the metal film of the sensor chip. Furthermore, resonance takes place. These resonating electrons are also known as a surface plasmons which are sensitive to the surrounding environment.

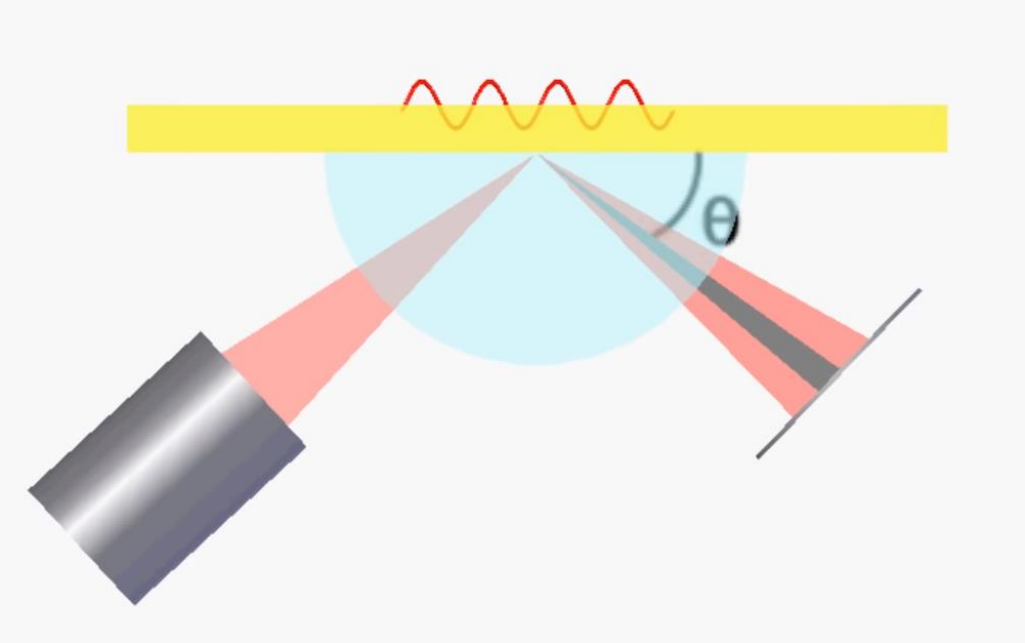

Figure 5 - Surface Plasmon Resonance phenomenon, light strikes a thin metal layer generating a wave through the metal layer (plasmon) and the light reflected is altered [33]

The result is an intensity loss in the reflected beam which appears as a dark band and can be seen as a dip in the SPR reflection intensity curve, the shape and location of the SPR dip can be used to convey information about the sensor surface.

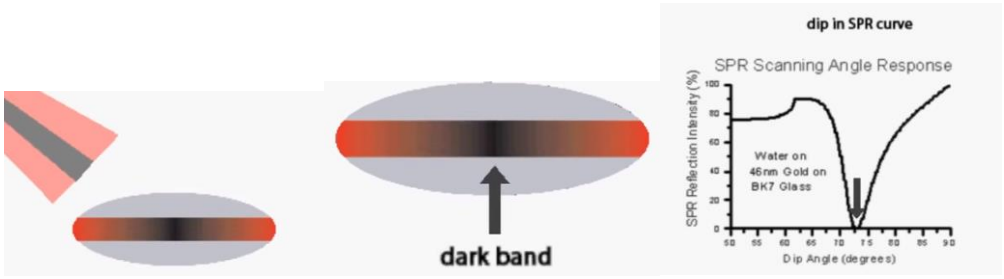

Figure 6 – Peak on the spectrum of the light reflected [33]

SPR technology is used for the study of molecular binding interactions between free analyte target molecules solution and probe molecules which are linked to or immobilize on to the sensor surface in charge of trap target particles. As a molecular binding event takes place, the angular position of this dark band shifts, and a shift in the reflectivity curve can be observed. This is a direct method of detection which avoids the inconvenience of labels.

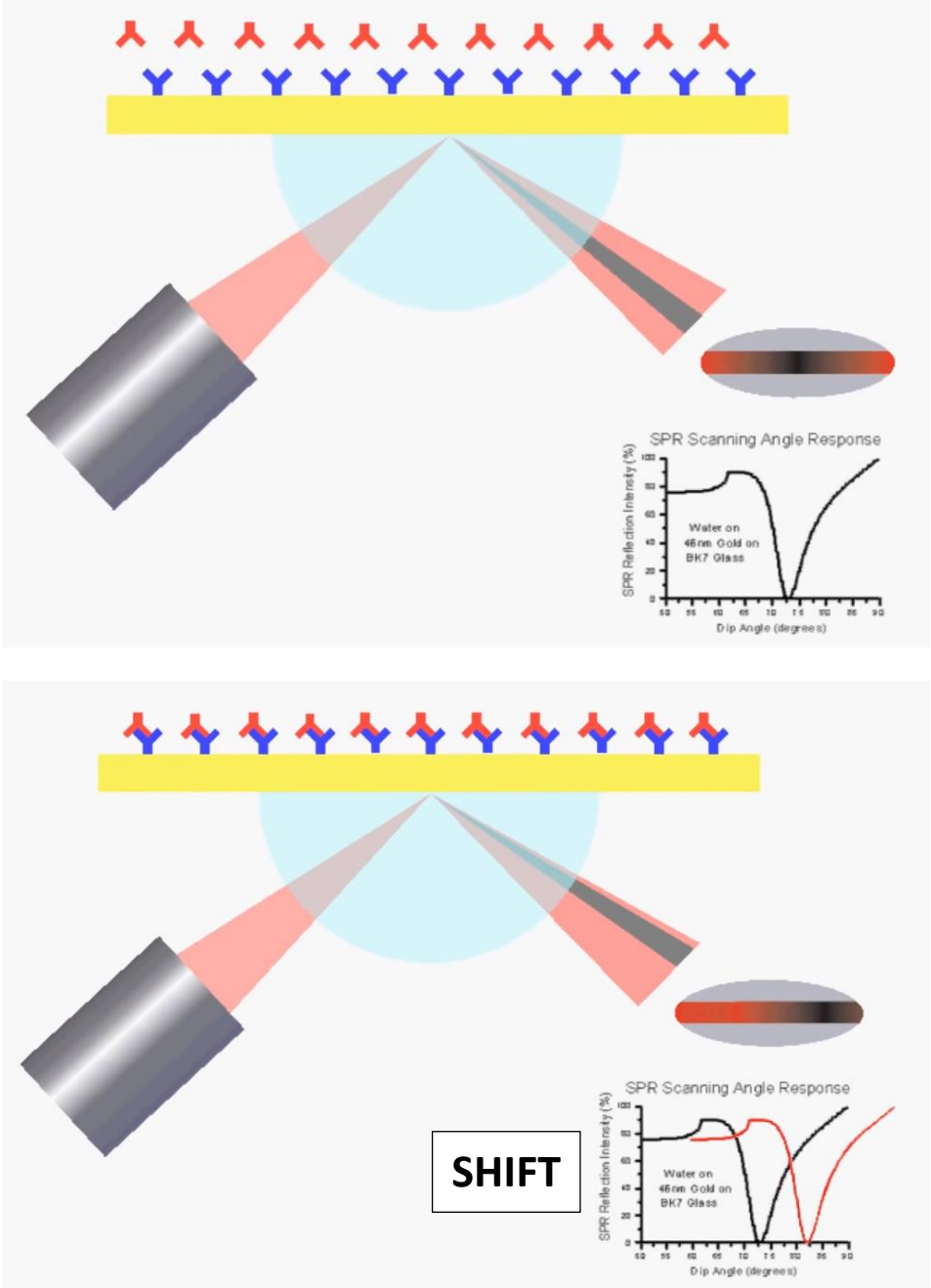

Figure 7 – Shifting effect in the spectrum occurs when dielectric environment alterations of the surface metal layer take place [33]

Another powerful aspect of SPR technology is the possibility to observe the time-dependent binding interaction between molecules by monitoring this change in SPR response over time, the kinetics of molecular binding effects can be studied.

One example, an analyte with low affinity to the immobilized ligand on the sensor surface is introduced and therefore negligible binding interaction is observed.

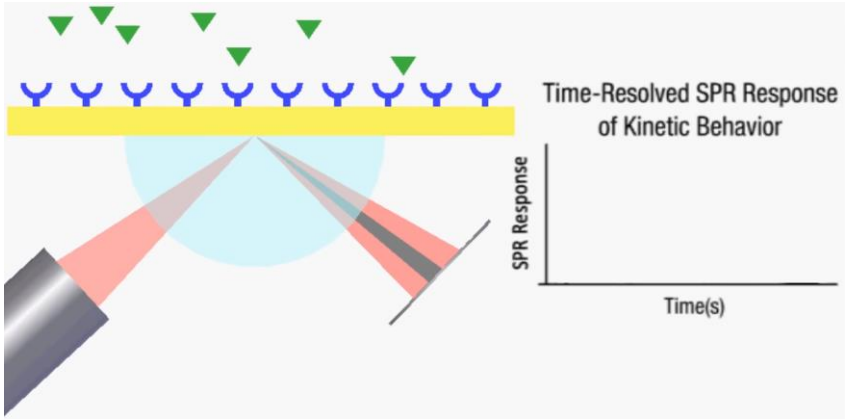

Figure 8 – No SPR response due to no specific bindings are present [33]

However, an analyte with higher affinity to the immobilized ligand is introduced into the system, then binding events are more readily observed. Initially there are many binding sites available resulting in a rapid increase in SPR response that occurs as analyte begins to bind to the ligand.

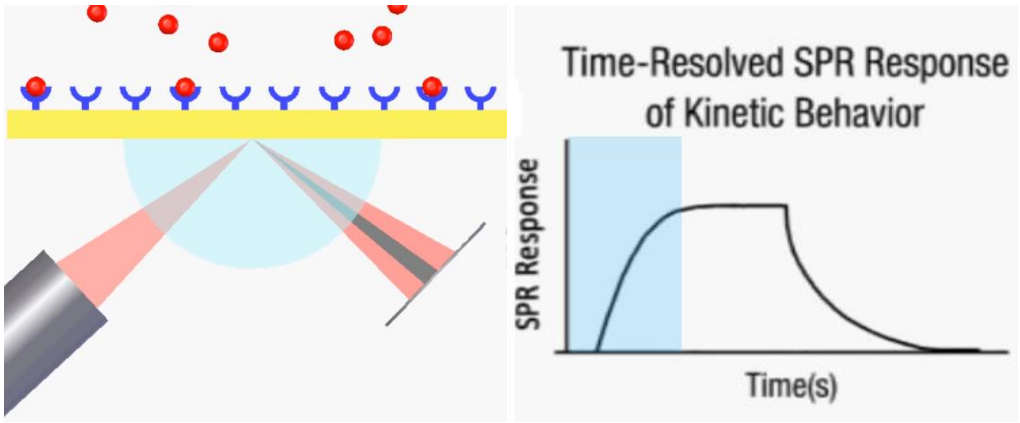

Figure 9 – Binding effects start to take place, SPR response increases with time [33]

While sample is continually delivered to the sensor surface, analyte molecules continue to bind in the number of available binding sites decreases, corresponding to a decrease in binding rate. As the SPR response levels off, the system approaches equilibrium in the number of molecules binding and unbinding become equal.

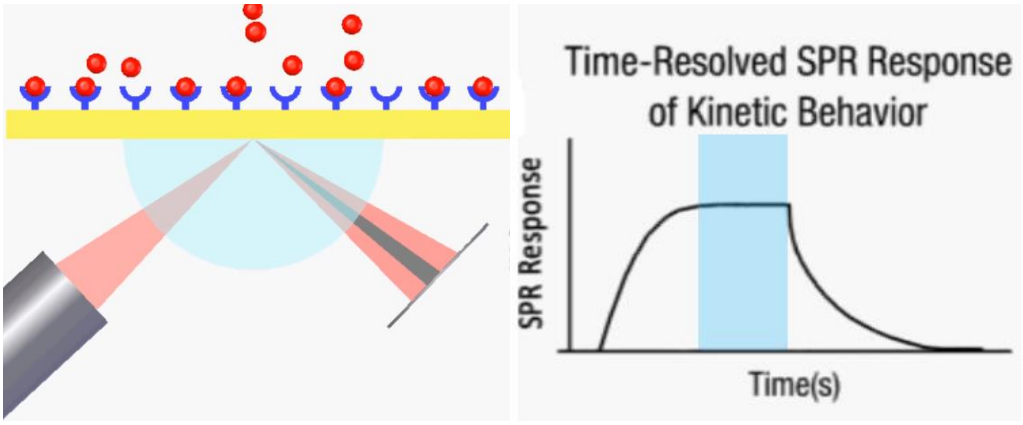

Figure 10 – At some point on time, system get to a saturation point and SPR remains constant [33]

when no more analyte in introduce into the system the molecules will continue to unbind resulting in a decrease in SPR response.

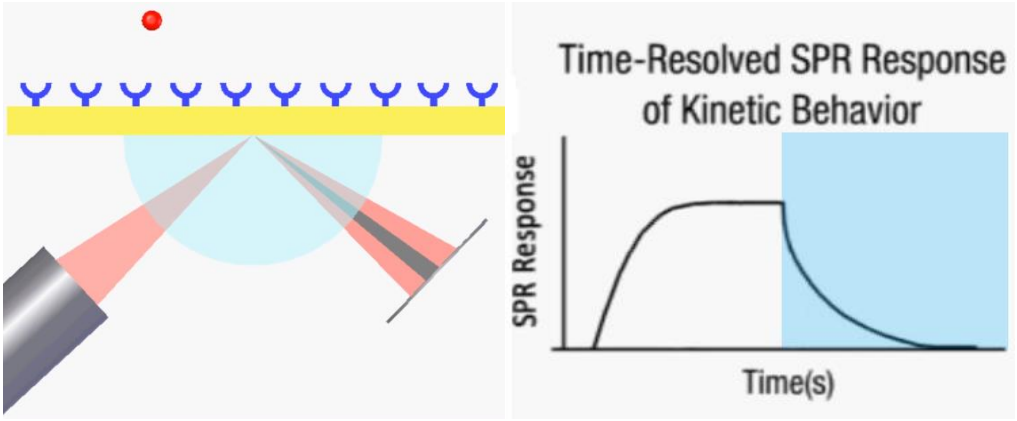

Figure 11 – When flushing the system with no analyte buffer and unbind of the particles happen resulting in a decrease of SPR response until reach the initial point. [33]

The association constant Ka, can be extracted from the behaviour of the binding response and likewise the dissociation constant Kd, can be extracted from the unbinding response. The ratio of these two rate constants can yield the binding affinity of the system.

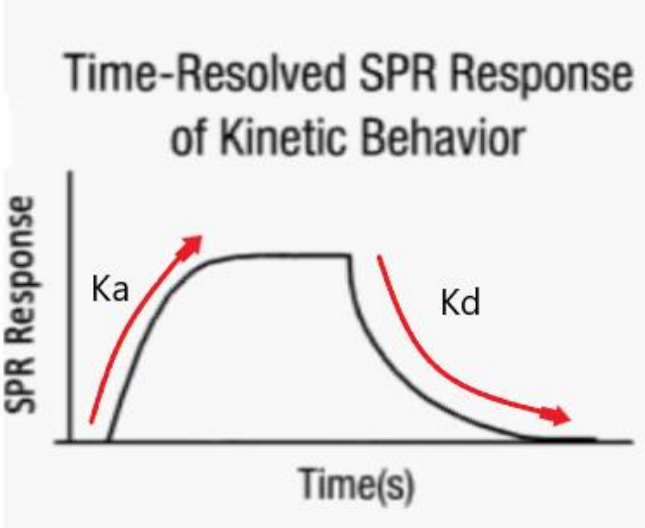

Figure 12 – Scheme of association constant (Ka) and dissociation constant (Kd) [33]

The information that can be obtained from SPR serves as a simple precise and label-free technique for quantitative analysis of molecular binding interactions [33].

In this project, same principle is used for the experiment performance. However, facility setup has a different configuration. The light transmitted from the sensor is recorded by the spectrometer instead of the light reflected, a configuration of the setup is shown in Figure 13.

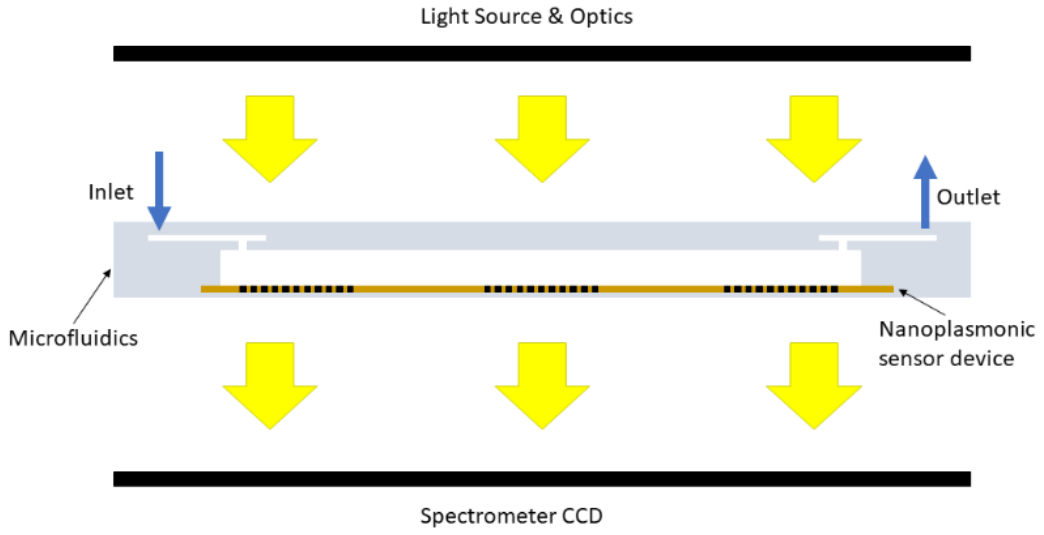

a)

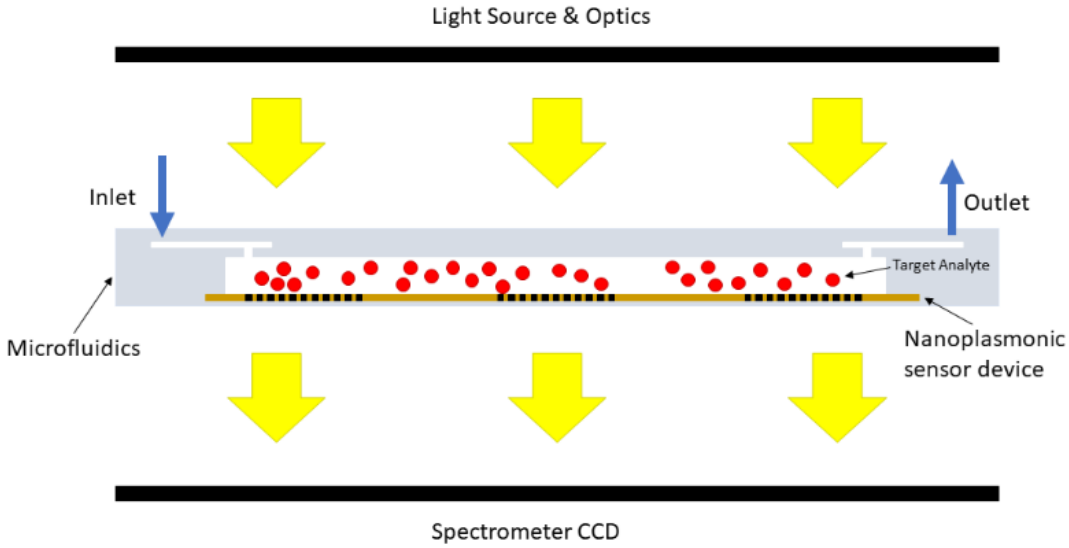

b)

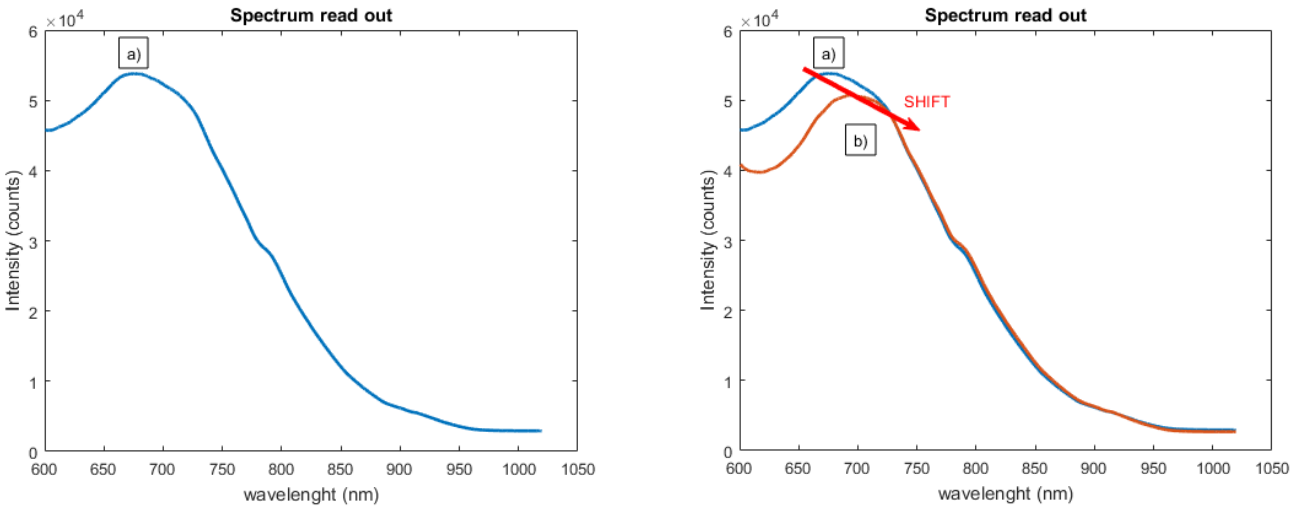

Figure 13 – Overview of the process: a) initial state b) particles are introduced to the system resulting in a spectrum shift

A nanoplasmonic sensors state-of-the-art is presented in the table below, showing the nanofabrication technique used for the thin metal layer nanoplasmonic sensor and the maximum sensitivity achieved by the device in different literature publications.

Technique	Features	Sensitivity	Reference
Interference lithography	Au square lattice holes D –240 nm P – 700 nm Au T – 100 nm Depth – 50 nm	271 ± 7 nm/RIU	[34] 2010
Soft interference lithography (SIL)	Au square lattice holes D – 100 nm P – 400 nm Au T – 50 nm	286 nm/RIU	[35] 2007
Light interference lithography	Au square lattice holes with Au nanoparticles D – 200 nm P – 450 nm Au T – 200 nm	0,2 a.u. (arbitrary unit) Transmition ~375 nm/RIU	[4] 2014
Electron beam lithography (EBL)	Au square lattice holes D – 40-520 nm P – 60-120 nm Au T – 50 nm Au nanodisks D – 60-200 nm P – 100-250 nm Au T – 50 nm	Hole array EF 4,2 x 10^5 nanodisks EF 1,3 x 10^3 Calculations performed for EF are in [36]	[37][36] 2008
Template stripping	Au square lattice holes D – 180 nm P – 500 nm Ag T – 100 nm	~450 nm/RIU	[38] 2011
Colloidal lithography	Au hexagonal lattice holes D – 687 nm Au T – 84.6 nm	471 nm/RIU Figure of merit 14.42	[39] 2018
Nanoimprinting	Au hexagonal lattice holes D – 300 nm P – 600 nm Au T – 100 nm	495 nm/RIU	[40] 2011
Laser holographic lithography technology and Ion milling	Au square lattice nanorings D –100 nm P – ~250 nm Au T – 30 nm height – 50 nm	544 nm/RIU Figure of merit 6	[41] 2018
Nanosphere lithography	Au hexagonal lattice holes D – 590 nm Au T – 50 nm	538 nm/RIU	[42] 2005
Templating nanofabrication	Au hexagonal lattice nanodonuts Out D – 322.6 ± 13.7 nm Inner D – 83.9 ± 6.6 nm Ring with – 119.4 ± 5.7 nm P – ~250 nm Au T – 100 nm	758 nm/RIU	[43] 2016

Table 1 - Review of different fabrication methods combined with electron beam evaporation of SPR sensor devices, devices features and sensitivity. Abbreviations: gold (Au), silver (Ag), diameter (D), pitch (P), thickness (T), enhancement factor (EF), refractive index unit (RIU)

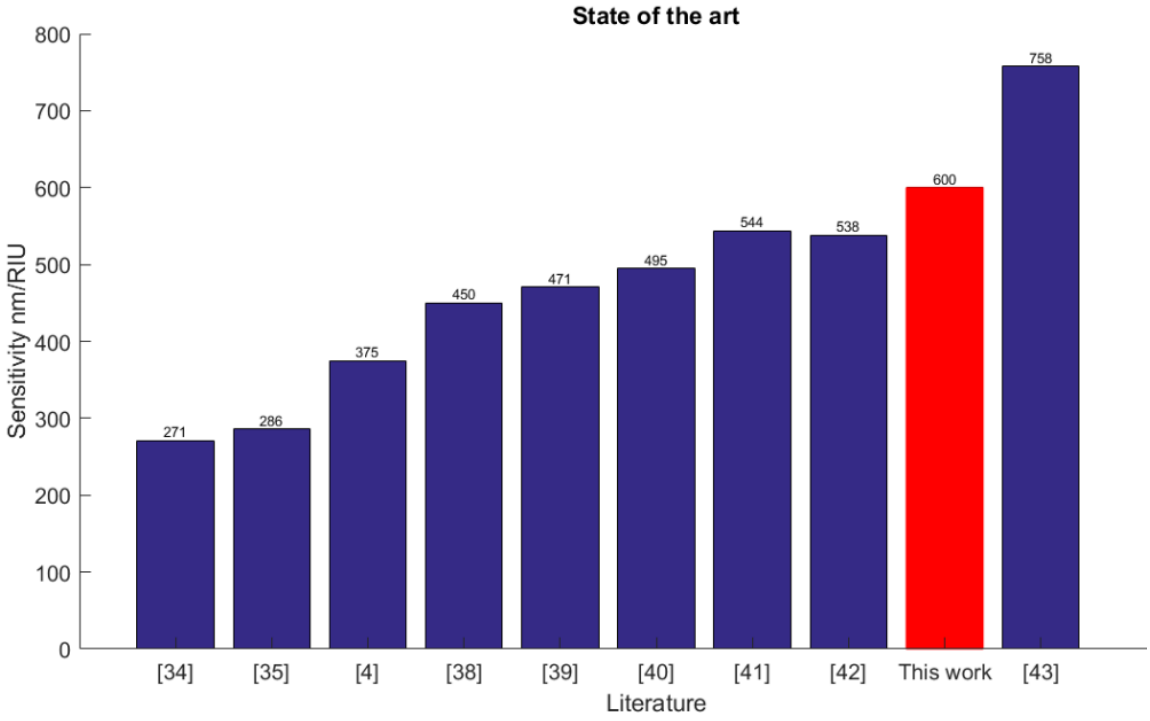

Figure 14 – State of the art of current literature about detection of nanosized particles with nanoplasmonic sensors, including this work data

4. Fabrication and characterization of nanoplasmonic sensors, IDTs and microfluidics

Fabrication processes presented in this chapter are based on the fabrication recipe that Jonas M. Ribe, NTNU postdoc was working with, it is validated, and parameter improvements are performed.

4.1. General process of nanoplasmonic sensors

Glass substrate is cleaned with acetone and isopropanol and dry with N2. Plasma cleaning is performed to remove dirtiness from the substrate surface and dehydration is done to prepare the sample for spin coating. After cleaning, sample is kept overnight under vacuum with HMDS to improve addition of the photoresist to the substrate. Deposition of CSAR 6200.13 positive photoresist is done, desire thickness of the photoresist depends on the desire final features, this is explained more in detail in Chapter 6 Results and Discussion. 1 min of soft baking at 150 ºC. Spin coating of Electra 92 AR-PC 5090.02 conductive layer is required to ensure a good exposure, 2000 rpm for 62 seconds and pre-exposure baking at 95ºC for 1 minute. EBL exposure is necessary to obtain the pattern on the photoresist layer, sensitivity analysis of different parameters such as beam diameter, writing time, dose exposed, thickness of the photoresist is performed and explained in Chapter 6 Results and Discussion. Water and AR 600-546 are used for 1 min for development, sample is rinsed with MIBK/IPA 1:3, clean with isopropanol and dry with N2. 200 nm of gold is deposited (most optimal performance parameter). Lift-off is done with remover 600-71 and ultrasonic bath for 2 min, clean with acetone, isopropanol and dry with N2.

For LinbO3 substrate, same process is followed, but changes in the temperature of the soft baking and pre-exposure are required due to pyroelectric charges will appear at temperatures around 120 ºC, to ensure a safe process temperature is decrease down to 90ºC for both steps, increasing time for soft baking to 8 min and 2 min for pre-exposure baking. It is recommended to use a wafer underneath to avoid the substrate get attached to the hot plate, also low heating and cooling speed provides a stable state of the LinbO3 state (5 deg/min).

Design of nanoplasmonic features is based on a square of 700 μm^2 with an array of holes in hexagonal lattice, holes features are 200 nm diameter and 400 nm pitch.

For detailed fabrication recipe description consult [44]. Summary of the steps is in Appendix A. Recipes.

Figure 15 shows step by steps the process used for the fabrication.

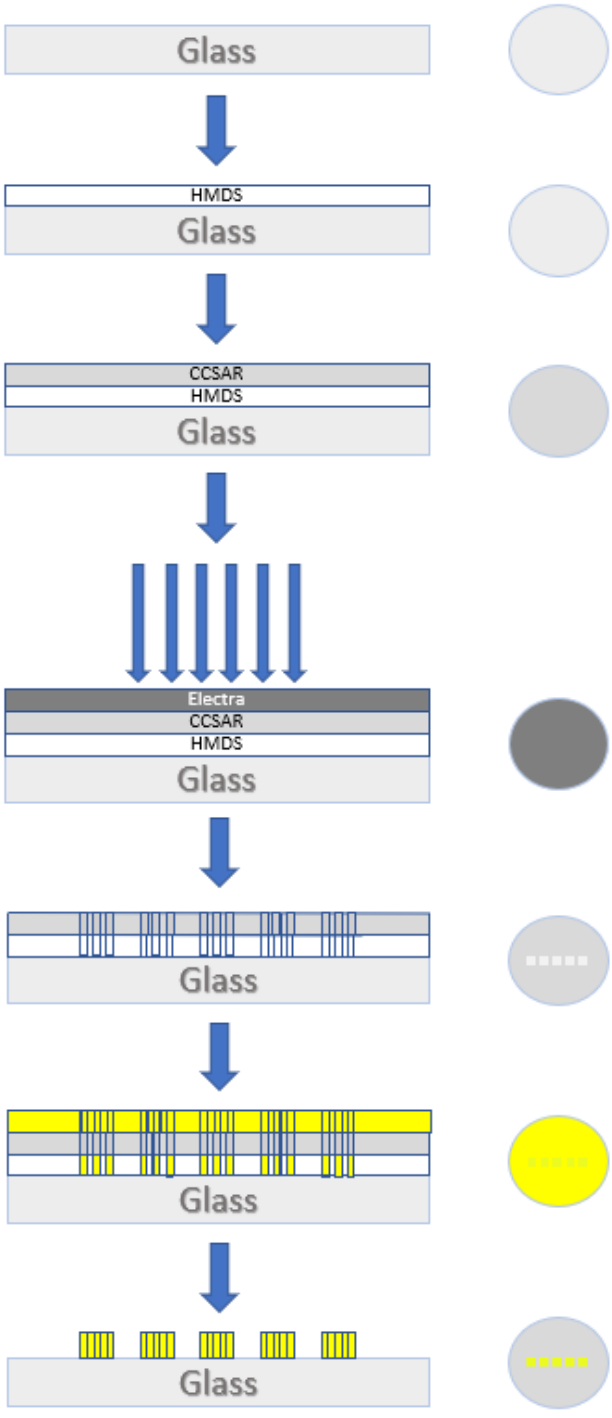

1 – Cleaning

2 – Plasma cleaning

3 – Dehydration

4 – Evaporation of HMDS deposition

5 – Photoresist spin coating

6 – Soft baking

7 – Conductive layer spin coating

8 – Checking thickness

9 – Pre-exposure soft baking

10 – EBL Elionix exposure

11 – Development

12 – Inspection

13 – Metal evaporation AJA E-beam

14 – Lift-off

Figure 15 - Overview of the process, five nanoplasmonic sensors. Cross section of the sample and top view [42]

4.2. General process of microfluidics

Desire pattern is fabricated with photoresist as a mould on top a silicon substrate before application of PDMS. To create the mould with the desire pattern, photolithography is used with Maskless aligner (MLA) machine in the NTNU Nanolab. Silicon wafer is cleaned with acetone and isopropanol and dry with N2, after that, plasma cleaning is performed to remove dirtiness from the substrate surface and dehydration is done to prepare the sample for spin coating. SU-8 3050 photoresist is deposited at specific speed in order to get the desire thickness, thus the height of the channel. The speed required is 3000 rpm to get 50 um thickness. Soft bake is performed to get optimal photoresist conditions for exposure. Desire pattern is expose in MLA with 375nm wavelength laser beam and 2000 mJ/cm2 are applied. Post-exposure bake at 65 ºC for 1 minute plus 95ºC for 4 minutes is needed. To get the final mould development is carried out stirring for 5 min the sample in a beaker with mr-Dev 600, rinse in acetone, isopropanol and it is dried with N2.

PDMS (polydimethylsiloxane) mixture is prepared with PDMS and curing agent (ratio 1:10) which is called cross linker and will create chemical bonds between the PDMS chains, thus being possible to harden the mixture and get a solid structure due to PDMS is liquid itself. During mixing bubbles will appear, to avoid this, the mixture is kept under vacuum for 10 minutes. After getting rid of the bubbles, PDMS mixture is applied on top of the silicon wafer with the mould inside a petri dish. To harden the mixture, petri dish is introduced into an oven at 60 ºC for 2 hours. After 2 hours, The PDMS mixture is solid and it is possible to be cut and obtain the microchannel.

Design of microchannel features is based on a channel width of 100 µm, 1 cm long with inlets and outlet with microtubes diameter size ~500 µm.

For detailed fabrication recipe description consult [45]. Summary of the steps is in Appendix A. Recipes.

Figure 16 shows step by steps the process used for the fabrication.

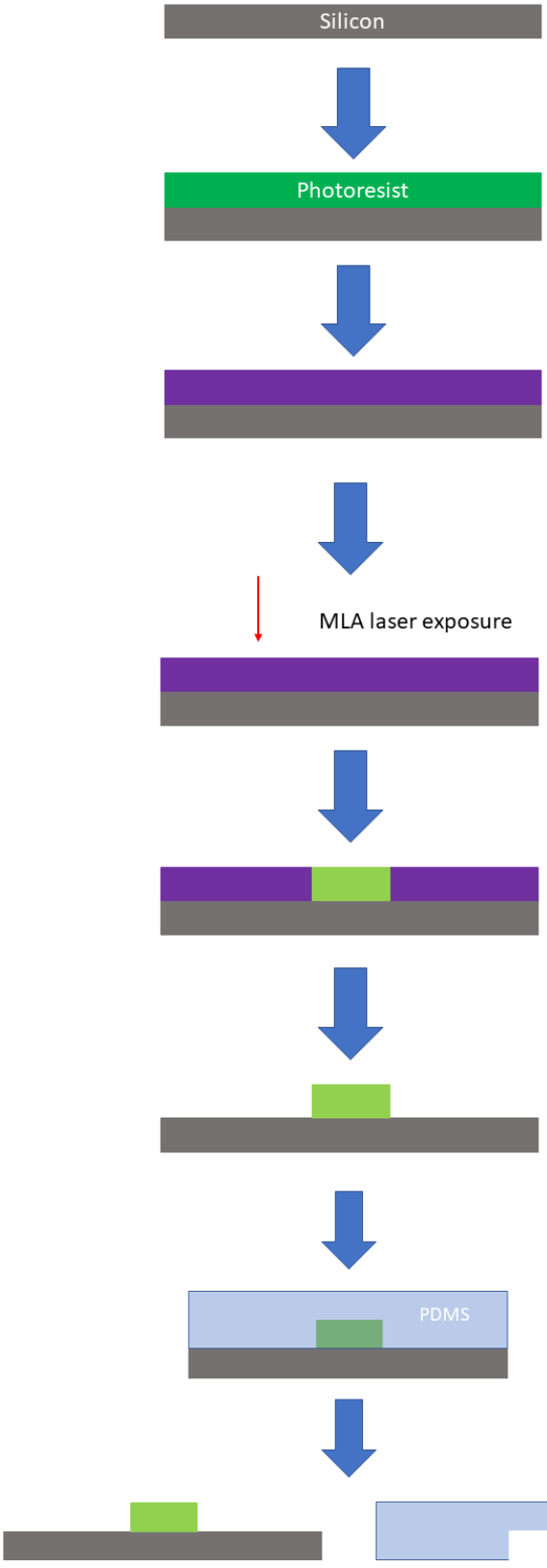

1 – Cleaning

2 – Plasma cleaning

3 – Dehydration

4 – Photoresist spin coating

5 – Soft baking

6 – Exposure MLA

7 – Post-exposure

8 – Development

9 – Tridecafluoro-silane deposition

10 – PDMS application

11 – Curing and peeling

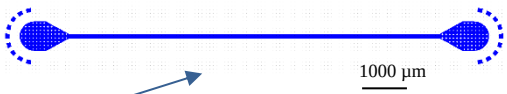

Figure 16 - Overview of the process not to scale, microchannel.
Cross section of the sample

4.3. General process of IDTs for SAW

The process followed for the fabrication of interdigital transducers (IDTs) is similar to the nanoplasmonic sensors explained above in Section 4.1. LinbO3 substrate is cleaned with acetone and isopropanol and dry with N2, after that, plasma cleaning is performed to remove dirtiness from the substrate surface and dehydration is done to prepare the sample for spin coating. 4000 rpm for 46 seconds are the parameters for spin coating of AZ5214E, positive photoresist with the image reversal properties, thus can be used as negative photoresist. Soft bake at 95ºC for 90 seconds is performed. Exposure of the invert design of the IDTs is done in the MLA 405 nm wavelength laser and a dose of 27 mJ/cm2 is applied. Image reversal bake at 113ºC for 2 minutes is required to obtain optimal angles of the pattern sides for improving the lift-off step (angle depending on the temperature). Flood exposure of the sample is needed to do the image reversal, sample is introduced in the MA6 mask aligner with correct parameters of intensity and time to reach a dose of 200 mJ/cm2. Development is performed to remove part of the photoresist and get the template for metal deposition. 5 nm of titanium and 80 nm of gold are deposited. Lift-off is done with 2 baths of acetone in ultrasonic bath.

To use the IDTs. a glass substrate is covered with string pattern of gold to have connections on the sides to the power supply, wire bonding is done to connect this glass substrate to the LinbO3 substrate. This way it is possible to apply power to the IDTs and produce surface acoustic waves (SAW) on the LinbO3 substrate.

LinbO3 is a piezoelectric substrate optimal for surface acoustic waves (SAW) which enable the transmittance of waves in a specific direction, also it has extraordinary optical properties making it a perfect property match for this project, more specifications are included in Appendix.

Design of interdigital transducers (IDTs) features is based on fingers width of 12.5 µm, with two big areas of gold as electrodes to connect the substrate to a power supply for surface acoustic waves generation with wire bonding to the glass substrate covered with string pattern of gold.

For detailed fabrication recipe description consult [45]. Summary of the steps is in Appendix A. Recipes.

Figure 17 shows step by steps the process used for the fabrication.

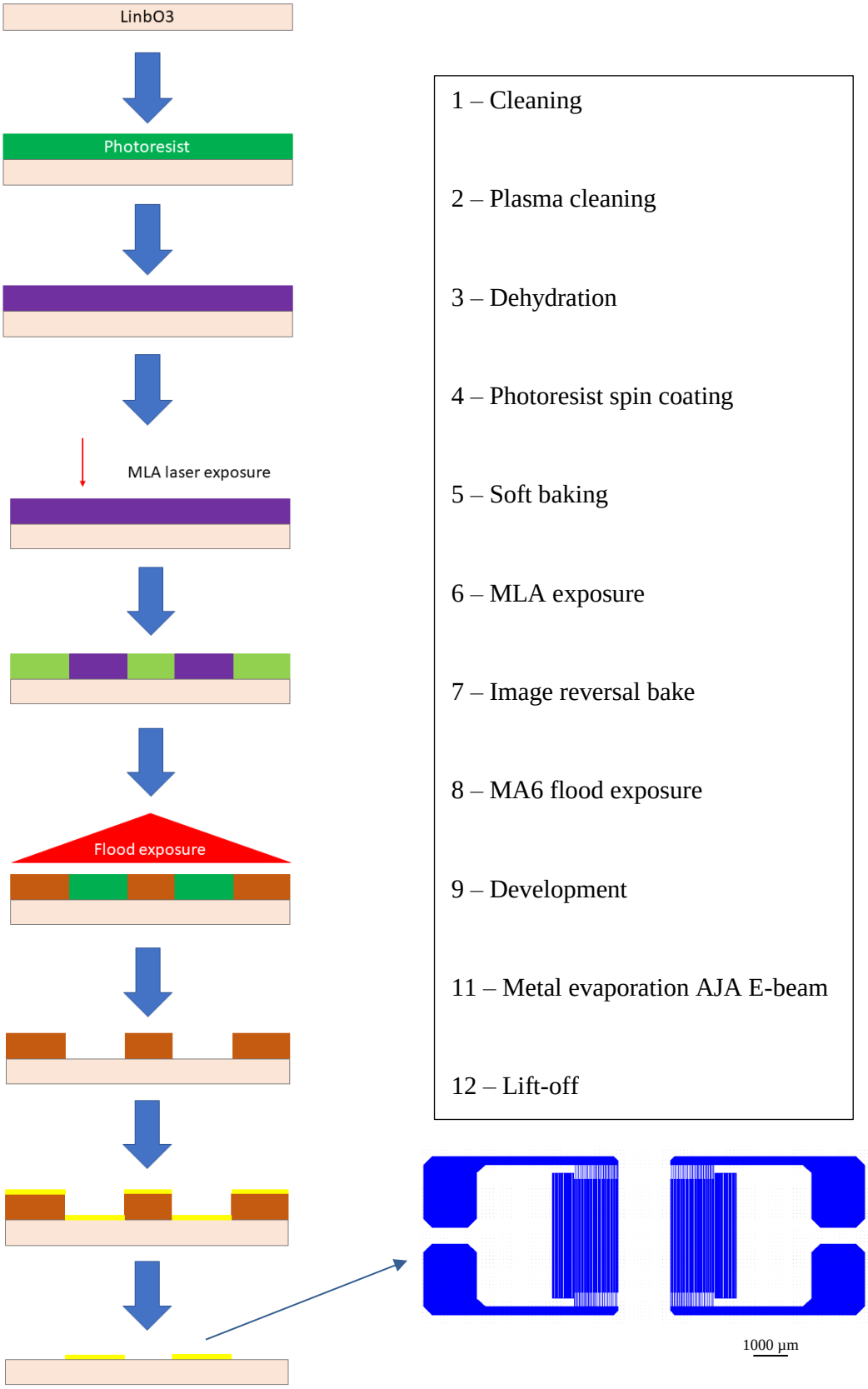

Figure 17 - Overview of the process not to scale, IDT.
Cross section of the sample

5. Experimental setup for nanoplasmonic sensor testing and methods

In this section it is described the facility setup for nanoplasmonic sensor testing including IDTs and microfluidics, also it is explained how the experiments are carried out.

5.1. Experimental setup description

5.1.1. Spectrometric analysis

The setup is based on an inverted microscope Nikon Eclipse Ti2 which enable us to perform spectrometric analysis and fluorescence experiments. For the spectrometric analysis of the nanoplasmonic sensors, light source is striking the sample from top as shown in Figure 18, and light is recorded by a magnification objective from bottom being possible to focus the area of interest, that way is possible to record the transmitted light form the sample with and optic fiber connected to a spectrometer which is connected to the computer for further process of the data. Different kind of light sources and spectrometers are tested and finally the most optimal results are obtained with a halogen lamp and spectrometer from ocean optics. Three main elements can be identified for the spectrometric analysis of the nanoplasmonic sensor alone: light source, nanoplasmonic device and detector of the light transmitted. It is shown a general scheme of the facility on Figure 18. SpectraSuite software is used to acquire the spectrum read out. A MATLAB script is used to display and evaluate the data obtained.

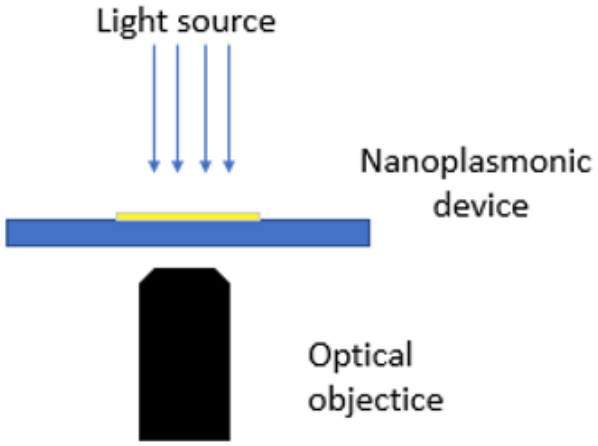

Figure 18 - Facility setup scheme for spectrometric analysis

5.1.2. Fluorescence analysis

Fluorescence experiments are performed in the same setup due to its multichannel option being possible to deviate the light with the internal mirrors and connect different cameras at the same time. Light source to take black and white images is a LED lamp and high-speed camera. For the fluorescence, 3 filters are installed blocking different wavelengths TE480/30x, ET395/25x and ET555/20x, enabling the possibility to excite specific fluorescence particles within the same setup and image the sample with a black background. A MATLAB toolbox and script are used to process the pictures obtained.

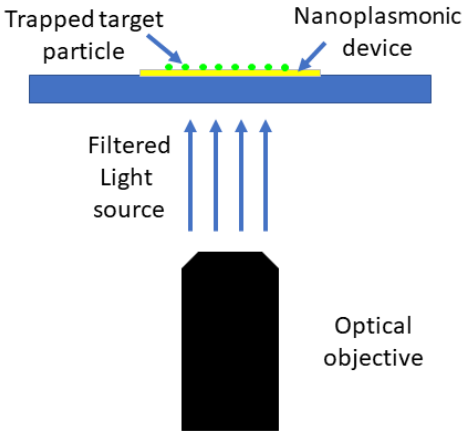

Figure 19 – Facility setup scheme for fluorescence analysis

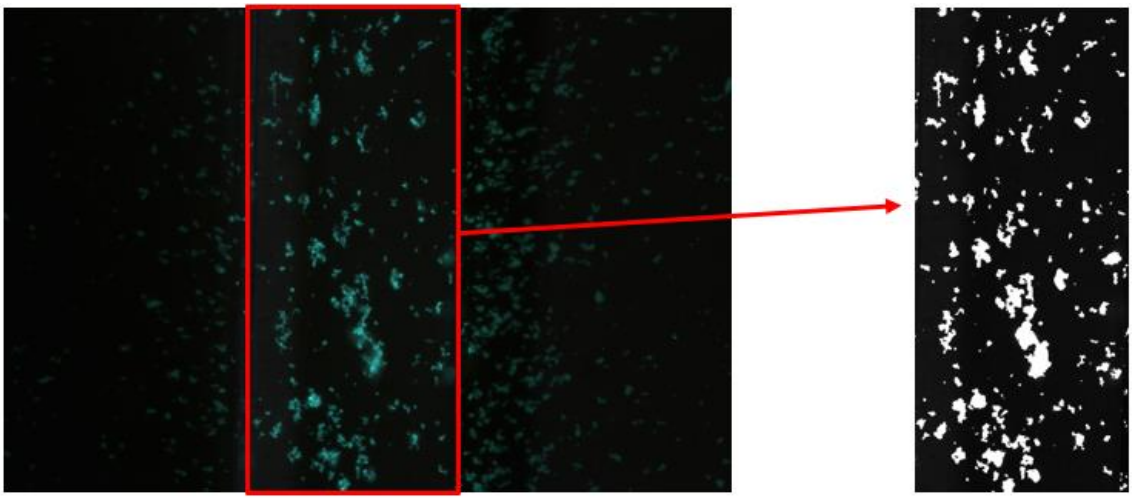

Figure 20 – Fluorescence image postprocessing. Differences in the level of intensity of the image pixels allow counting the area covered by fluorescence beads trapped on the surface

5.1.3. SAW generator and microfluidics

Power supply and cable connections to the IDTs for generation of SAW are used for the glycerol-water experiments of the mixing prototype with

nanoplasmonic sensor. Pump system and tube connections are required to flow specific volumes through the microchannels to have stability during experiments and ensure constant flow rates for online detection.

5.2. Experimental method and data processing

5.2.1. Spectrometric analysis

Several mixtures of glycerol diluted with water are prepared to calibrate the nanoplasmonic sensor device. A scale is used to measure the weight of the solute and final solution and get the mixture mass concentrations. Refractive index (RI) is associated to the different mixtures with data tested and published in other articles [46].

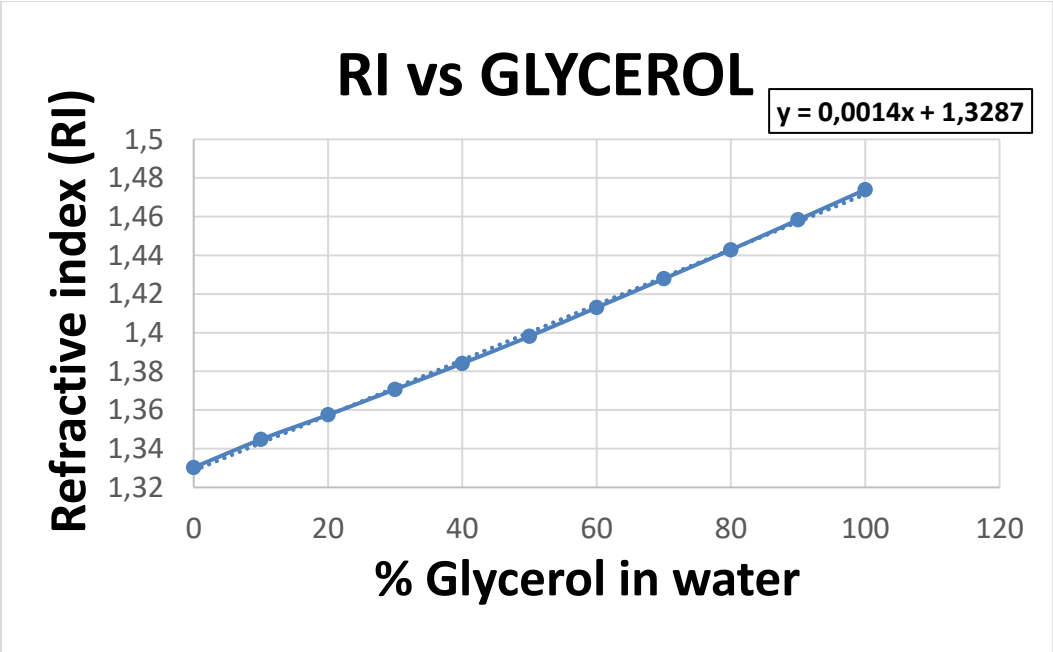

Figure 21 – Linear relation between the concentration of glycerol diluted in water and refractive index, plot of data shown in [46]

Calibration of the sensor is based on a batch experiments, it is performed applying a droplet of 10 µl on top of the nanoplasmonic sensor placed between the light source and the magnification connected to the spectrometer shown in Figure 24, then spectrum of light transmitted through the device is read out with a spectrometer. Cover slips are used as initial setup before implementing microfluidics to keep repeatability while performing the experiments, making the incident light strikes the device the same way avoiding light deviation due to droplet curvature.

Software controlling the spectrometer, being possible to acquire the spectrum read out, is SpectraSuite software (OceanOptics spectrometer software). Small fluctuations take place while measuring, for this average of 100 readings is possible to do in the SpectraSuite software to avoid measure a high fluctuation reading, minimizing noise obtaining. This way a smooth spectrum curve for better polynomial fitting.

Data postprocessing is done in a MATLAB script. The smooth spectrum curve obtained from the spectrometer is analysed and the intensity peak of the wavelength is found. The curve is fitted to a polynomial show in Figure 22, in the script the polynomial grade and the width of the spectrum from the peak can be selected (the higher grade the more accurate is the wavelength tracking), a maximum point of the fitted polynomial is found matching with the wavelength peak of maximum intensity. It is possible to track the wavelength peak of the intensity for different glycerol mixtures. Furthermore, a calibration curve can be defined shown in Figure 23.

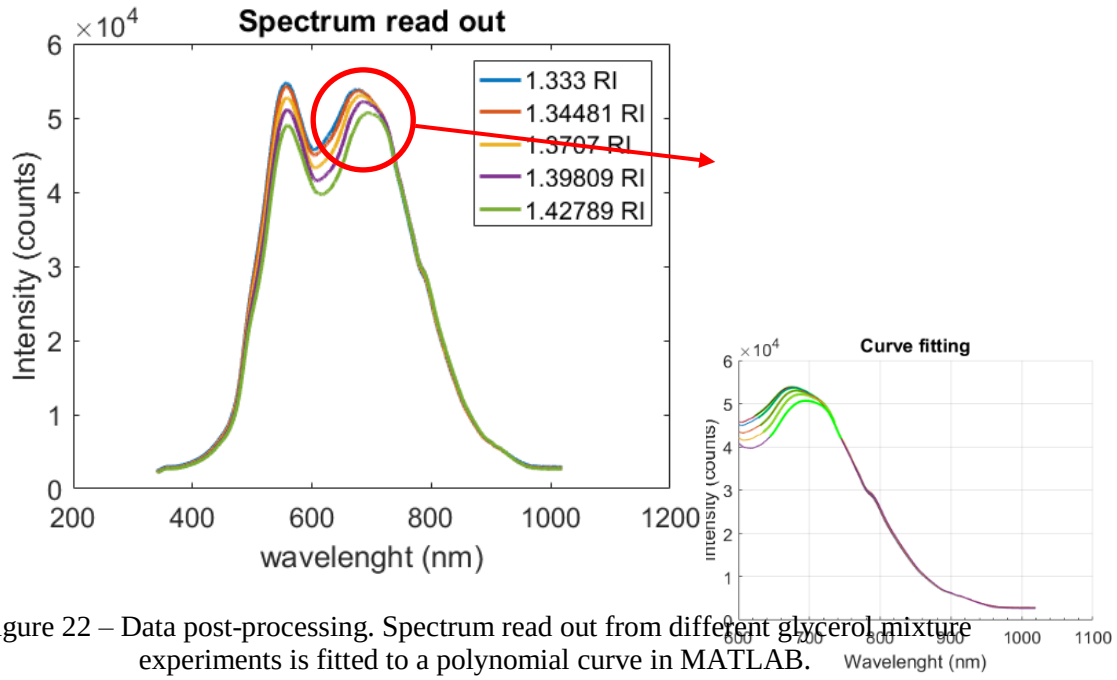

Figure 22 – Data post-processing. Spectrum read out from different glycerol mixture experiments is fitted to a polynomial curve in MATLAB.

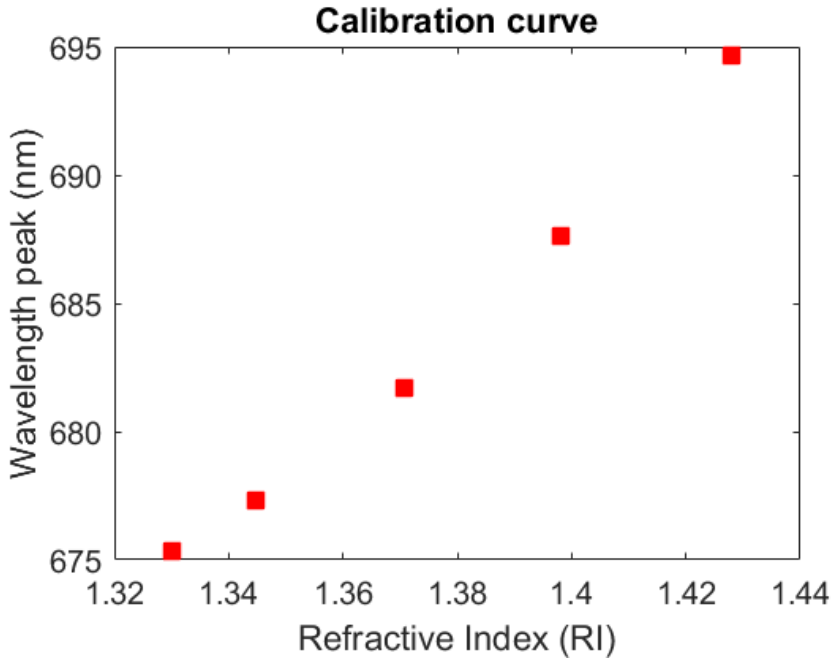

Figure 23 – Calibration curve generated from the tracking of the polynomial curve peaks, for different refractive index the spectrum is shifting. Furthermore, a detection of the fluid refractive index can be obtained.

Figure 24 – Left hand image, overview of the facility setup. Right hand image, close view of the setup, light source on top, nanoplasmonic sensor and magnification on the bottom.

Different light sources and spectrometers are tested. A spectrometer from Thorlabs and a LED light source is used as initial setup. Experiments show that the Thorlabs spectrometer measures changes in intensity while taking readings from the sample, this is not what literature explains about this phenomenon and experimental results. First preliminary results using different glycerol mixtures are used for comparing different pitches and lattice arrays of the holes, square versus hexagonal, are shown in Figure 25 and Figure 26.

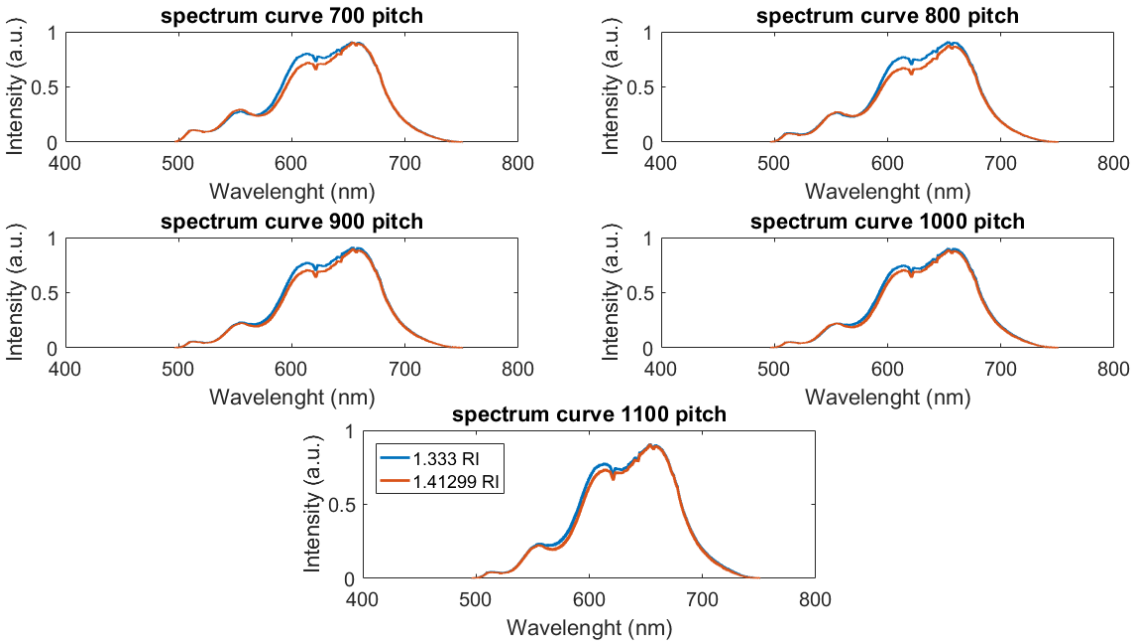

Figure 25 – Spectrum Read out of square lattice holes array pattern for the nanoplasmonic sensor, 400 nm diameter and different pitches.

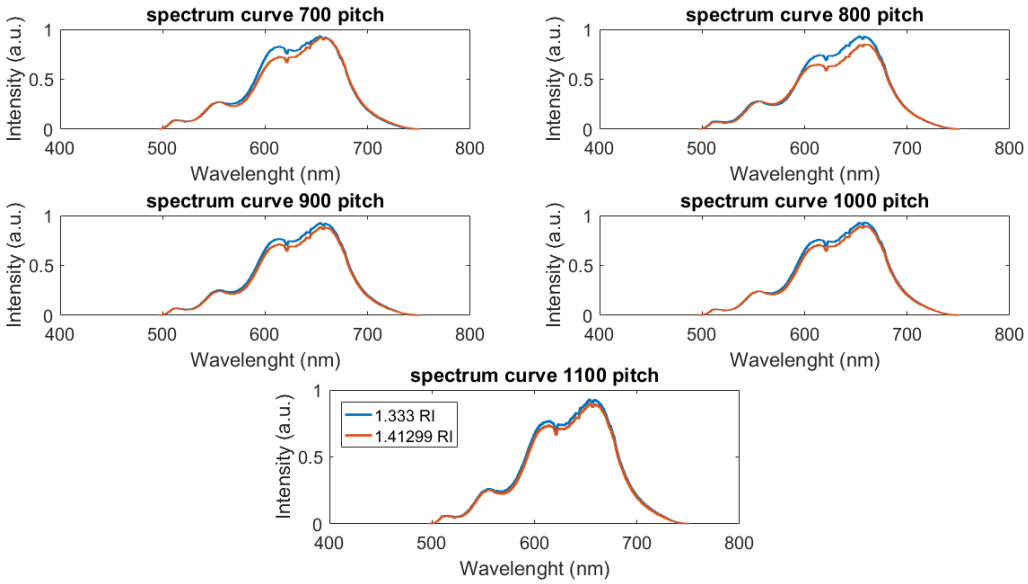

Figure 26 - Spectrum Read out of hexagonal lattice holes array pattern for the nanoplasmonic sensor, 400 nm diameter and different pitches.

Gauss approximation of the data is performed in order to define a better shift of the spectrum based on the centroid of the wavelength (centre of mass of the spectrum) or the intensity shift. Furthermore, an improvement the process of the data and shift measurement is obtained.

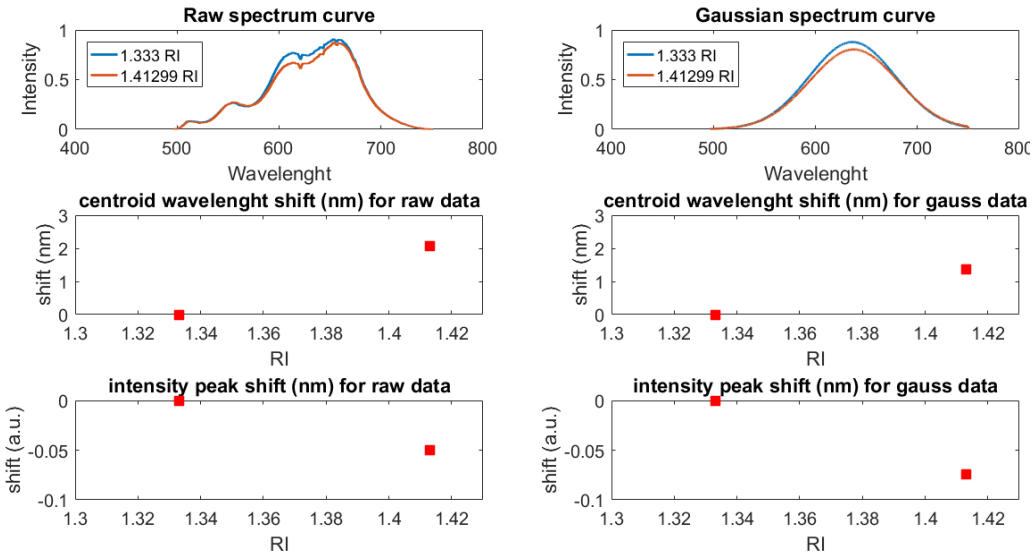

Figure 27 – Comparison of the raw data and Gaussian approximation data postprocessing. Shift is evaluated in terms of centroid wavelength shift and intensity shift.

New light sources and different setups, shown in Figure 28, are tested in order to analyse what is inducing error while performing the experiments due to not significant shift of the spectrum is found. New optic fibers, new setups and new light sources are tested with no significant changes when processing the data are found.

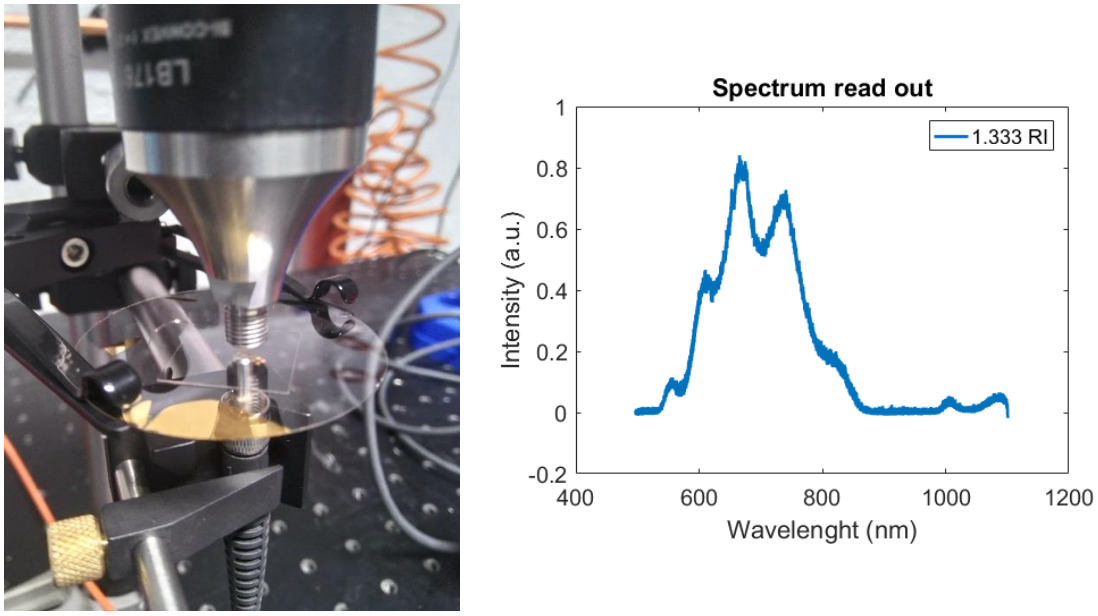

Figure 28 – Left hand side, alternative setup for testing the nanoplasmonic sensor. Right hand side, Spectrum reading from a halogen lamp.

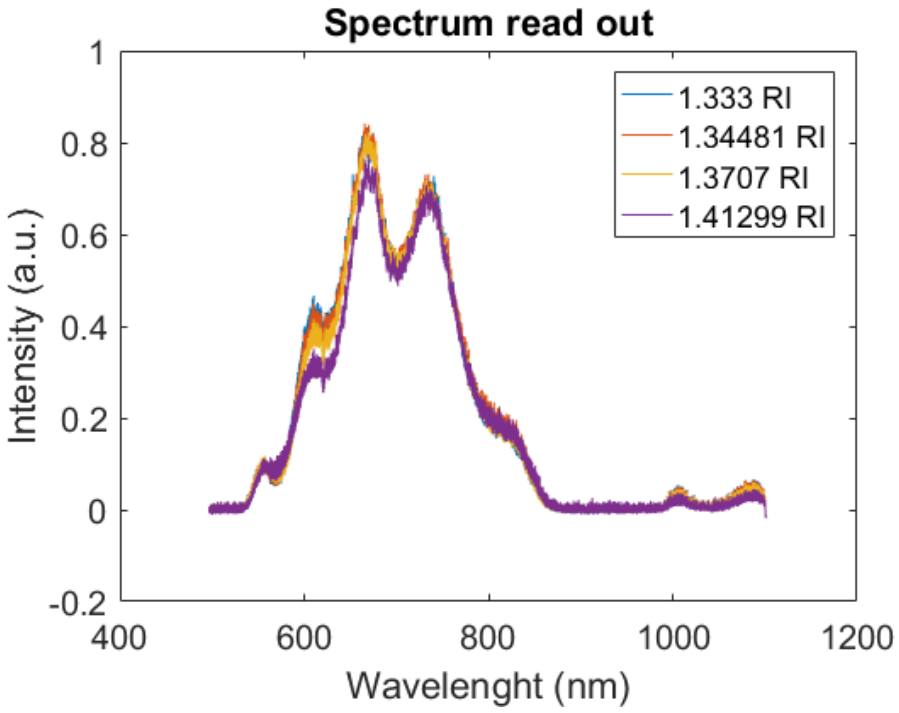

Figure 29 – Spectrum read out from different glycerol samples with different refractive index (RI), no significant shift of the spectrum is observed.

In these tests, no significant shifts of the wavelength peak are present as shown in Figure 27. Optimal design is determined by the bigger intensity shift, 400 nm diameter of the hole array, 800 nm pitch distance and 200 nm of gold deposited observed in Figure 26.

Literature shows a shift on the wavelength peak of the spectrum, for this reason another spectrometer from Ocean Optics is test for the same experiments. Results compared with Thorlabs spectrometer are present in figure 30.

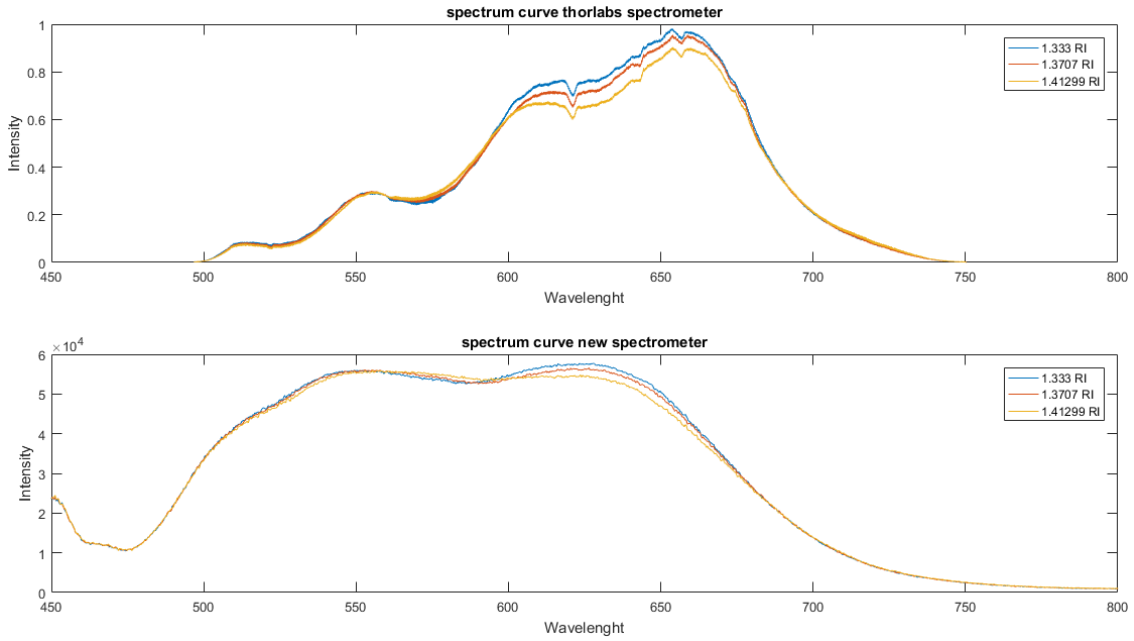

Figure 30 – Spectrum read out from different glycerol samples with different refractive index (RI) comparison between Thorlabs spectrometer and Ocean Optics spectrometer, significant differences on the spectrum are observed. Wavelength in nm and Intensity in a.u.

Significant differences on the spectrum read out are present in the comparison of both spectrometers, Thorlabs and the new spectrometer (Ocean Optics). New experiments are carried out with Ocean Optics spectrometer, results show a clear shift of the wavelength peak of the spectrum, being possible to make a better analysis of the data and interpretation of the results. Inverted microscope, halogen lamp light and Ocean Optics spectrometer are selected as most optimal setup combination to perform the experiments. Experiment results, with most optimal setup, are displayed in Figure 31.

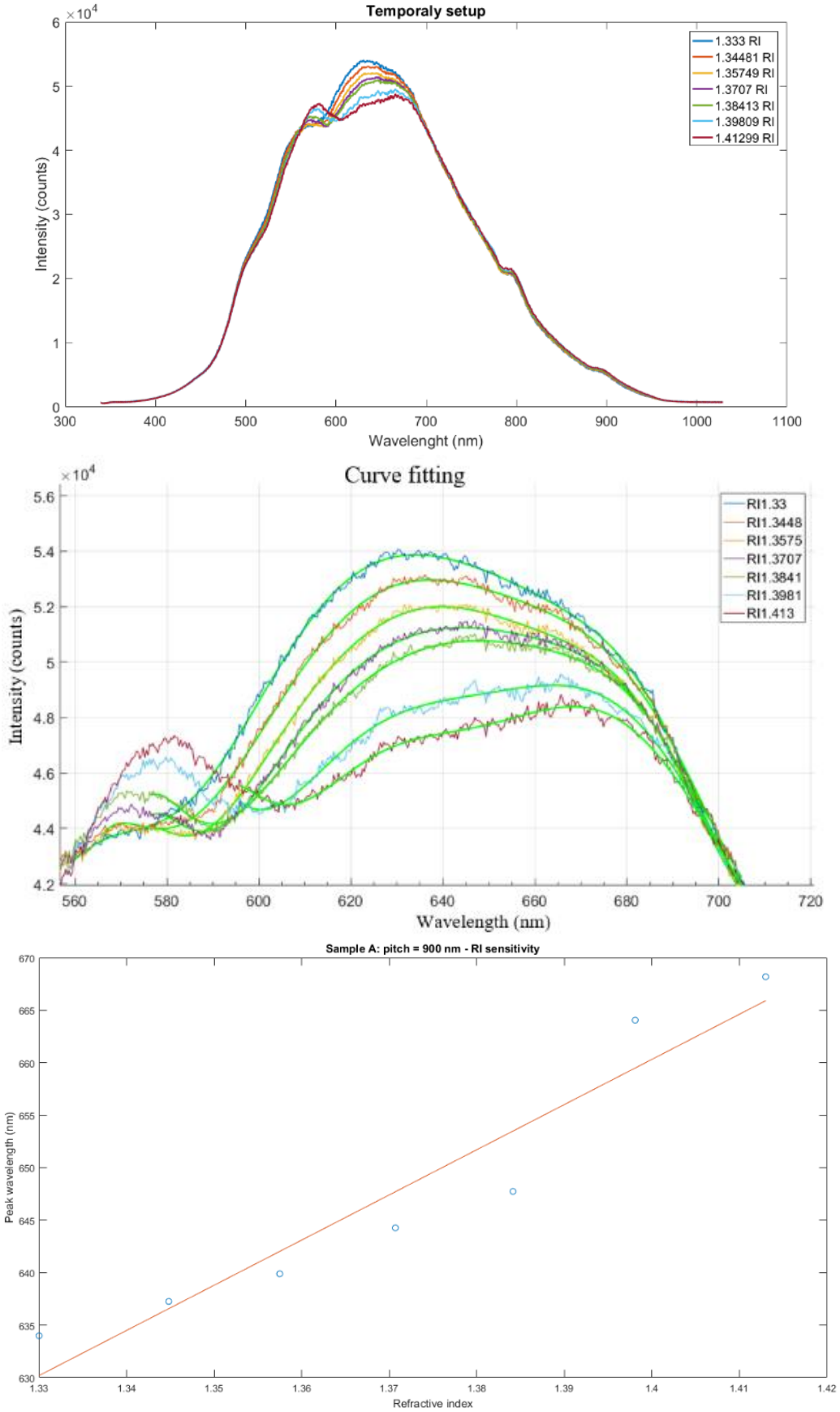

Figure 31 – Experimental data of 400 nm diameter 800 nm pitch 200 nm gold sample, using the most optimal setup based on inverted microscope, halogen lamp light and Ocean Optics spectrometer.

5.2.2. Fluorescence analysis

Mixtures of fluorescence beads diluted with Phosphate Buffered Saline (PBS) as a buffer are prepared to test the functionalization of the sensor. Different concentrations are tested to get enough intensity density from the beads, thus enabling fluorescence imaging.

Type of beads	Size (nm)	Excitation - Emission (nm)	Concentration (particles/ml)
Dragon green (streptavidin)	196	480-520	2.4 E 10
Plum Purple	503	360-420	7.3 E 09
Suncoast Yellow	210	540-600	2.1 E 10

Table 2 – Bead specification used for fluorescence experiments and the most optimal concentration for functionalization tests

This analysis is based on a batch experiment, it is performed applying a 10 µl droplet on top of the glass slide, filtered light through specific wavelength filters strikes the glass slide. When the focus is correct and the density of beads is optimal, black background images can be taken from the bottom of the beads emitting light with a high speed camera and the software PIV controller. Images of the correct concentration of beads display in Table 2 are shown in Figure 32.

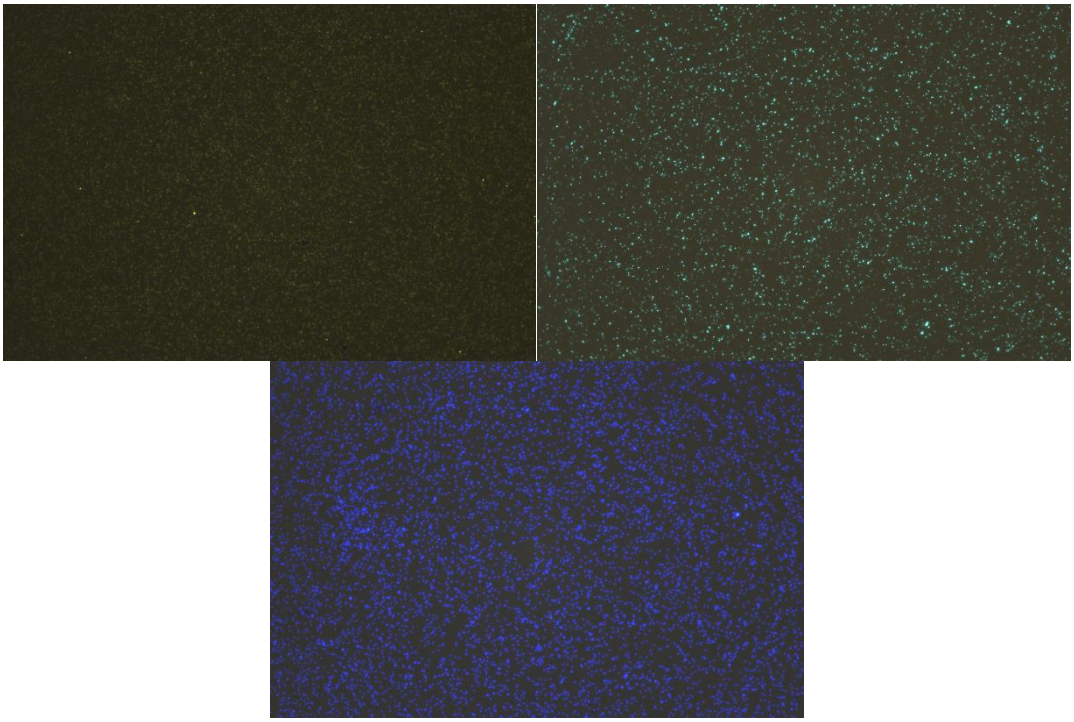

Figure 32 – Upper left image, black background image of Suncoast Yellow beads at a concentration of 2.1 E 10 particles/ml. Upper right image, Dragon green beads at a concentration of 2.4 E 10 particles/ml. Bottom image, Plum Purple beads at a concentration of 7.3 E 09 particles/ml.

Different devices for testing functionalization are designed. Preliminary device is based on a glass substrate with 5 nm of titanium and 10 nm of gold on top, almost transparent, being possible to image the device from bottom. Incubation of the beads after functionalization of the surface is performed for 2 hours in order to test the binding effect. Optimization of the device is achieved with implementation of microfluidics on the glass substrate. Furthermore, improve in the performance of the fluorescence analysis is obtained. To perform the experiments, a 10 µm sample of mixed beads is prepare and introduce inside the different microchannels of the microfluidics test device, shown in Figure 63 Section 6.3. Mixture is incubated for 2 hours, and then a fluorescence analysis imaging is performed.

Data postprocessing is done in a MATLAB toolbox and MATLAB script. The black background image is imported to MATLAB, where a matrix with the image pixels showing different intensities can be obtained. For black pixel the value in the matrix is 0, and for pixels with different intensity the value in the matrix is 1. Furthermore, generating a binary matrix with the image. A MATLAB script is used to count the values with intensity different to 0 out of the total pixels. Therefore, a percentage of the area cover by beads is obtained, an example is shown in Figure 33 with an area covered by 8.9977%.

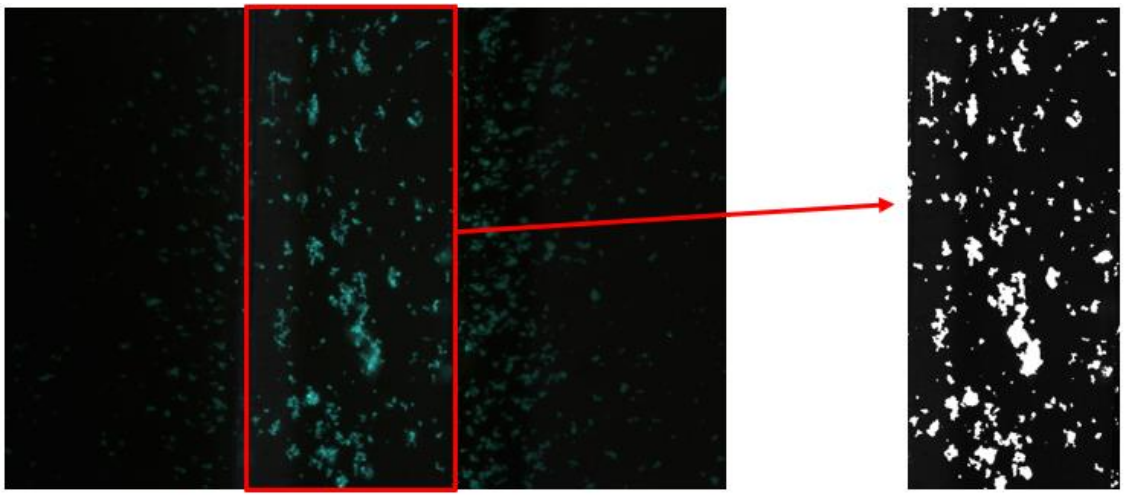

Figure 33 – Fluorescence image of the sample with microchannel implemented after incubation of fluorescence beads. Area of interest is analysed with MATLAB toolbox. Black and white image is obtained for generation of binary matrix and determined the percentage of area covered.

5.2.3. SAW generator and microfluidics

Inside microchannel, laminar flow is commonly found due to low Reynolds number and high Péclet number [45]. These conditions will hinder the nanoparticles attachment on the surface, particles will follow the velocity vectors of the liquid flow, enabling few nanoparticles get in contact with the surface of the sensor. To improve this limitation surface acoustic waves (SAW) can be implemented.

Saw generator is used for applying power to the interdigital transducers (IDTs), thus surface acoustic waves (SAW) are generated on the surface of the LinbO3 substrate which will affect the flow inside the microchannel. The main goal is to break the laminar flow inside the microchannel and improve the mixing, this way more particles will be in contact with the sensor surface improving the detection performance.

Pumps are used to control the flows and enable an online detection of nanosized particles.

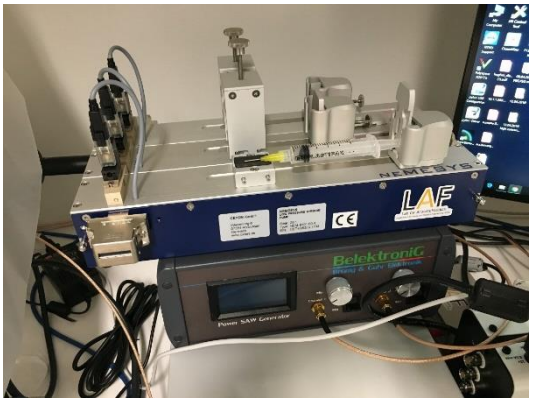

Figure 34 – Saw generator and syringe pumps

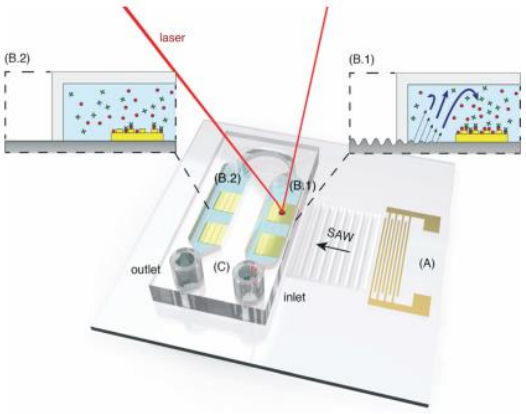

Figure 35 – Scheme of surface acoustic waves (SAW) perturbing the laminar flow inside microfluidics for mixing improvement, achieving higher number of nanoparticles getting attached to the surface [47]

5.3. Experiment uncertainties and validation

In this section, uncertainties and validation of the experiments are presented. Sample with features of 200 nm diameter and 400 nm pitch on LinbO3 substrate with microfluidics implementation is tested. Experiments are analysed to determine the accuracy in comparison with other projects published in literature and how precise these experiments are. A model scheme of precision and accuracy is shown in Figure 36.

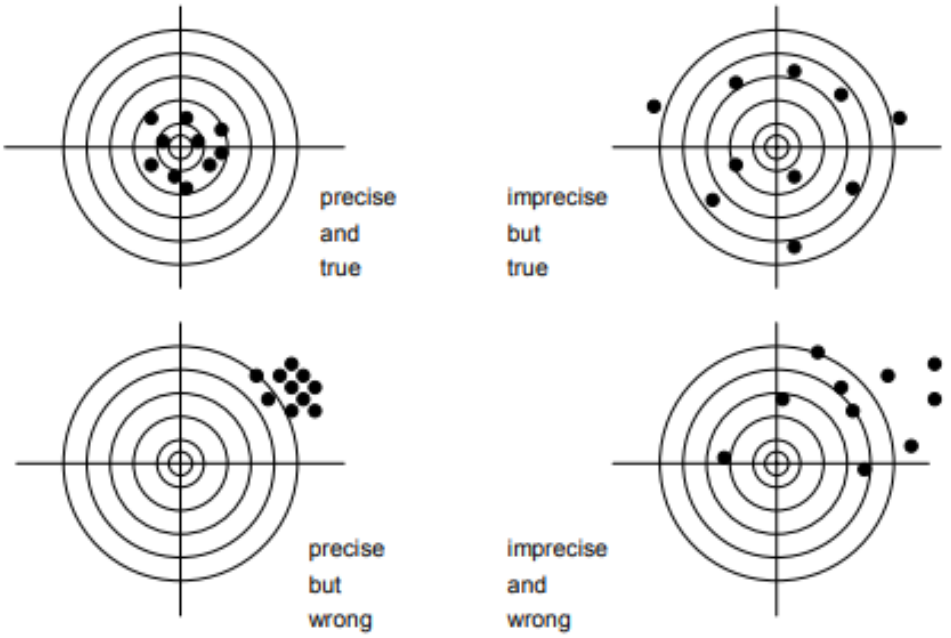

Figure 36 – Scheme of precision and accuracy. The canter of the target represents the (unknown) true value [48]

To determine how accurate are the experiments presented in this work, a comparison with the research papers shown in Chapter 3 Spectrum Shifting effect of the nanoplasmonic sensor Table 1. To perform the comparison, the wavelength peak of the spectrum is display for the refractive index 1.3333 with similar nanostructures as the ones used in this work.

The range of the peak wavelength measured on the literature is from 640 – 745 nm, this work presents a wavelength peak of 675 nm which is a reasonable number and really close to the literature. Reference number [4] from Nature journal, used same features of the nanostructures and the same substrate (glass) with a wavelength peak on 660 nm, which validate these experiments meaning what it is measured is trustful. the other references used slightly different

nanostructures which affects the wavelength peak presented in comparison with this work. Data is presented in Figure 37.

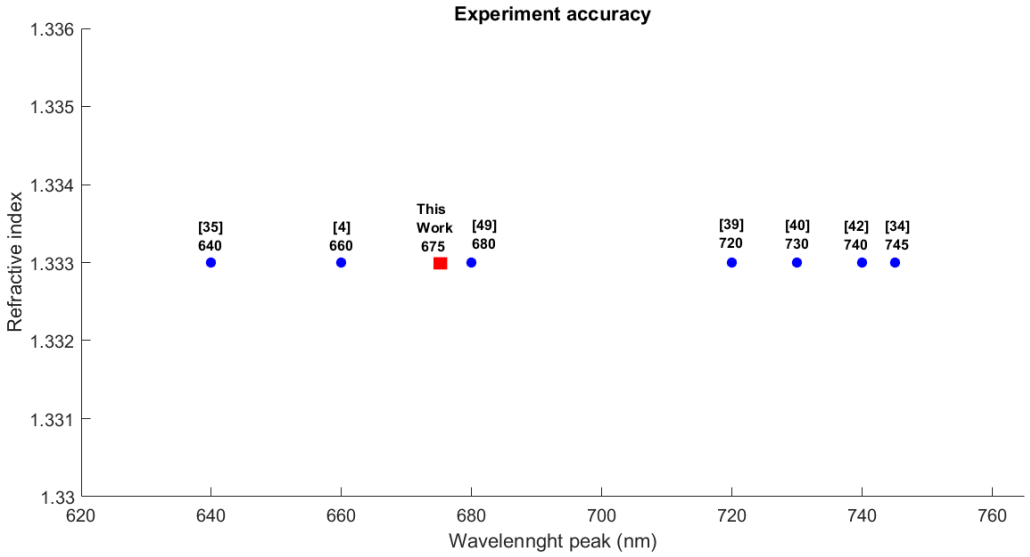

Figure 37 – Peak of the spectrum wavelength of the literature review related with this work, similar nanostructures are tested. 1.333 refractive index is selected as a reference to compare how accurate is the measurement of this work.

To determine how precise are the experiments of this project, 4 measurements are performed with the same sample features of 200 nm diameter, 400 nm pitch, 200 nm of gold deposited and microchannel implemented on LinbO3 substrate. The experiments are carried out with the procedure explained in Section 5.1.1. Spectrometric analysis.

Data collected from the experiments is displayed in Figure 38. Outlier points are calculated with the recommended method Measurement Uncertainty (ASME,1998) called modified Thompson τ technique which enable reject data collected. Mean value of wavelength peak, variance and standard deviation are calculated with 4 data measured samples on the experiments, shown in Table 3.

The sensitivity is calculated based on the data calculated in Table 3 showing a linear trend, with the standard deviation as error in the measurement. Maximum uncertainty of the measurements is 625.95 ± 0.62250 nm (0.1 %), which means the experiments have high accuracy level. In order to improve accuracy, more experiments can be carried out, this will be necessary if low refractive index changes want to be detected with this device (changes lower than 0.01 refractive index units are not trustful due to the levels of uncertainty).

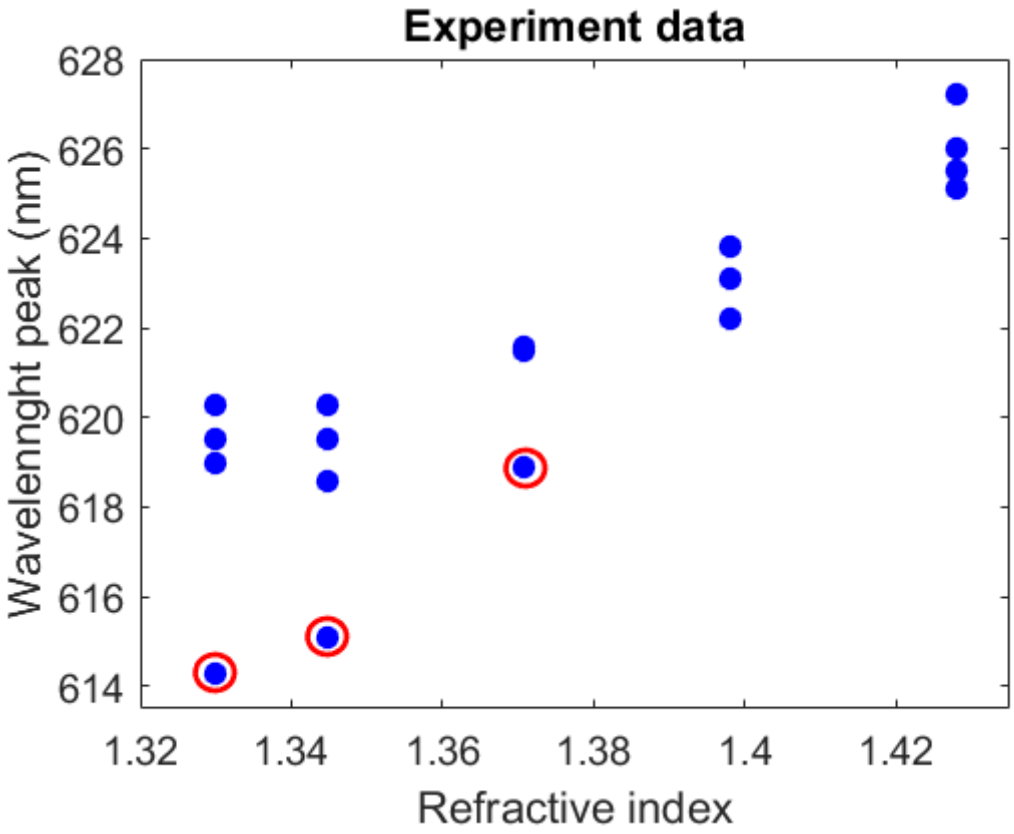

Figure 38 – Experiment data displayed of the 4 measurements performed. Data points in red are outlier points which can be rejected to calculate the mean value, variance and standard deviation

Refractive index	Mean value wavelength peak (nm)	Variance	Standard deviation
1.3333	619.60	0.28667	0.5354
1.3448	619.47	0.48222	0.6944
1.3707	621.53	0.00222	0.0471
1.3981	623.05	0.32250	0.5679
1.4279	625.95	0.62250	0.7889

Table 3 – Properties of the data measured, Mean value of the spectrum wavelength peak, variance and standard deviation

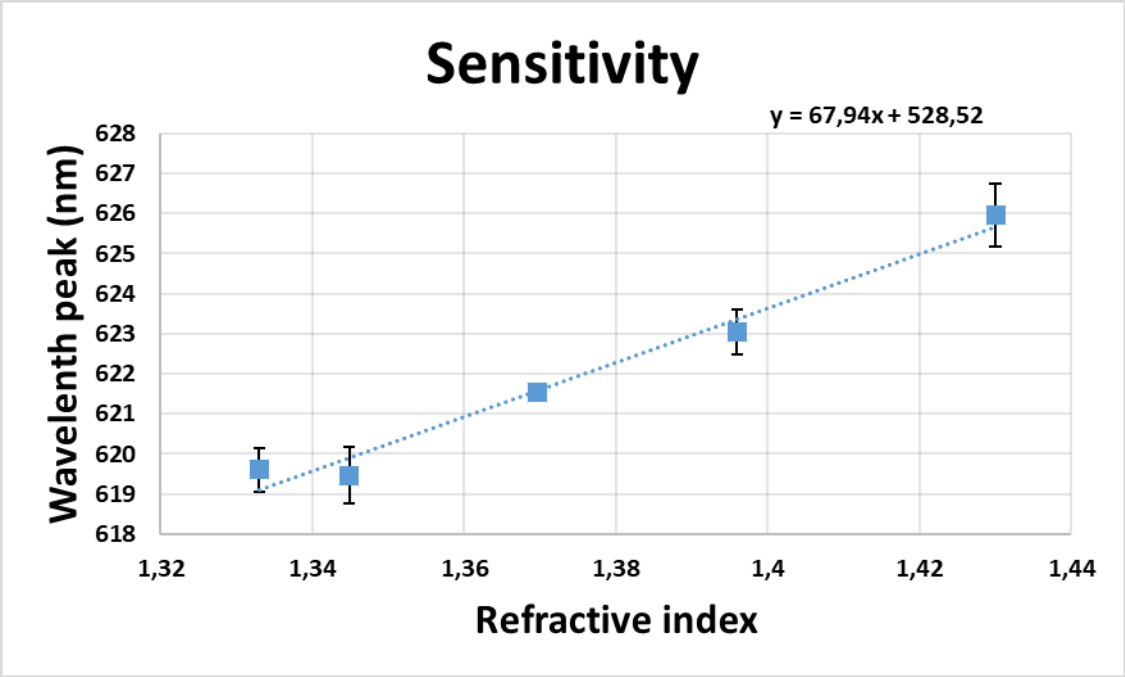

Figure 39 – Calibration curve showing the device sensitivity, error bars are included representing the standard deviation of the measurements. Linear function is fitted with the data points plotted

6. Results and Discussion

In this thesis work, an optimization of the nanoplasmonic sensor fabrication is carried out to obtain desired nanostructures features. Nanoplasmonic sensor testing is performed to determine the sensitivity performance of the different nanostructure features, with a highest sensitivity of ~600 nm/RIU. Functionalization of the sensor is achieved in order to get binding effects on the surface, thus trapping the desire nanosized particles.

Combining these results, it is possible to test a successful online detection of nanosized particles. Also, a combination of interdigital transducers (IDTs), microfluidics and nanoplasmonic sensor fabrication is presented. Further test can be carried out to test performance improvement of online detection of nanoparticles with the implementation of surface acoustic waves (SAW).

Different subtasks are discussed:

1. Optimization of process recipe
   1.1. Performance of different beam diameter and pitch
   1.2. Writing time for different beam diameters
   1.3. Dose test
      1.3.1. Features of 200 nm diameter and 400 nm pitch and different thicknesses of photoresist deposited for the lift-off step performance on glass
      1.3.2. Features of 200 nm diameter and 400 nm pitch and different thicknesses of photoresist deposited for the lift-off step performance on LinbO3 substrate
2. Nanoplasmonic sensors optimization results
   2.1. Different geometric features and gold thicknesses deposited
   2.2. Implementation of microfluidics
3. Functionalization of the sensor
4. Online detection with functionalized sensor experimental results
5. Microfluidics, SAW and nanoplasmonic sensor prototype fabrication

6.1. Optimization of process recipe

6.1.1. Performance of different beam diameter and pitch

It is important to select the optimal parameters for the exposure in the EBL Elionix, in this section the performance of different beam diameter and pitch is discussed.

When introducing the pattern file in the EBL software, it is possible to divide this image in different writing files, dividing the image in pixels/dots, a table with different resolution possibilities is shown below.

Dots	100µm	250µm	500µm	1000µm	1500µm	3000µm
50,000	2	5	10	20	30	60
200,000	0.5	1.25	2.5	5	7.5	15
500,000	0.2	0.5	1	2	3	6
1,000,000	0.1	0.25	0.5	1	1.5	3

Table 4 – Dot size table, first column is the number of dots and in the first row is the writing field size (Units are nm). Combination used is highlighted.

On the first column is shown the number of dots and in the first row is shown the writing field size, thus resulting in a specific dot size. The lower the value of the dot size is the better the resolution is obtained. Higher resolution provides better shape of the desire pattern on the sample.

The pattern is divided into a dot number, and it is possible to select the dot step size which the electron beam is going to follow, this is the pitch. For example, selecting pitch 2, which means during the writing, the beam is going to jump every 2 dots in a specific direction, being possible to reduce the writing time but also this affects to the quality of the final performance. It is possible to select the beam diameter changing the current of the electron beam, different beams and currents leading to a different beam diameter are shown in table 4. The diameter beam must be selected to overlap the dots exposed as shown in Figure 40.

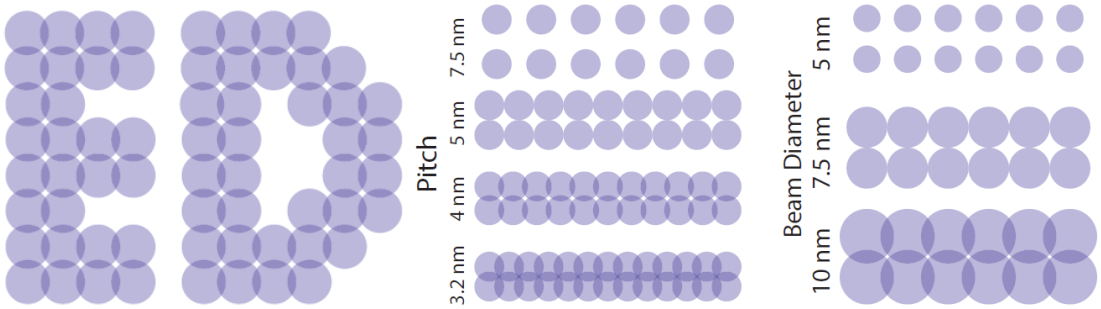

Figure 40 – Overlapping effect with the optimal pitch and beam diameter [50]

Dose area (dose is the time the beam spends in a dot) determines the final writing time and quality of the exposure, this can be calculated with Formula 1. Dots required a minimum dose to change the properties of the photoresist (reference dose is given by the data sheet of the photoresist), it is required a dose test to find the correct dose for the specific processes. For deeper explanation of the relation between different beam diameter and pitch consult [50] provide by some NTNU students.

$$Dose\ area = \frac{(Beam\ current \times base\ dose)}{(step\ size(pitch))^2} \qquad (1)$$

Beam Current	OLAP	Beam Diameter
100pA	120µm	1.8nm
200pA	120µm	2nm
500pA	120µm	2.1nm
1nA	120µm	2.3nm
2nA	120µm	3nm
5nA	120µm	5nm
10nA	120µm	10nm
10nA	240µm	15nm
20nA	240µm	25nm
50nA	240µm	90nm
100nA	240µm	300nm

Table 5 – EBL parameters, combination of beam current and OLAP aperture generates different beam diameters. In yellow, selected parameters for the fabrication. Combination used is highlighted.

Feasible writing time and optimal quality of the final features need to be found with a different combination of number of dots, writing field size, pitch, beam diameter and dose.

A test is performed to find optimal parameters for the exposure. Figure 41 shows a SEM image of the nanostructures when photoresist is exposed with different parameters, pitches from 10 nm to 4 nm are tests in combination with currents from 5 nA to 1 nA. Furthermore, the most optimal overlapping effect is

found when reducing the beam diameter (lowest beam current) and small pitch, 4 nm pitch and 1nA as a current.

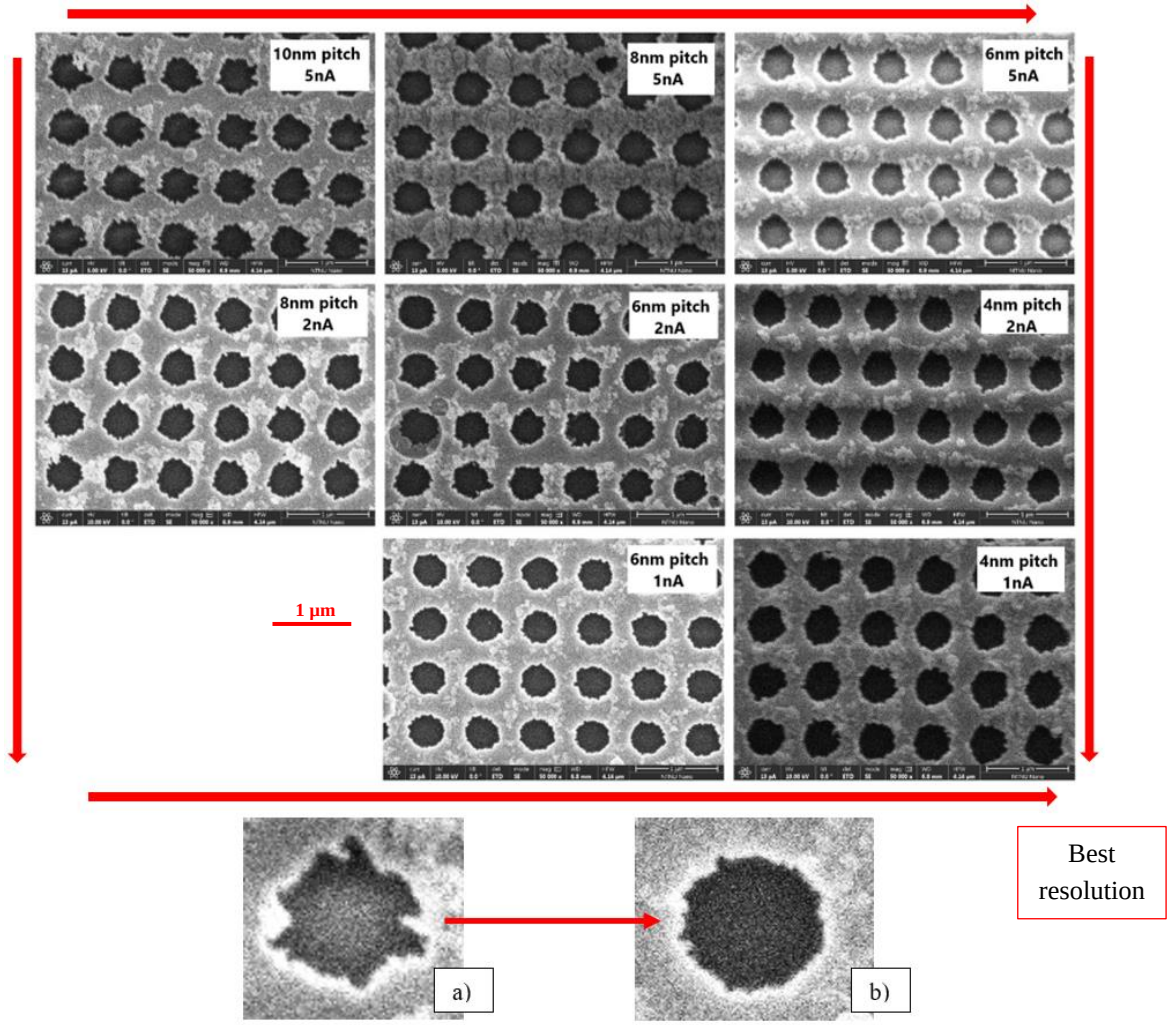

Figure 41 – Nanostructures SEM images of the exposures in the EBL with the optimal dose of different pitches and beam currents (beam diameter). a) Left upper image single hole, not optimal overlapping results in not well-defined shape, b) Bottom right image single hole, reduced beam diameter and pitch result in high resolution results

6.1.2. Writing time for different beam diameters

The relation between pitch and beam diameter require a specific dose area, and thus different writing time as explained in Section 1.1 of Chapter 6 results and discussion. Also, the path followed by the beam changes with different pitches leading to a change in the writing time. Simulations are performed to find a feasible writing time for the different features. Although for a small pitch (1 nm) the quality of the features is most optimal, it requires a long time (plus than 30000 seconds) in comparison with bigger pitch (10 nm) which takes shorter time (~2500 seconds). This is a limiting factor due to availability of the EBL machine in the NTNU nanolab. Bigger pitch for faster exposure is selected as a final parameter for the fabrication. Quality of the final features do not affect significantly the performance during spectrometric experiments of this nanoplasmonic sensor.

For the features of 400 nm diameter 800 nm pitch is 10 pitch and it requires 36 min of exposure for the desire area (700 μm^2) and features of 200 nm diameter 400 nm pitch is 5 pitch due to smaller features require higher resolution to be obtained and exposure takes 1 hour and 45 min.

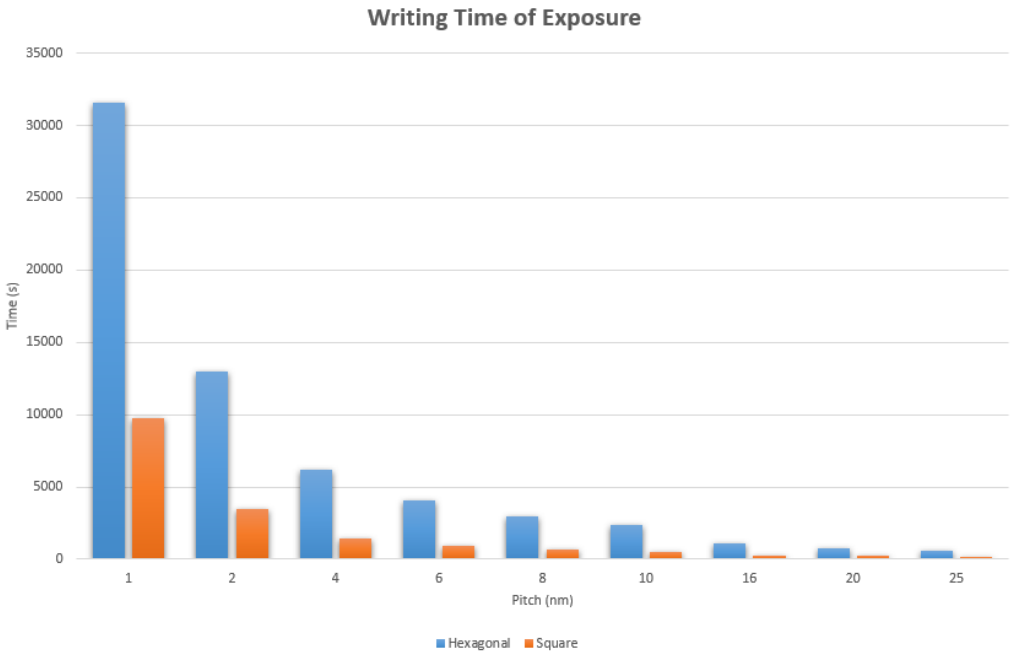

Figure 42 – Writing exposure time simulation for features of 400 nm diameter 800 nm pitch with hexagonal and square lattice array.

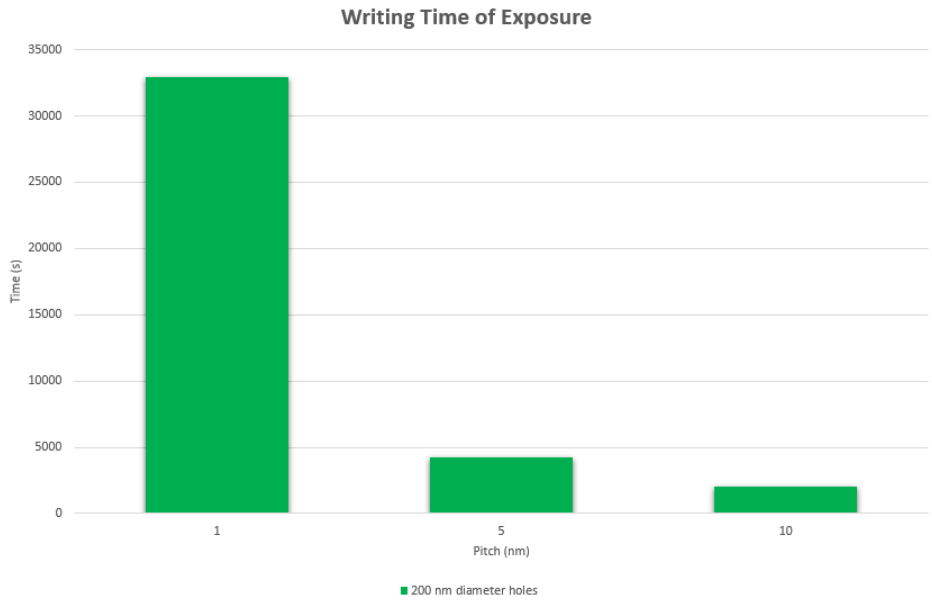

Figure 43 - Writing exposure time simulation for features of 200 nm diameter 400 nm pitch.

6.1.3. Dose test

6.1.3.1. Features of 200 nm diameter and 400 nm pitch and different thicknesses of photoresist deposited for the lift-off step performance on glass

For the glass substrate, sensitivity analysis of the photoresist thickness deposited is carried out and for each specific thickness a dose test is performed. In Figure 44 it is shown the dose test for 5000 rpm during photoresist spin coating, best dose for this parameter is 180 μm/cm². For 5000 rpm speed, the thickness achieved is ~0.35 μm following the experimental data sheet (thickness cannot be check in reflectometer due to substrate properties). Figure 44 demonstrates that although the optimal dose is reached during the dose test, the photoresist thickness is not optimal to get the desire geometrical features (200 nm diameter and 400 nm pitch) for the metal evaporation and lift-off step, columns of photoresist after development are too weak and tend to get together, Figure 45 shows areas where the photoresist dots are together and it is not possible to remove during lift-off step. Also, when photoresist columns bend together, more area of the surface is exposed to the deposition without any pillar of photoresist, that way covering completely the surface without any pattern.

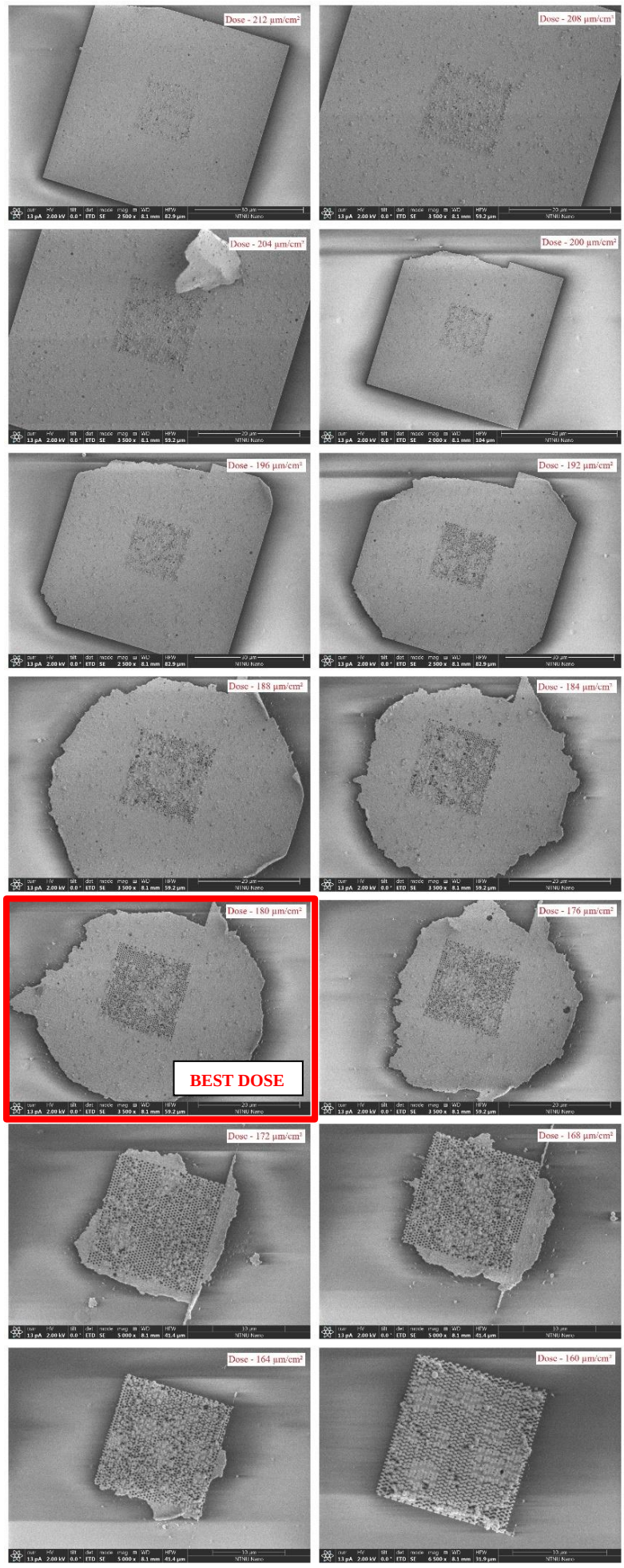

Figure 44 – SEM images of nanostructures dose test on glass. Optimal dose 180 µm/cm²

Experiment is repeated for different thicknesses of photoresist, including a dose test for each thickness. Results are displayed below and in Table 6, best dose of the different thicknesses is shown.

Speed spin coating (rpm)	Thickness (µm)	Optimal dose (µm/cm²)
4000	0,4	180
5000	0,35	180
5500	0,325	180
6000	0,3	184

Table 6 – Optimal dose for the different speed coating test of the photoresist

Most optimal parameters for the fabrication of 200 nm diameter and 400 nm pitch on glass substrate are 0,3 µm thickness of photoresist exposed with a dose 184 µm/cm², depositing 200 nm of gold and performing lift-off.

In Figure 38, different optimal doses are shown of the different thicknesses of photoresist spin on top of the substrate. In the 4000-rpm spin coating it can be seen numerous gaps and areas completely cover all over the sample due to the height of the columns are so high, the columns reach the aspect ratio limit becoming weak and bending together which does not allow an optimal deposition and further lift-off.

As long as the thickness of the photoresist is thinner, increasing speed during spin coating, the height of the columns gets an optimal aspect ratio and less gap areas are disappearing, it is found that the optimal parameter for getting the optimal thickness is 6000-rpm.

It is possible to go thinner, this way the features are improving and less gaps are found, but in this work 200 nm of gold is required for the sensor fabrication, and going lower than 6000-rpm for the thickness is a problem due to columns of photoresist starts to be the same thickness of the wanted gold to deposit, thus the photoresist columns are completely cover by gold being impossible to perform the lift-off step, so getting thinner layer than the one obtained with 6000-rpm is not optimal for the nanoplasmonic sensor fabrication.

200 nm diameter features recipe fabrication is obtained the same way as the followed to get the 400 nm diameter features.

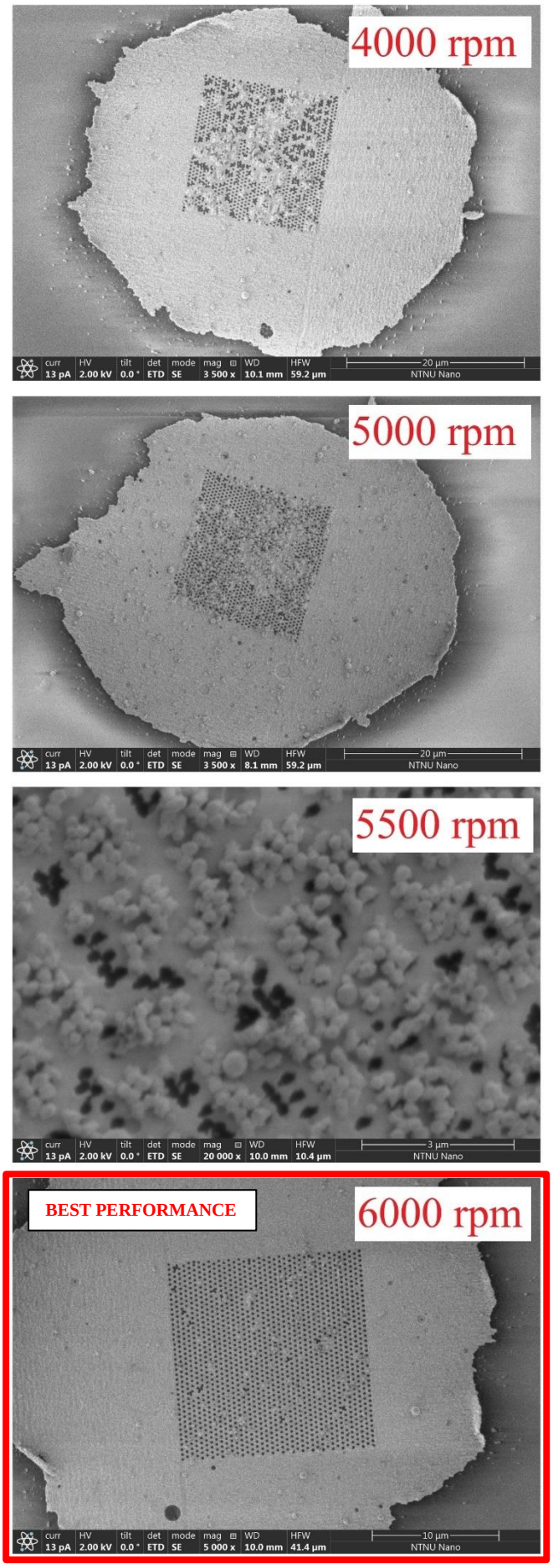

Figure 45 - SEM images of nanostructures on glass of lift of performance. Optimal thickness of photoresist for 6000 rpm during spin coating.

Summary of EBL parameters for nanoplasmonic sensor fabrication on glass:

For the bigger features, 400 nm diameter and 800 nm pitch optimal parameters are: 1,000,000 number of dots, 1000µm writing field size, 10 pitch, 5 nA current to get 5 nm as beam diameter, dose 172.5 µm/cm². 6000 rpm spin coating.

For the smaller features, 200 nm diameter and 400 nm pitch optimal parameters are: 1,000,000 number of dots, 1000µm writing field size, 5 pitch, 2 nA current to get 3 nm as beam diameter, dose 180 µm/cm². 6000 rpm spin coating.

6.1.3.2. Features of 200 nm diameter and 400 nm pitch and different thicknesses of photoresist deposited for the lift-off step performance on LinbO3 substrate

Same methods as in Section 1.3.1 of Chapter 6 results and discussion for glass substrate are followed to get the desire features on LinbO3 substrate. The most optimal parameters for glass substrate are the starting point of the thickness sensitivity analysis.

The optimum thickness on LinbO3 is for the spin coating speed of 5750 rpm (~0,315 µm) due to recipe fabrication slightly changes in the prebake temperatures because of LinbO3 limitations. Prebake temperature changes leads to different evaporation of the solvents in the photoresist and thus different thickness is achieved (test is silicon wafers is performed to check thickness changes with different prebaking time and temperature).

Optimal dose changes due to different properties of the LinbO3 substrate with 168 µm/cm² as the most optimal dose. Dose test images are displayed in Figure 47.

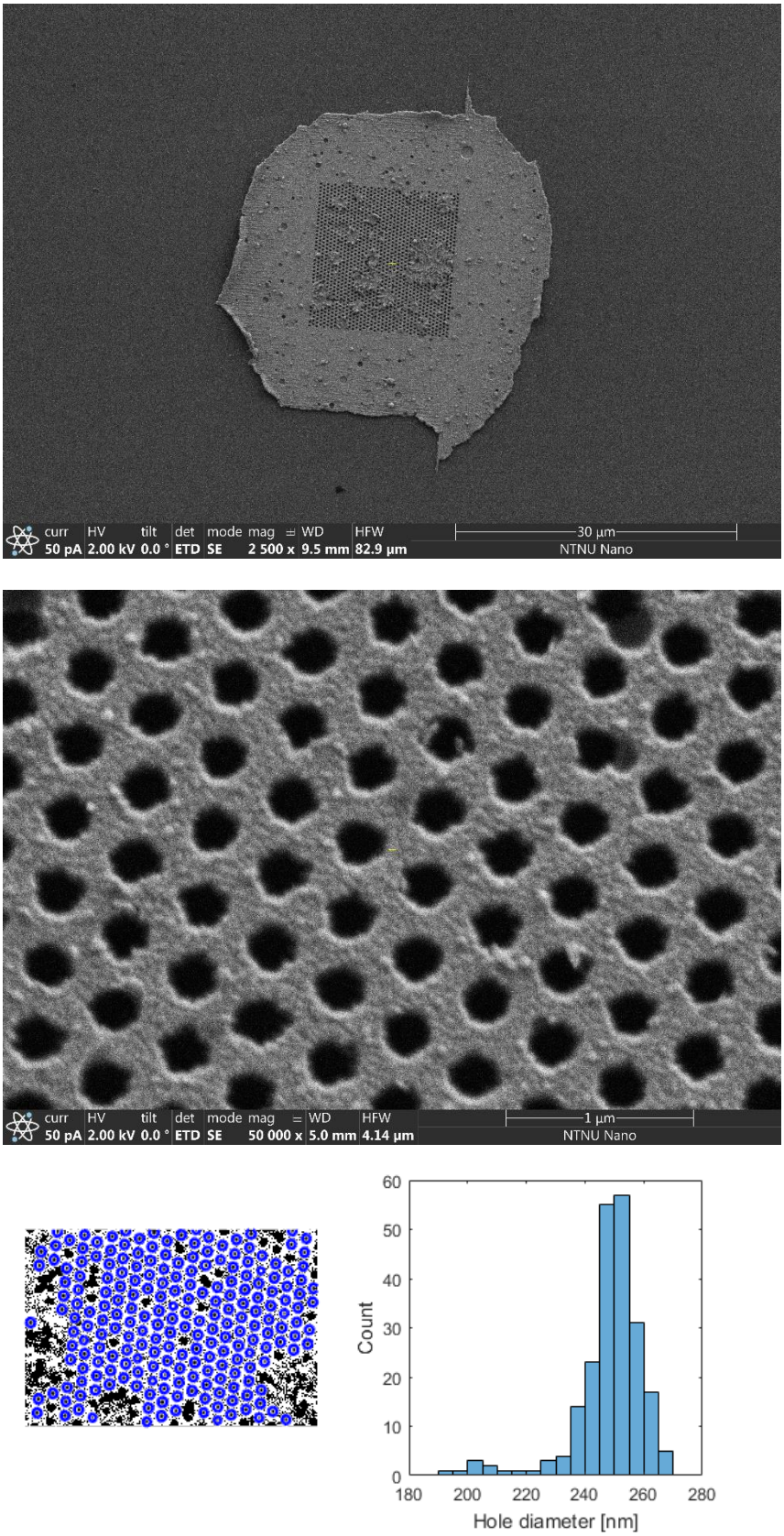

Figure 46 – SEM images of hexagonal array lattice holes of 200 nm diameter and 400 nm pitch on LinbO3 for the most optimal dose. Hole size estimation, hole sizer script in MATLAB is used to determine the actual mean hole diameter. Mean diameter 248.2 ± 12.1 nm.

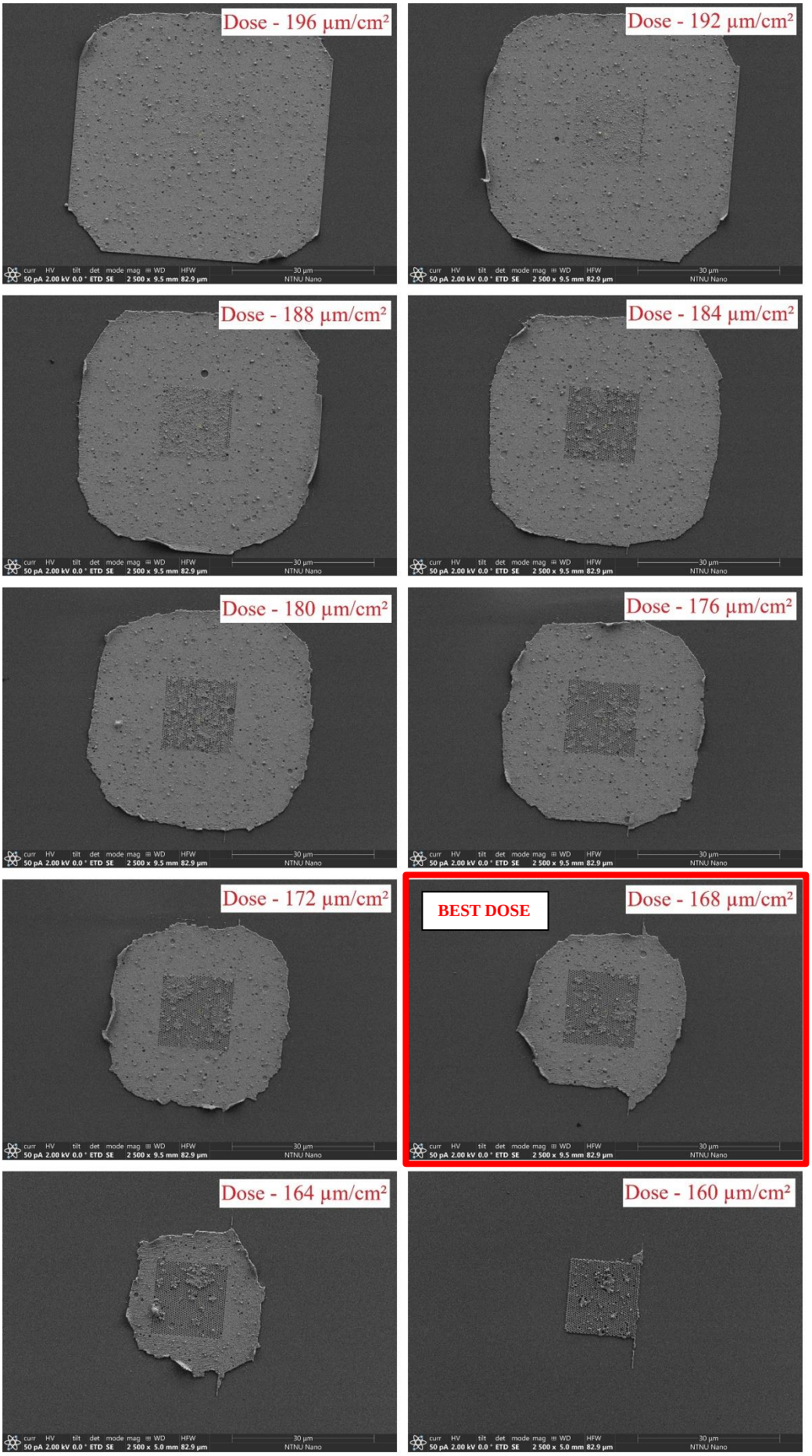

Figure 47 – Dose test SEM images of nanostructures on LinbO3. Optimal dose 168 µm/cm²

6.2. Nanoplasmonic sensors optimization results

6.2.1. Different geometric features and gold thicknesses deposited

In this section, results of the experiments testing the nanoplasmonic sensor optimization is described.

Surface plasmon response (SPR) of the device is measured as wavelength peak shift of the spectrum. Glycerol mixtures are analysed from 0 - 70 % mass concentrations, with refractive index 1.333 – 1.428 to perform the device calibration. A general scheme of how calibration is performed is presented in Figure 48. Calibration curve presents a linear relation between the shift of the spectrum wavelength peak and the change in the refractive index close to the surface.

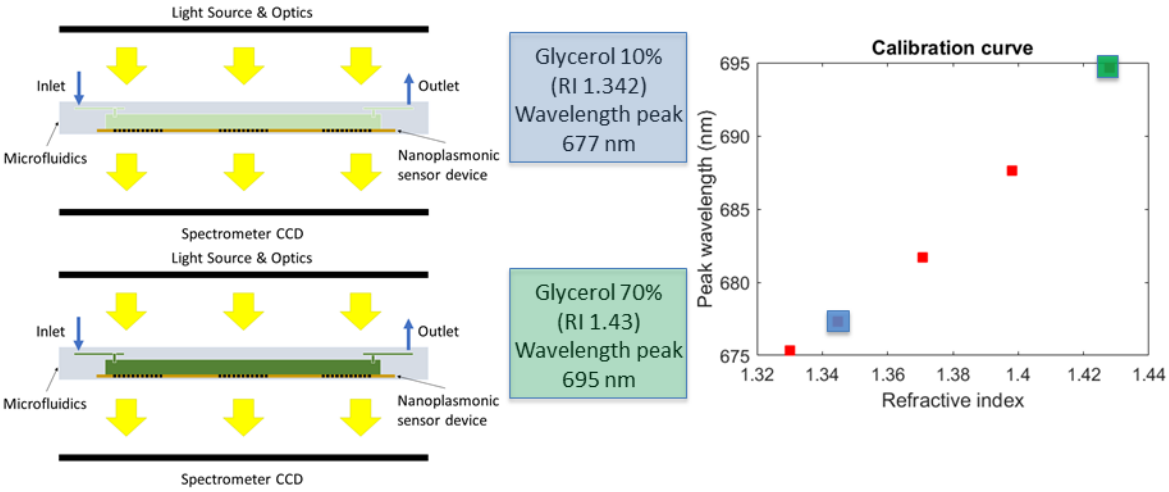

Figure 48 – Glycerol calibration scheme including microfluidics. Different glycerol mixtures are tested giving different peaks of the spectrum measured being possible to track the shift. Calibration curve is determined, sensitivity ~210 nm/RIU.

Devices with different thicknesses and geometric features are tested. A sensitivity analysis is performed testing features with different pitches from 700 nm – 1100 nm and different lattice array of the holes, square lattice and hexagonal lattice, hole diameter is kept constant 400 nm.

Previous studies [51] demostrate theoretically that hexagonal lattice array shows better performance than square lattice array. Surface plasmon resonance is more present in hexagonal array due to more density of holes are present in the same area in comparison with square lattice array. In this thesis, experimental

results demostrate that hexagonal lattice array shows higher sensitivity for the spectrum shift when mesuring different refractive index. Results are shown in the Figures 49-50-51.

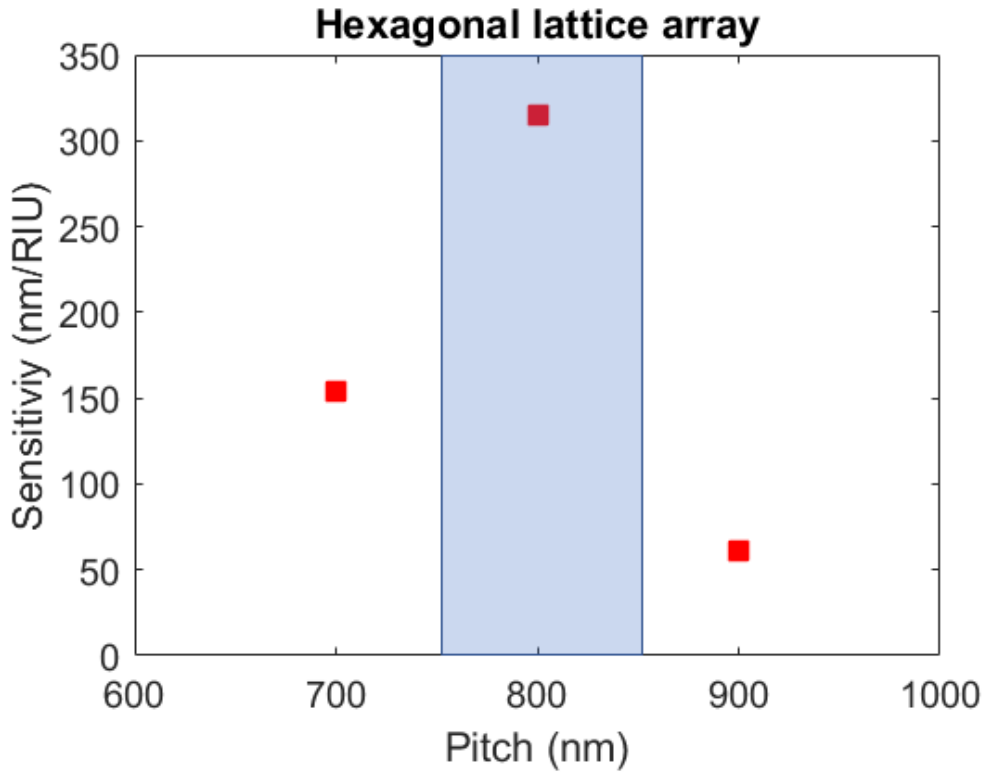

Figure 49 – Experimental results of hexagonal lattice hole array with 400 nm diameter, pitch sensitivity analysis. Best sensitivity is found for 800 nm pitch.

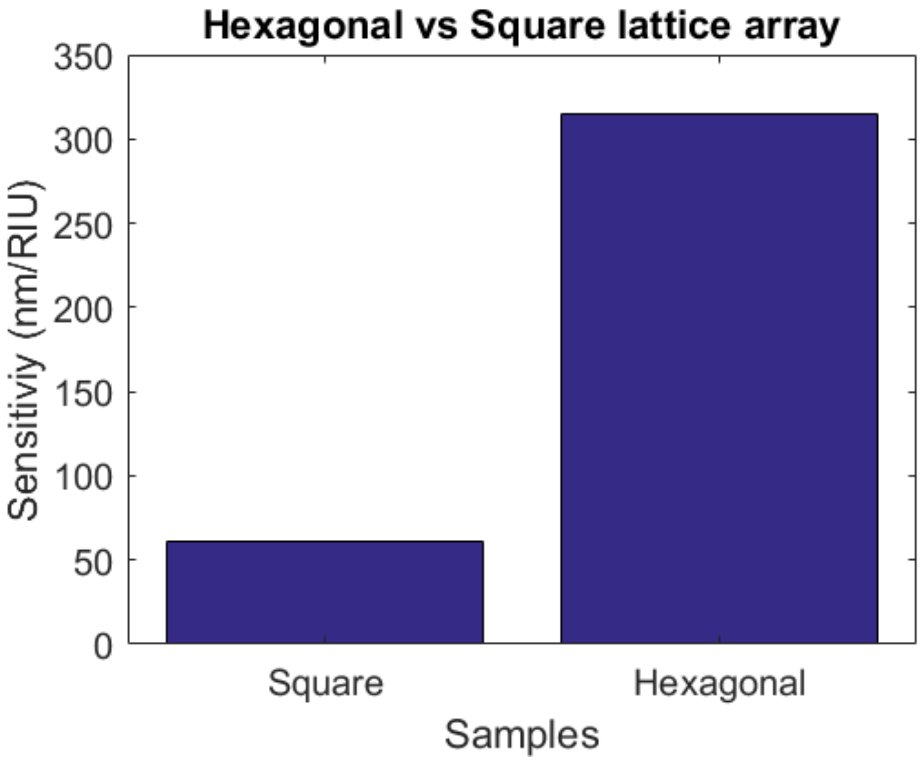

Figure 50 – Experimental results comparing hexagonal vs square lattice hole array with 400 nm diameter and 800 nm pitch. Best sensitivity is found for hexagonal lattice hole array.

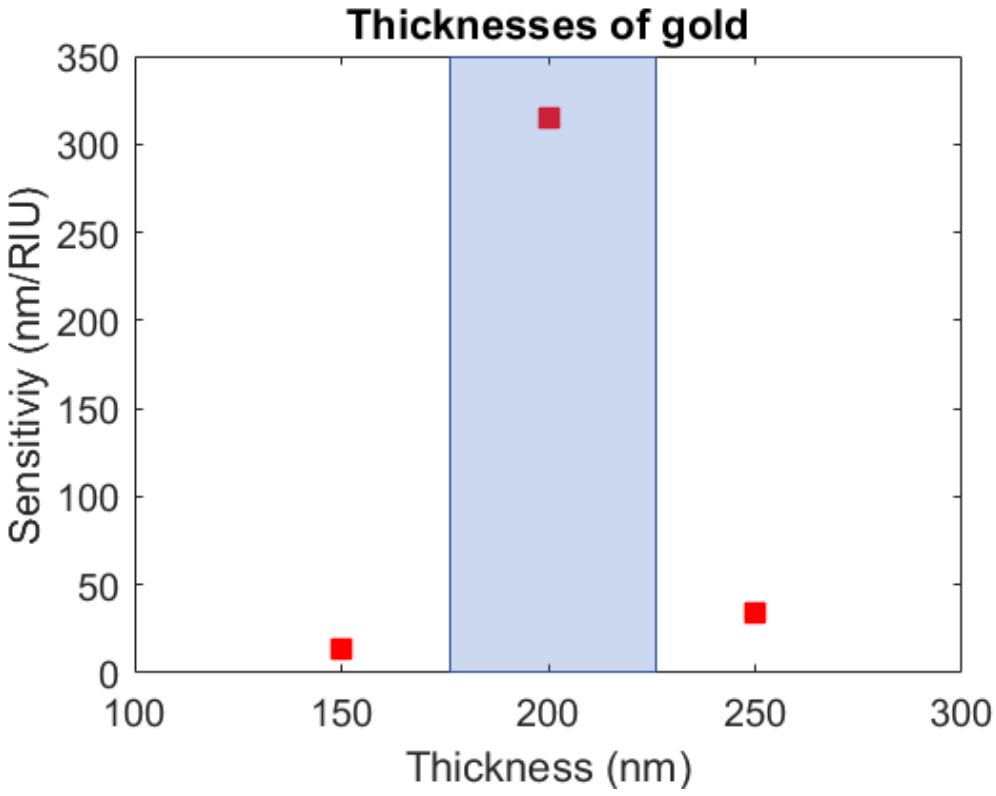

Figure 51 – Experimental results of hexagonal lattice hole array with 400 nm diameter, gold thickness deposited sensitivity analysis. Best sensitivity is found for 200 nm gold.

Most optimal features for the nanoplasmonic sensor device as a first stage of the optimization with diameter 400 nm constant are: 800 nm pitch, hexagonal array lattice and 200 nm gold deposited.

To improve sensitivity of the sensor, features are reduced to the half size, following feature sizes of previous studies [4], 200 nm diameter 400 nm diameter and thickness of gold deposit is kept constant to 200 nm. A new fabrication process is developed due to smaller size of the features implies higher resolution in the fabrication as explained in Section 1. Optimization of process recipe. Experiments are carried out the same manner as with the bigger features. Device sensitivity increases significantly in comparison with the bigger size diameter of 400 nm from ~300 RIU/nm to ~600 RIU/nm, shown in Figure 52.

Highest sensitivity of the sensor is found with features of 200 nm diameter, 400 nm pitch and 200 nm of gold deposited.

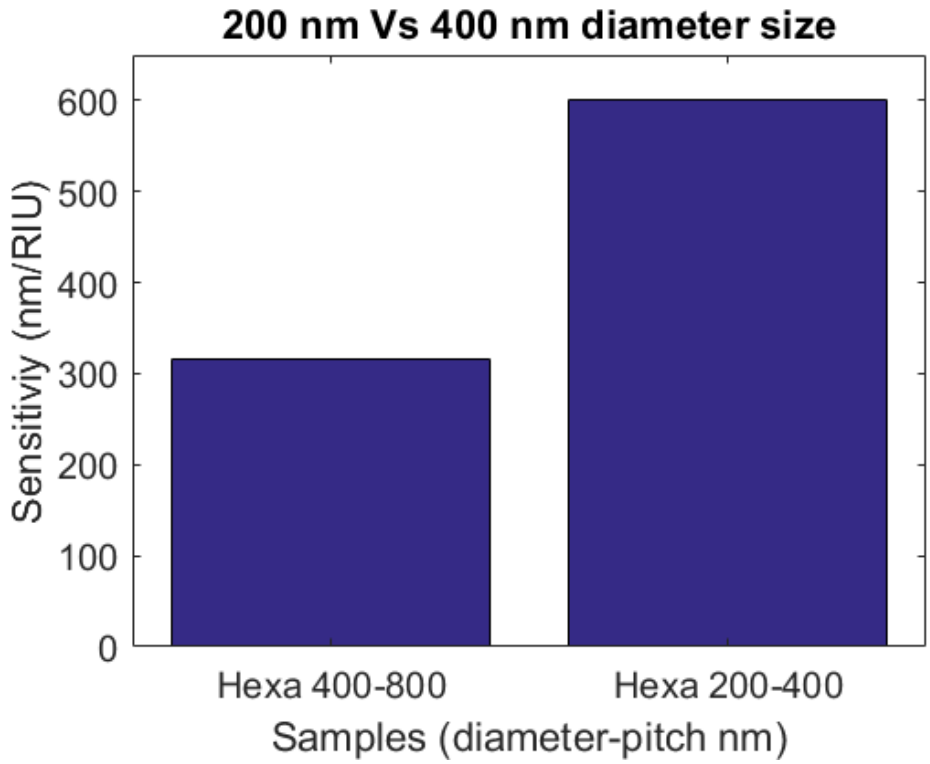

Figure 52 – Experimental results of hexagonal lattice hole array, big features of 400 nm diameter and 800 nm pitch versus small features of 200 nm diameter and 400 nm pitch. Best sensitivity is found for 200 nm diameter features.

6.2.2. Implementation of microfluidics

For a better controllability and reduction of liquid sample usage, microfluidics are implemented to the nanoplasmonic sensor in order to test and calibrate this configuration for further detection of nanosized particles.

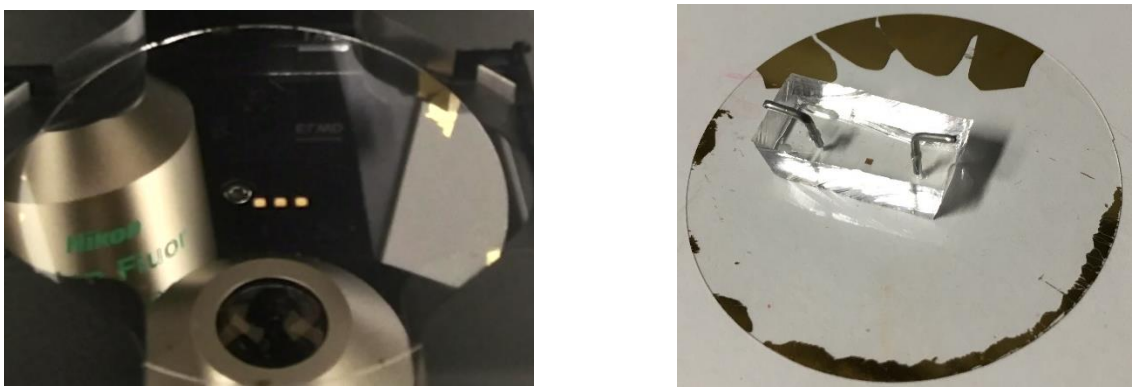

Figure 53 – Left hand side image, nanoplasmonic sensors array on glass substrate without microfluidics implementation. Right hand side image, nanoplasmonic sensors array with microfluidics implementation.

Detection performance comparison is carried out on both configuration of the nanoplasmonic sensor, without microfluidics and with microfluidics implementation. Nanostructures of hexagonal lattice hole array of 200 nm diameter and 400 nm pitch on glass substrate are tested with both configurations and a loss of sensitivity is observed for microfluidics implementation.

The PDMS microchannel induces another layer with a different refractive index during experiments which affects in the read out of the spectrum reducing the total shift of the spectrum. Intensity is also affected by the PDMS microchannel, although it is transparent, light is mitigated due to its thickness.

However, Microfluidics implementation improves the calibration curve fitting, due to more controllability is achieved during experiments. A better fitted linear relation is found for the spectrum peak and refractive index.

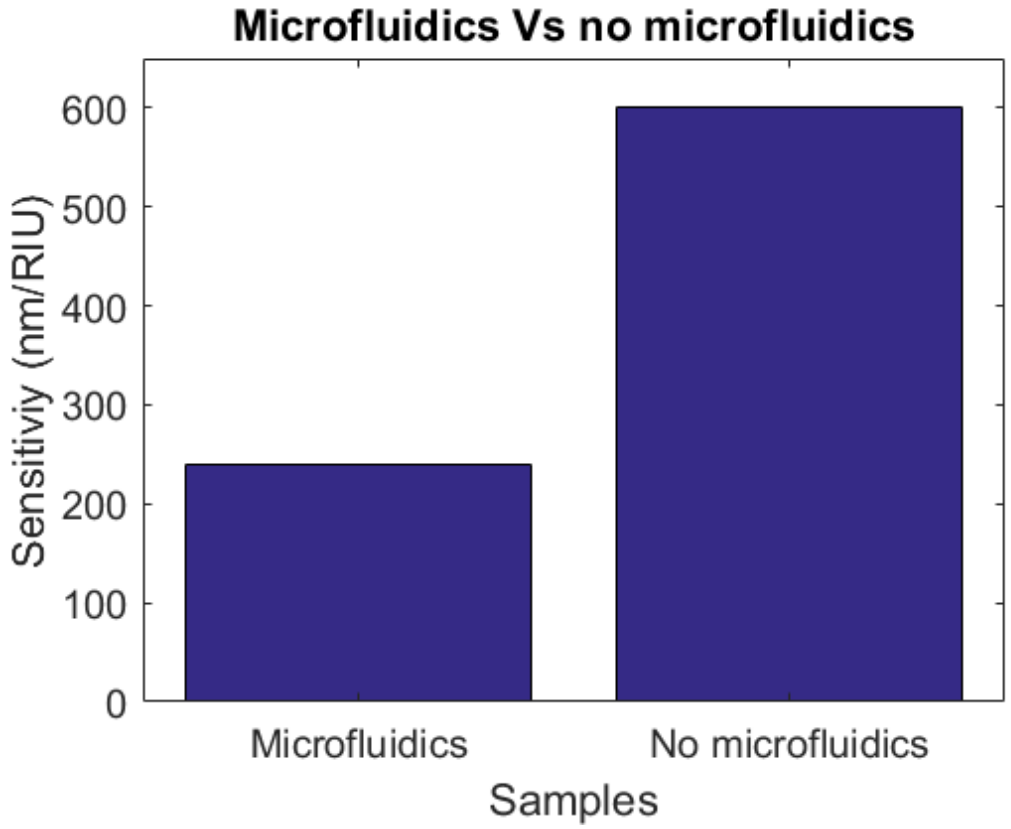

Figure 54 – Experimental results of hexagonal lattice hole array with 200 nm diameter and 400 nm pitch. Sensitivity comparison of microfluidics implantation.

Test with chamber and microchannel is performed to compare different configuration performance. Not significant differences using microchannel or chamber are found. Experiments are carried out with microchannel due to microfluidics problems are avoid (bubbles, alignments with the sensor) and better performance of functionalization is obtained, with chamber troubles are found when flushing due to formation of bubbles preventing the completely wetting of the sensor surface.

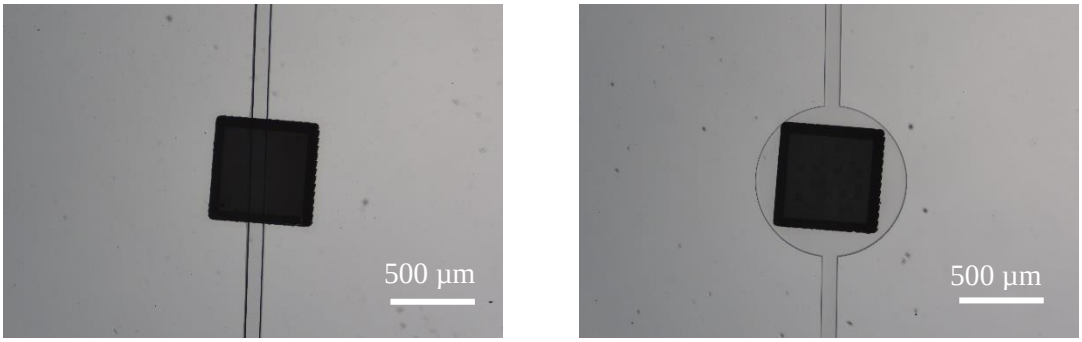

Figure 55 – Bottom view image of different nanoplasmonic sensor and microfluidics configurations. Left hand side image, microchannel implementation, Right hand side image, chamber implementation.

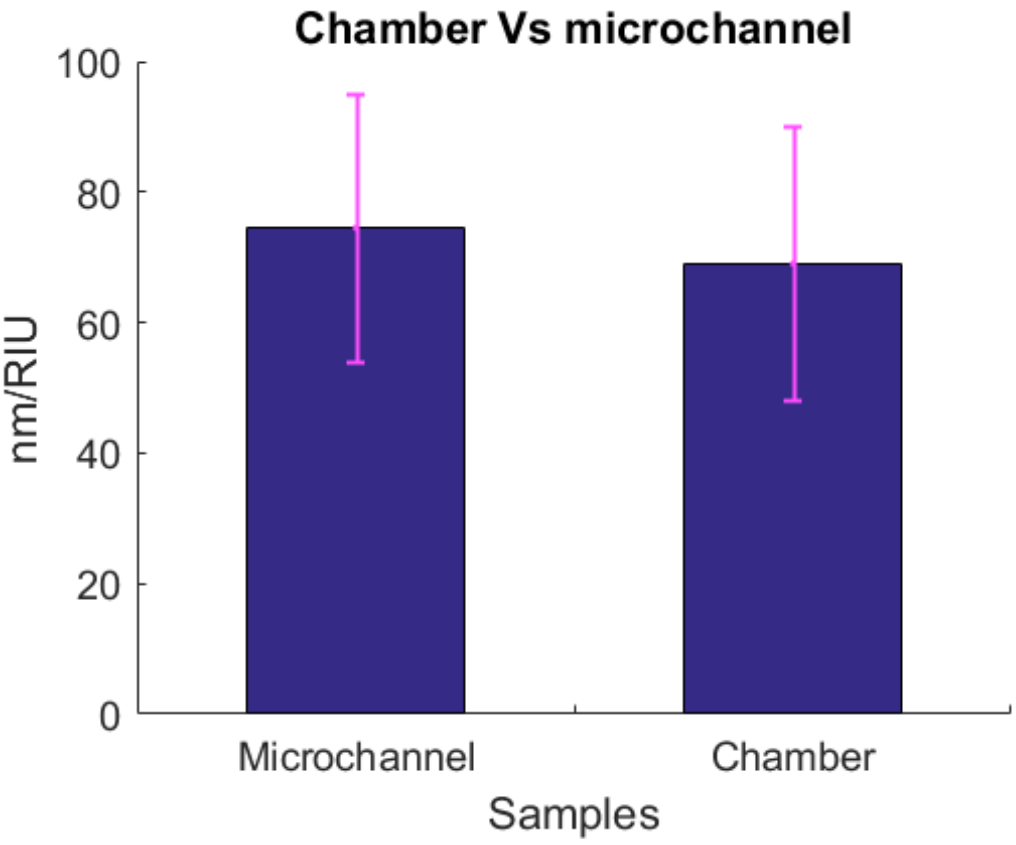

Figure 56 – Spectrometric experimental results of different nanoplasmonic sensor and microfluidics configurations. Features of the nanostructures 400 nm diameter and 800 nm pitch.

LinbO3 substrate is tested with the most optimal parameters for the nanoplasmonic sensor testing and performance on glass. Features of 200 nm diameter, 400 nm pitch, 200 nm of gold deposited and microchannel implemented.

Results with LinbO3 as a substrate give a lower sensitivity, ~125 nm/RIU, due to the properties of the substrate such us how light is transmitted through this medium, the thickness of the substrate which dampen the shifting effect.

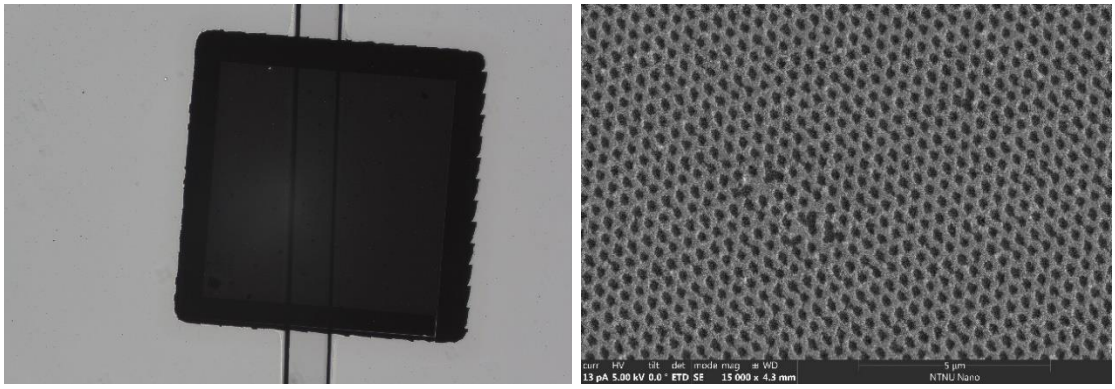

Figure 57 – Left hand side, image from the bottom of the nanoplasmonic sensor and microchannel implementation. Right hand side, zoomed image of the nanoplasmonic sensor, features of 200 nm diameter and 400 nm pitch on LinbO3 substrate

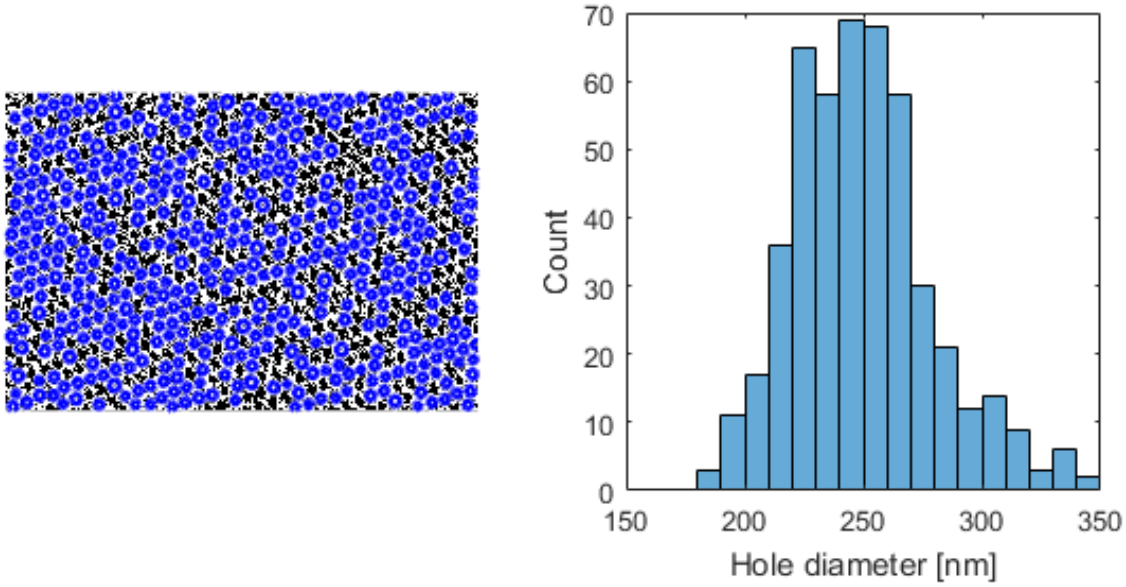

Figure 58 – Hole size estimation, hole sizer script in MATLAB is used to determine the actual mean hole diameter. Mean size hole diameter: 249.75 ± 29.41 nm

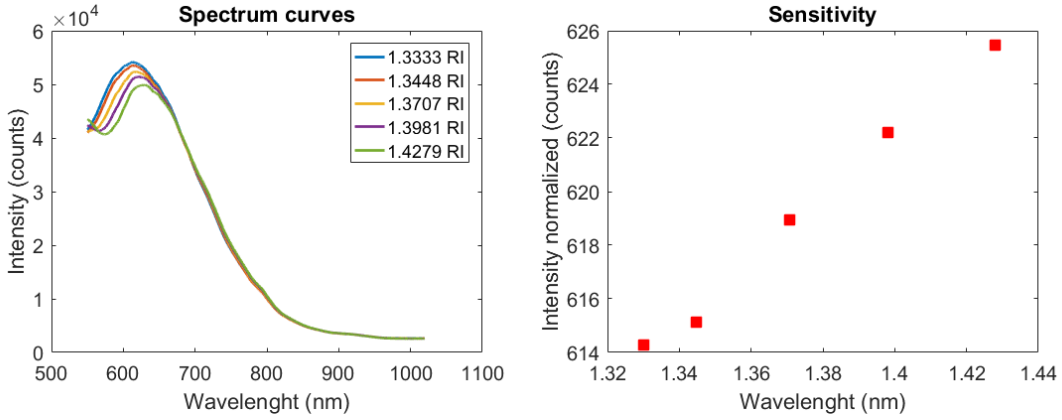

Figure 59 – Single experiment spectrum curves obtained from the calibration spectrometric analyses of glycerol mixtures. Track of the spectrum peak can be perform obtaining a

calibration curve. Nanoplamonic sensor with features of features of 200 nm diameter and 400 nm pitch on LinbO3 substrate

This experiment proves that LinbO3 substrate is optimal for the spectrometric analysis. It is possible to detect a change in the refractive index, enabling to detect nanosized particles in a fluid. Therefore, this substrate can be combined with the fabrication of interdigital transducers (IDTs) for generation of surface acoustic waves (SAW) and possible improvement of the detection performance.

6.3. Functionalization of the sensor

To obtain binding effects on the surface of the sensor, a chemical process is required. Application of polyethylene glycols (PEGS) chemicals are used.

Polyethylene glycols (PEGS) are used to avoid non-specific bindings, undesired target particles getting attached to the surface, acting as surface blocking agents. This chemical treatment generates a hydrophilic coating on gold nanoparticles.

For spectrometric experiments, PEGs chains need to be short enough to avoid a dampen effect of the surface plasmon resonance phenomenon, normally PEG chains are composed of molecules with longitude on the order of thousand subunits. The thicker the coating layer of the gold nanoparticles is, the more decreases the electric field, thus the evanescence wave in charge of the plasmon effect is attenuated. This dampen effect increases exponentially until the coating layer reaches the thickness of the nanoparticle size, which reduce the plasmonic resonance effect [27], therefore it decreases the detection sensitivity.

In this project, a combination of MT(PEG)4 and CT(PEG)12 is used to modify sensor surface and minimize nonspecific binding, the numbers 4 and 12 refers to the PEG spacers units. The longitude of the PEG subunits does not affect significantly the resonance plasmon effect. A possible shift of the spectrum is recorded for detection of nanoparticles (200 nm size) shown in next chapter 4 Functionalized sensor experimental results.

Procedure methods to perform the chemical treatment of the sensor surface recommended by Thermo Scientific and follow in this project are attached in the Appendix B. PEG procedure methods. For better handling and storage, solutions are prepared dissolving the reagent in dimethylsulfoxide (DMSO).

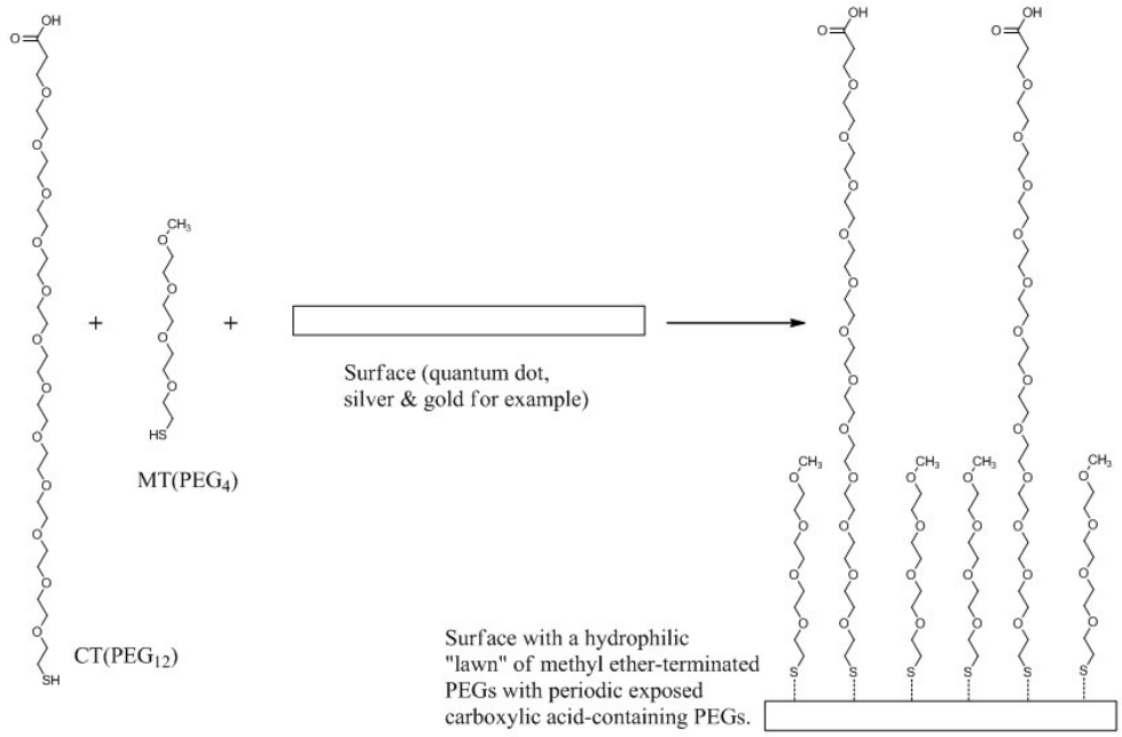

Figure 60 - Surface modification with MT(PEG)4 and CT(PEG)12 [52].

Coating experiments are performed in different solution of PEG concentrations and coating time. The effectiveness of the coating is tested by incubation of fluorescence green beads coated with streptavidin that will bind to the PEGylated surface with biotin in the end of the CT(PEG)12.

Experiments are carried out applying different solutions of PEGs shown in Table 7. A thin metal layer is deposited on a glass surface, 5 nm thickness of titanium and 10 nm thickness of gold which enable to image the attached beads from the bottom with the inverted microscope Nikon Eclipse Ti2 and fluorescence spectroscopy.

Square samples	A1	A2	A3	A4	B1	B5	B6
Ratio (CT(PEG)12:MT(PEG)4)	Control PBS	Control PBS + MT(PEG)4	1:1	1:3	Control PBS	1:5	1:10

Table 7 – Different sample areas of Figure 52 and the different solutions of CT(PEG)12:MT(PEG)4 applied for testing the binding effect of the functionalization process

After 2 hours of incubation of the PEGs and 2 hours of beads mixture incubation, binding test results are not successful due to the contact with air reduce effectiveness and PEGylated gold surfaces become hydrophilic, thus resulting difficult to flush the incubated beads, as a result of this non-specific bindings are present, Figure 62 shows all beads incubated are attached to the functionalized surface instead of the expected result in which only green beads coated with streptavidin react with biotin at the end of the PEG chain and get attached to the surface. Figure 62 is obtained from the imaging of all squares in sample A and B, not differences are observed meaning the performance of this experiment is not optimal.

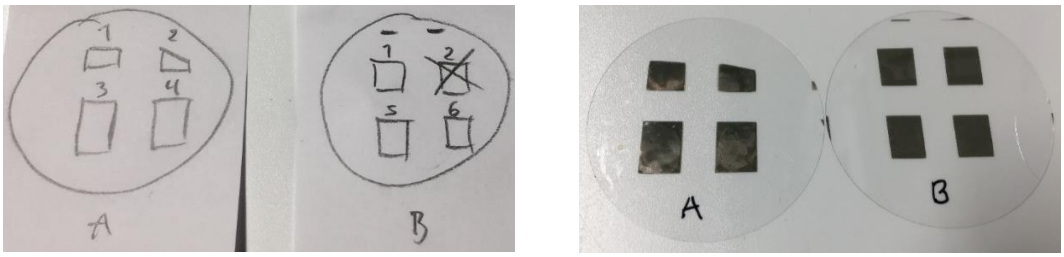

Figure 61 – Glass substrate covered with 5 nm of titanium and 10 nm of gold for functionalization experiments and its respective reference.

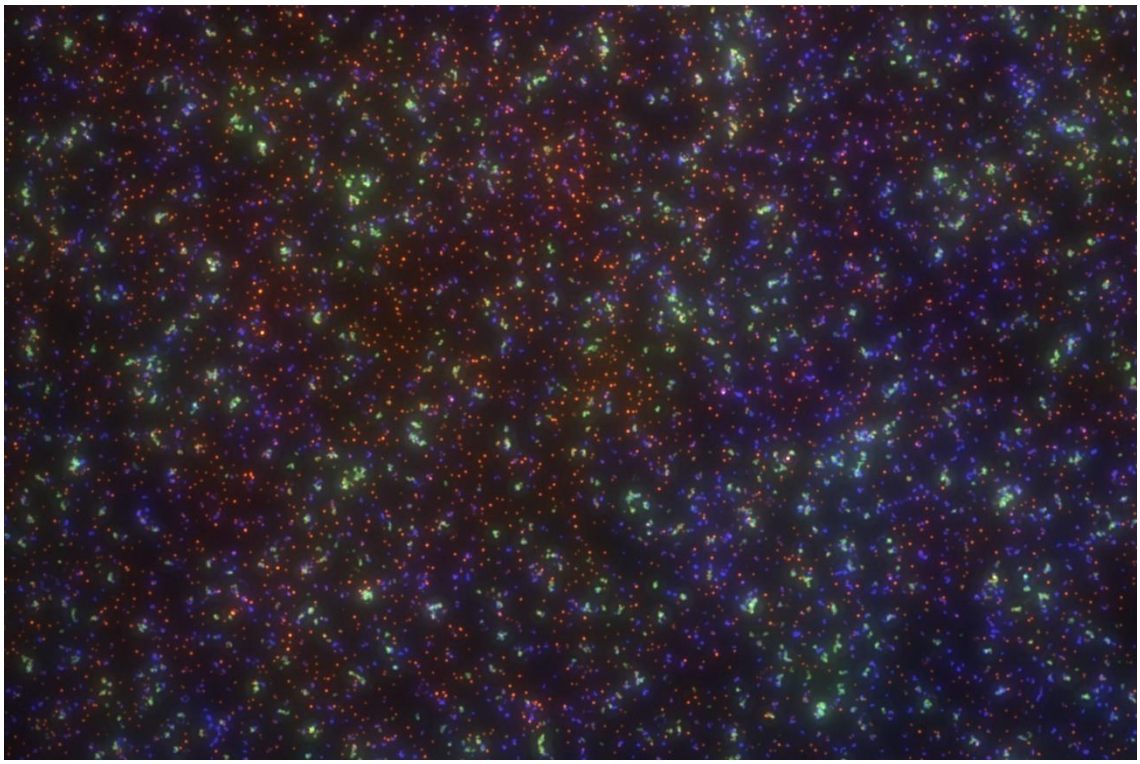

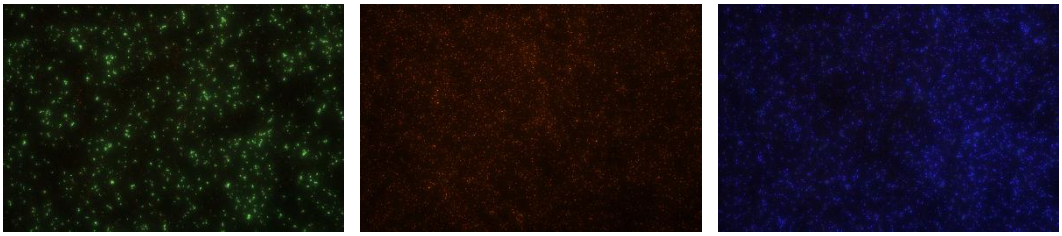

Figure 62 – Black background images of sample A and B. Non-specific bindings are present on the sample due to loss of functionalization effectiveness during the PEGylation process. Bottom images are taken with different filters with specific beads wavelength emission.

Microfluidics are implemented on the glass surface and gold layer to avoid contact with air and improve flushing of the surface. A prototype for this experiment is show in Figure 63. Different coating times and concentrations of PEG are tested, shown in Table 7. Best procedure for surface PEG functionalization is incubate PEGs for 5 hours using a concentration of 1:5 (CT(PEG)12:MT(PEG)4). Shorter coating time shows less binding effect after flushing the incubated beads, longer coating time is detrimental for the binding effect. 1:5 ratio shows the higher density of attached beads on the surface after processing the fluorescence spectrometric images shown in Figure 64-65-66.

Controls are tested in channel 1 with only PBS expecting some non-specific bindings due to surface is not treated chemically. Channel 2 is treated with only MT(PEG)4 which is in charge of protecting the surface from non-specific bindings and shows no beads attached, images of these channels after testing are shown in Figure 66.

A summary of the results is presented in plots of Figure 71.

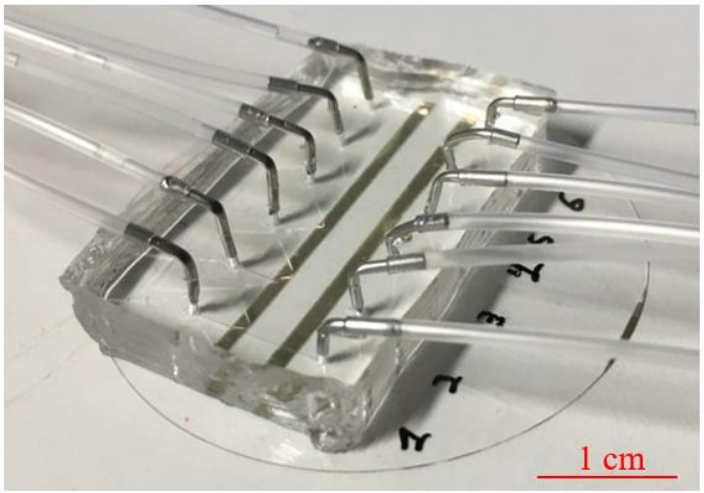

Figure 63 – Microfluidics prototype for functionalization test

Channels	1	2	3	4	5	6
Ratio (CT(PEG)12:MT(PEG)4)	Control PBS	Control PBS + MT(PEG)4	1:1	1:3	1:5	1:10
Area covered (%)	3.9344	0.1672	0.2166	2.2272	8.9977	4.6580

Table 8 – Area covered by beads and ratios of PEG applied for the different microchannels

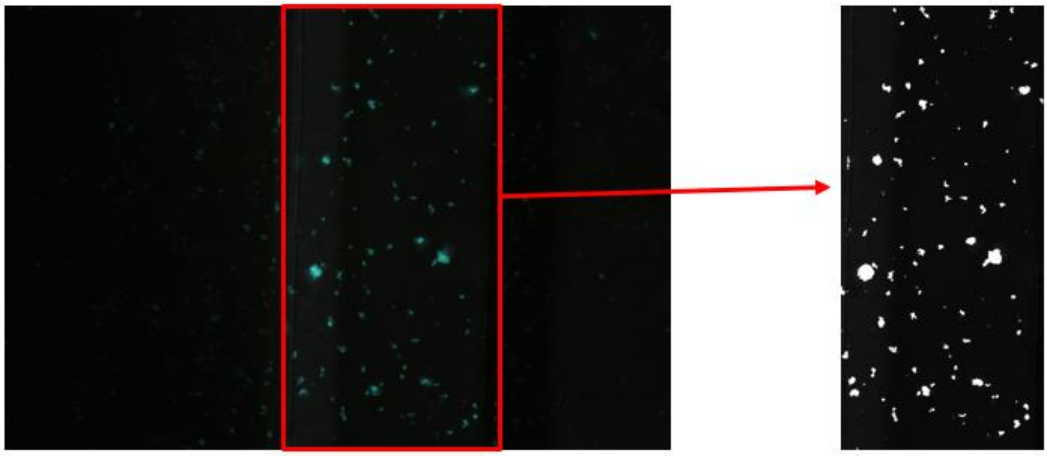

Figure 64 - Black background image of the microchannel width 100 µm and the processed black and white image, 1:3 ratio of (CT(PEG)12:MT(PEG)4) tested

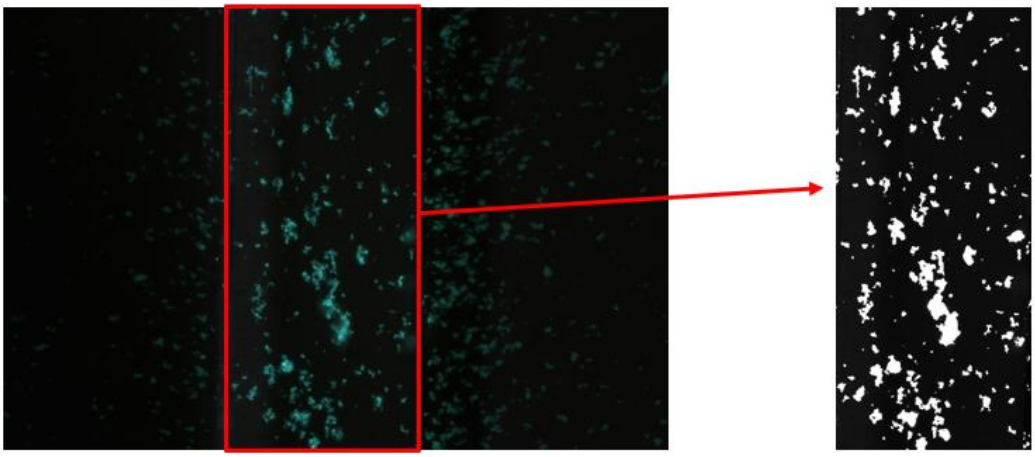

Figure 65 - Black background image of the microchannel width 100 µm and the processed black and white image, 1:5 ratio of (CT(PEG)12:MT(PEG)4) tested

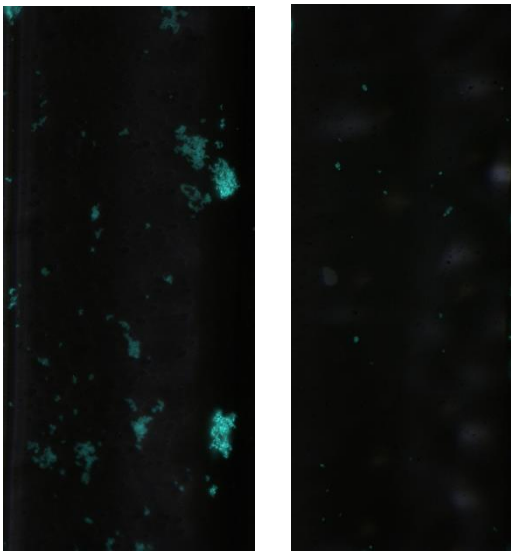

Figure 66 – Black background image of the microchannel width 100 µm. Left hand side image, PBS control test. Right hand side image, PBS + MT(PEG)4 control test

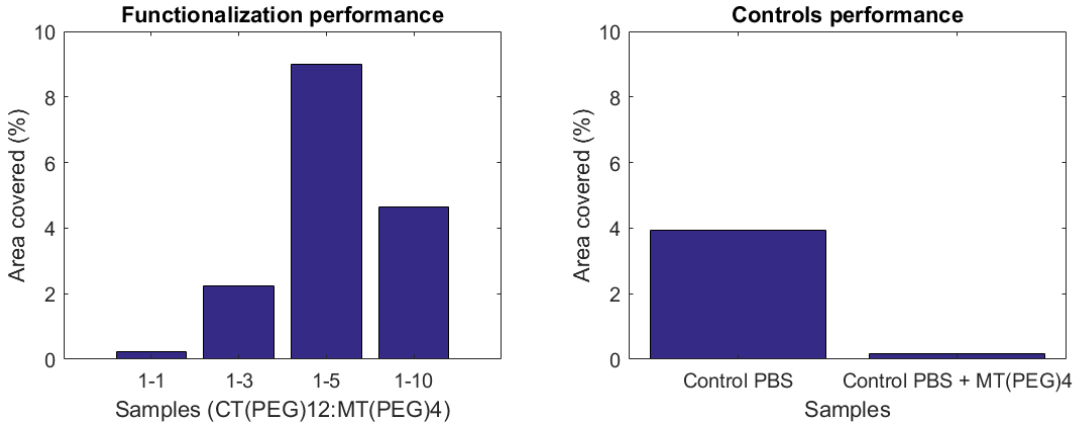

Figure 67 – Functionalization test results for the different microchannels

6.4. Online detection with functionalized sensor experimental results

Online detection results of nanoparticles test using functionalized nanoplasmonic sensor with microfluidics implementation are presented in this chapter.

Nanoplasmonic sensor with most optimal parameters described in Section 2. with features of 200 nm diameter, 400 nm pitch and 200 nm of gold deposited, functionalized inside a microchannel with procedure explained in Section 3. is tested with Dragon green beads (200 nm size) covered with streptavidin that will bind to the PEGylated surface with biotin linker.

The experiment starts flowing buffer solution of PBS into the microchannel generating a SPR response on the sensor. At time zero, nanosized particles are introduce into the system. Nanoparticles start to bind to the sensor inducing a change in the refractive index on the surface, thus generating a different SPR response as shown in Figure 68. When the system is saturated no more changes are induce to the sensor and the SPR response remains constant.

Different concentration and velocities of the flow are tested. High flows and low concentration of beads leads to no signal response from the sensor. Most optimal parameters for the experiments are Reynolds number of 40 and concentration of particles of 2.4 E 11 particles/ml.

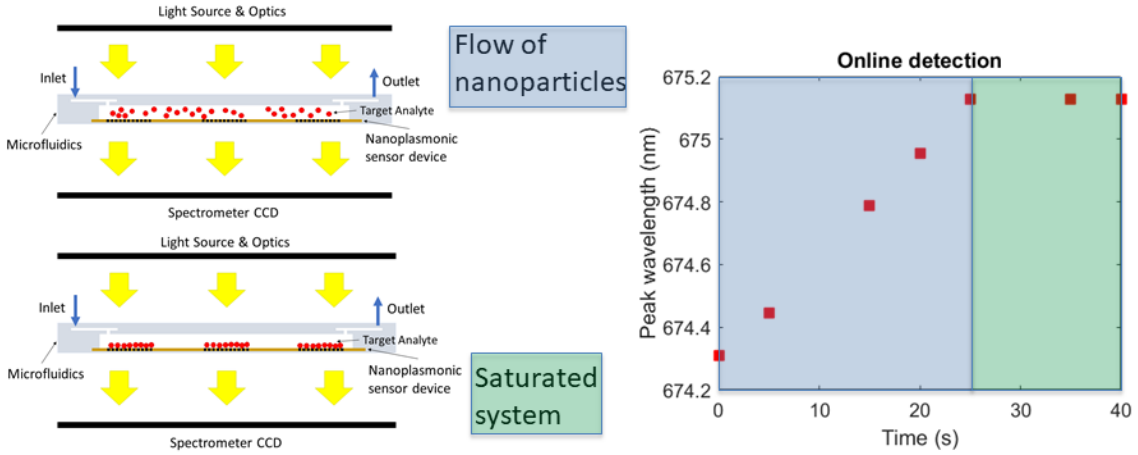

Figure 68 – General scheme of the online detection experiment. Binding effects generates a shift on the spectrum with time until the system is saturated.

Beads are incubated overnight to measure the difference in the wavelength transmitted after the online detection saturated and the overnight incubation. More beads might bind to the sensor because of deposition. Beads attached to the sensor are shown in Figure 69.

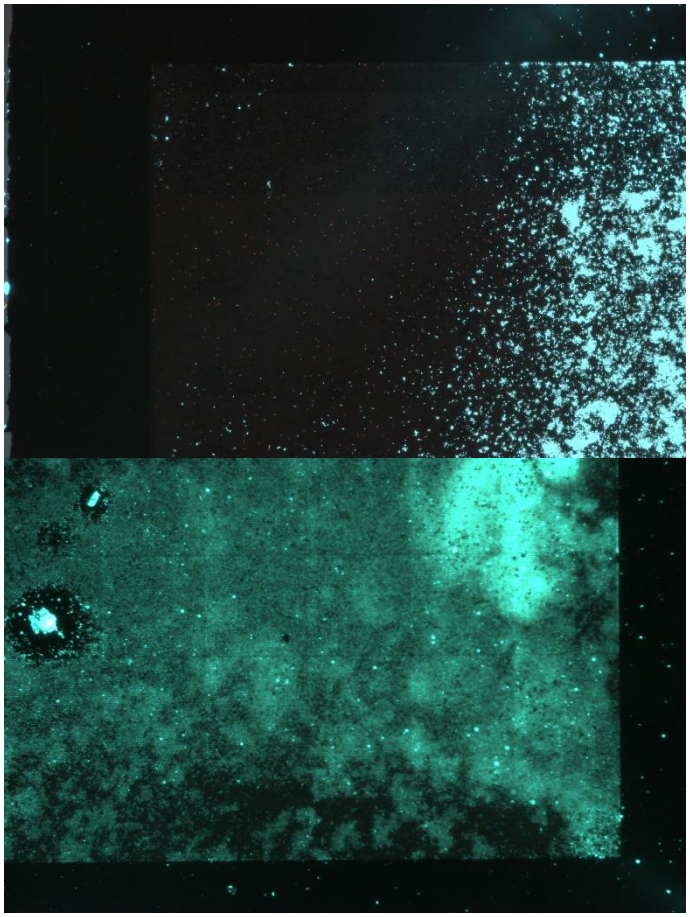

Figure 69 - Black background image of the fictionalized nanoplasmonic sensor corners with specific bindings of Dragon green beads covered with streptavidin

Peak of the spectrum after the incubation overnight is found at ~684 nm, while the saturated system for the online detection is found at ~675 nm, meaning more beads are attached and bigger shift of the wavelength peak is detected. Flushing with PBS is performed, after certain time some of the beads are removed from the sensor, thus decreasing the SPR response and shifting the spectrum the opposite way, Figure 70 shows a general view of the process. Not completed flush of the beads is observed due to the wavelength peak of the spectrum has to come to the initial state with no beads on the system, this can be explained as the covalent join formed by the streptavidin of the beads and the biotin in the end of the PEG chains is strong enough to resist the flush with PBS buffer, furthermore a special elution is required to separate the beads form the sensor.

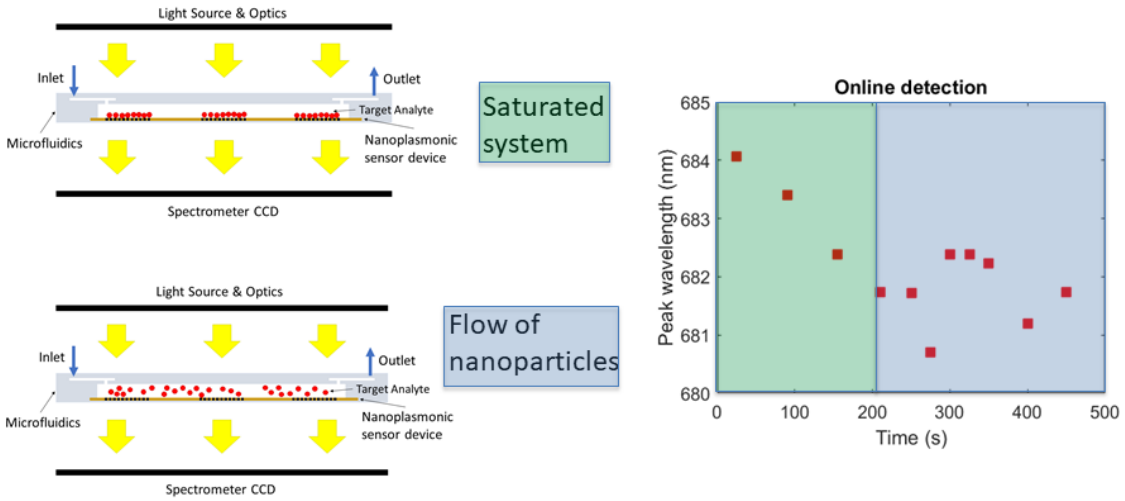

Figure 70 – General scheme of the online detection experiment. Flushing the system with buffer removes beads from the sensor surface shifting the spectrum.

6.5. Microfluidics, SAW and nanoplasmonic sensor prototype fabrication

In this chapter, results of nanofabrication combination of nanoplasmonic sensor, interdigital transducers (IDTs) and microfluidics is presented. A detection prototype device is fabricated to perform an online detection of nanoparticles, with little amount of sample (few microliters). Improvement of the sensing performance is attempted with the implementation of surface acoustic waves (SAW) which increases the mixing inside the microchannel and furthermore increasing the nanoparticles contact with the sensor surface.

Fabrication process is carried out with LinbO3 substrate following the process described in Chapter 4. Fabrication and characterization of nanoplasmonic sensors, IDTs and microfluidics. In the exposure design, mark alignments are included to align the IDT design with the nanoplasmonic sensor design and be able to place the microchannel in between the IDTs and on top of the nanoplasmonic sensor.

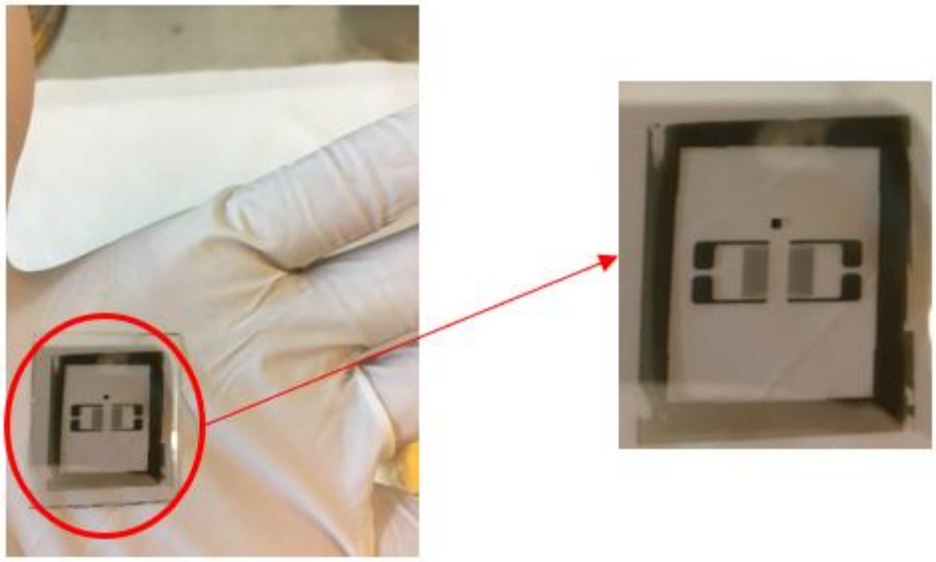

Figure 71 – Nanoplasmonic sensor and IDT fabrication sample.

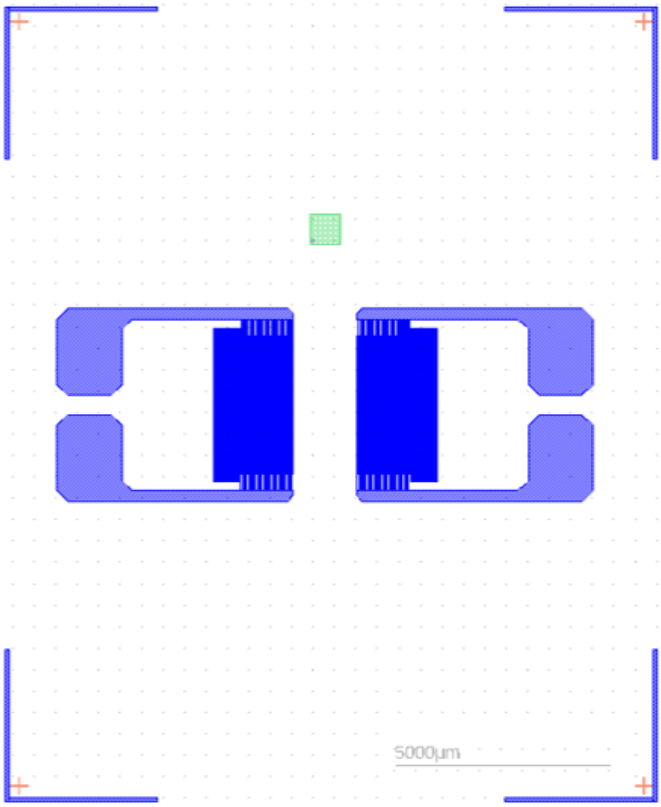

Figure 72 – Nanoplasmonic sensor and IDT fabrication design including alignment marks for the EBL exposure.

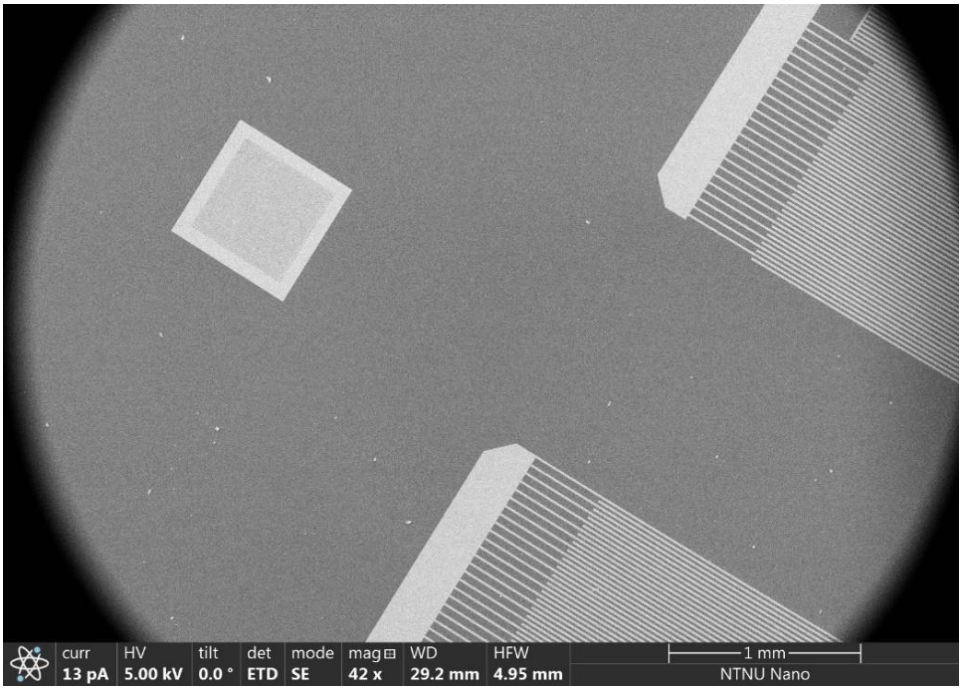

Figure 73 – SEM images of nanoplasmonic sensor and IDT on LinbO3 substrate.

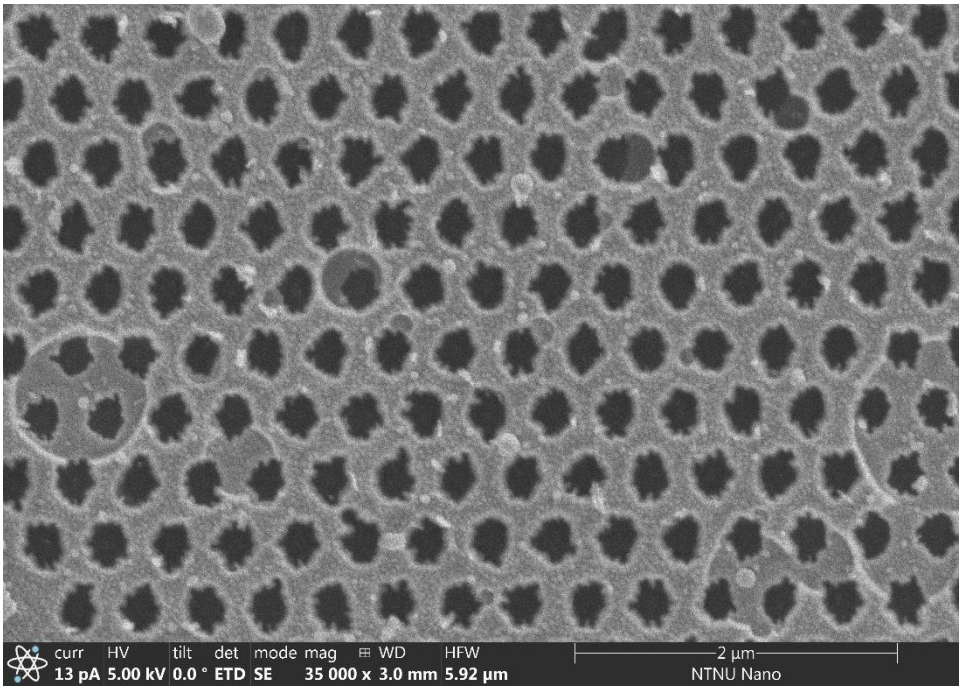

Figure 74 – SEM images of Figure 64, zoomed area of the nanoplasmonic sensor, features of 200 nm diameter, 400 nm pitch can be observed.

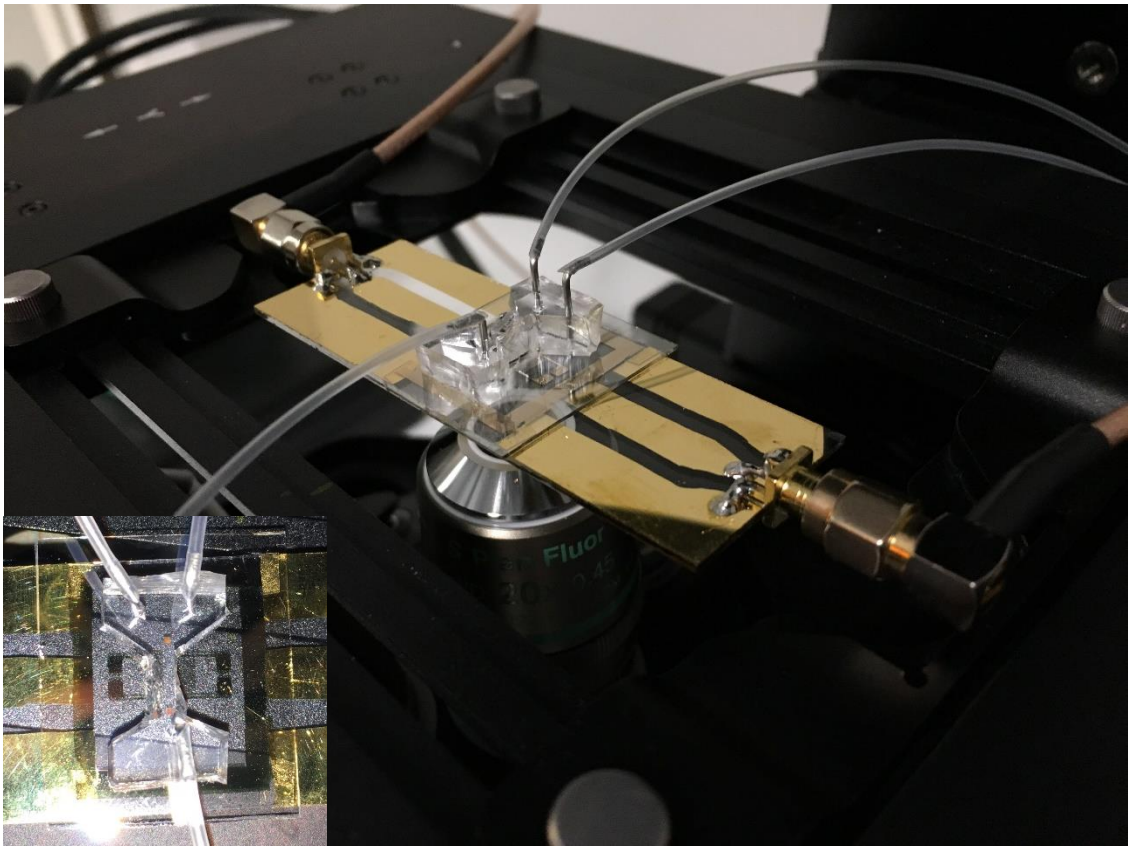

Figure 75 – Microfluidics, SAW and nanoplasmonic sensor prototype on the facility setup. Sample is attached to a glass covered by gold being possible to apply current to the IDTs for SAW generation, also microtubes are connected to the microfluidics

7. Conclusion

7.1. Summary and conclusions

State-of-the-art of nanoplasmonic sensor fabrication and performance is presented comparing the work done in this report with literature. The fabrication results achieved are comparable to the devices fabricated in current literature for further sensor applications. The physics and main working mechanism of the nanoplasmonic sensor device are explained.

Combination of electron beam lithography (EBL) and electron beam evaporation metal deposition is performed for the fabrication of nanoplasmonic sensors. Optimization of the recipe is carried out to find the optimal dose related with different photoresist thicknesses and metal deposition is achieved analysing differences in lift-off step for different geometric features of the nanostructures.

Nanoplasmonic sensors experiments are performed. Different geometric features and gold deposited thicknesses are selected to analyse device sensitivity during experiments resulting features of 200 nm diameter, 400 nm pitch and 200 nm of gold deposited as most optimal features with a sensitivity of ~600 nm/RIU. Microfluidics are implemented to the nanoplasmonic sensors device decreasing the sensitivity to ~250 nm/RIU, however more accurate device calibration and less sample usage is achieved. Binding effect on the sensor surface with PEG chemical is studied, obtaining as most optimal binding performance relation 1:5 ratio of (CT(PEG)12:MT(PEG)4) and application procedure is described.

Prototype device including functionalized nanoplasmonic sensor and microfluidics is fabricated. Online detection is performed being possible to detect nanosized particles target of 200 nm in a mixture of different nanosized particles. Fabrication of a prototype including nanoplasmonic sensor, microfluidics and interdigital transducers (IDTs) is fabricated.

7.2. Further work

Further work can include the study of the different pattern designs varying the geometric features and the geometrical distribution of the features to find higher sensitivity of the device. Different strategies for enhancing the sensitivity of the nanoplasmonic sensor [53] can be studied. Different functionalization processes [54] can be analysed for detection of specific target particles.

Nanoplasmonic sensor experiments with different types of liquids can be tested to validate the optimization performed in this report. Environmental pollution samples can be tested to detect level of pollutants concentration or detect specific target particles in a mixture of different nanoparticles, such us blood.

Further development of the device prototype including nanoplasmonic sensor, microfluidics and interdigital transducers (IDTs) can be studied. Improvements on the facility setup and postprocessing software can be performed enabling surface acoustic waves generation for better mixing inside the microchannel, online spectrometric analysis for detection of the specific target particles, online characterization of the device with high speed camera and fluorescence imaging and control liquid flow using syringe pump.

Prototype including nanoplasmonic sensor, microfluidics and interdigital transducers (IDTs) calibration. Mixing test with different glycerol solution can be performed to test the mixing inside the microchannel performance of the surface acoustic waves (SAW) on the device. Detection of nanoparticles with mixing inside the microchannel can be carried out and a compare the results with and without surface acoustic waves (SAW) mixing the microchannel inside, observing if any improvement on the detection performance of the sensor is found.

References

[1] D. Li, W. Zhai, Y. Li, and Y. Long, “Recent progress in surface enhanced Raman spectroscopy for the detection of environmental pollutants,” *Springer Microchim Acta*, pp. 23–43, 2014.

[2] P. Singh, “Sensors and Actuators B : Chemical SPR Biosensors : Historical Perspectives and Current Challenges,” *Sensors Actuators B. Chem.*, vol. 229, pp. 110–130, 2016.

[3] M. Soler, A. Belushkin, A. Cavallini, C. Kebbi-Beghdadi, G. Greub, and H. Altug, “Multiplexed nanoplasmonic biosensor for one-step simultaneous detection of Chlamydia trachomatis and Neisseria gonorrhoeae in urine,” *Biosens. Bioelectron.*, vol. 94, no. January, pp. 560–567, 2017.

[4] H. Im *et al.*, “Label-free detection and molecular profiling of exosomes with a nano-plasmonic sensor,” *Nat. Biotechnol.*, vol. 32, no. 5, pp. 490–495, 2014.

[5] J. Crocker and J. Bartram, “Comparison and Cost Analysis of Drinking Water Quality Monitoring Requirements versus Practice in Seven Developing Countries,” pp. 7333–7346, 2014.

[6] H. Recommendation, “Water Infrastructure and Investment,” no. 2015, 2016.

[7] W. Cheng and R. G. Compton, “Trends in Analytical Chemistry Electrochemical detection of nanoparticles by ‘ nano-impact ’ methods,” *Trends Anal. Chem.*, vol. 58, pp. 79–89, 2014.

[8] M. T. Blom, E. Chmela, R. E. Oosterbroek, and R. Tijssen, “On-Chip Hydrodynamic Chromatography Separation and Detection of Nanoparticles and Biomolecules,” *Anal. Chem.*, vol. 75, no. 24, pp. 6761–6768, 2003.

[9] C. You *et al.*, “Detection and identification of proteins using nanoparticle – fluorescent polymer ‘ chemical nose ’ sensors,” *Nat. Nanotechnol.*, vol. 2, no. May, 2007.

[10] X. Xu, J. Wang, K. Jiao, and X. Yang, “Biosensors and Bioelectronics Colorimetric detection of mercury ion (Hg 2 +) based on DNA oligonucleotides and unmodified gold nanoparticles sensing system with a tunable detection range,” *ELSEVIER Biosens. Bioelectron.*, vol. 24, pp. 3153–3158, 2009.

[11] C. Huang and H. Chang, “Fluorescent Sensors for Detection of Mercury (II) in ing Hg (II) ions in aqueous solution has been developed . in bulk solution fluoresce weakly when they are adsorbed,” vol. 78, no. 24, pp. 8332–8338, 2006.

[12] B. Hak *et al.*, “Biosensors and Bioelectronics Detection of Hepatitis B Virus (HBV) DNA at femtomolar concentrations using a silica nanoparticle-enhanced microcantilever sensor,” *ELSEVIER Biosens. Bioelectron.*, vol. 25, pp. 130–135, 2009.

[13] N. Cho, J. A. Jackman, R. Ferhan, and N. Cho, “Nanoplasmonic sensors for biointerfacial science,” *Chem. Soc. Rev.*, vol. 46, no. 12, 2017.

[14] M. C. Estevez, M. A. Otte, B. Sepulveda, and L. M. Lechuga, “Trends and challenges of refractometric nanoplasmonic biosensors: A review,” *Anal. Chim. Acta*, vol. 806, pp. 55–73, 2014.

[15] V. Spampinato, M. A. Parracino, R. La Spina, F. Rossi, and G. Ceccone, “Surface Analysis of Gold Nanoparticles Functionalized with Thiol-Modified Glucose SAMs for Biosensor Applications,” vol. 4, no. February, pp. 1–12, 2016.

[16] Y. Chen and H. Ming, “Photonic Sensors Review of Surface Plasmon Resonance and Localized Surface Plasmon Resonance Sensor □,” vol. 2, no. 1, pp. 37–49, 2012.

[17] G. J. Parks, “On a Remarkable Case of Uneven Distribution of Light in a Diffraction Grating Spectrum,” *Proc. Phys. Soc. London*, 1902.

[18] L. Rayleigh, “On the Dynamical Theory of Gratings,” *R. Soc. London*, vol. LXXIX, 1907.

[19] R. W. W. D, “Anomalous Diffraction Gratings,” *Phys. Rev.*, 1935.

[20] H. Palmer, “Parallel Diffraction Grating Anomalies,” *J. Opt. Soc. Am.*, vol. 42, no. 4, 1952.

[21] D. Bohm and D. Pines, “A Collective Description of Electron Interactions. I. Magnetic Interactions,” *Phys. Rev.*, vol. 82, no. 5, pp. 625–634, Jun. 1951.

[22] C. J. Powell and J. B. Swan, “Effect of Oxidation on the Characteristic Loss Spectra of Aluminum and Magnesium,” *Phys. Rev.*, vol. 118, no. 3, pp. 640–643, May 1960.

[23] E. Burstein, W. P. Chen, Y. J. Chen, and A. Hartstein, “Surface polaritons — propagating electromagnetic modes at interfaces,” *J. Vac. Sci. Technol.*, vol. 1004, no. 1974, 2015.

[24] H. Kretschmann, E. and Reather, “Radiative Decay of Non Radiative Surface Plasmons Excited by Light,” *Z.Naturf*, no. November 1968, pp. 0–1, 1968.

[25] A. Otto, “Excitation of nonradiative surface plasma waves in silver by the method of frustrated total reflection,” *Zeitschrift für Phys. A Hadron. Nucl.*, vol. 216, no. 4, pp. 398–410, 1968.

[26] B. Liedberg, C. Nylander, and I. Lunström, “Surface plasmon resonance for gas detection and biosensing,” *Sensors and Actuators*, vol. 4, pp. 299–304, 1983.

[27] A. S. Hughes and M. Reeves, “Biosensing on the End of an Optical Fiber,” *Fac. Columbian Coll. Arts Sci. Georg. Washingt. Univ.*, no. May 2011, 2015.

[28] “Detlef Smilgies. Boundary Conditions for theWave Vector at an Interface between Two Media. http://sta .chess.cornell.edu/~smilgies/re /BoundaryConditions.html.”

[29] “Rob Kooyman. Handbook of Surface Plasmon Resonance. RCS Publishing, AE Enschede, The Netherlands, 2008.”

[30] “Sophocles Orfanidis. Electromagnetic Waves and Antennas. ECE Rutgers, New Jersey, 2008.”

[31] M. Graetzel, “Nanoplasmonic Sensing,” pp. 5288–5300, 2013.

[32] H. Raether, “Surface plasmons on smooth surfaces. In: Surface Plasmons on Smooth and Rough Surfaces and on Gratings,” *Springer Tracts Mod. Physics, vol 111. Springer, Berlin, Heidelb.*, 1988.

[33] SPRtech101, “Surface Plasmon Resonance Explained [video file].” [Online]. Available: https://www.youtube.com/watch?v=sM-VI3alvAI&list=PLNFHuvZlMPOL9cki0mZ3gy94LbIlgrIPm.

[34] P. Photovoltaics, B. J. W. Menezes, J. Ferreira, M. J. L. Santos, L. Cescato, and A. G. Brolo, “Large-Area Fabrication of Periodic Arrays of Nanoholes in Metal Films and Their Application in Biosensing and,” pp. 3918–3924, 2010.

[35] J. Henzie, M. H. Lee, and T. W. Odom, “Multiscale patterning of plasmonic metamaterials,” *Nat. Nanotechnol.*, vol. 2, no. 9, pp. 549–554, 2007.

[36] “Supporting information Table S1 .,” no. cm, pp. 1–10, 2000.

[37] Q. Yu, P. Guan, D. Qin, G. Golden, and P. M. Wallace, “Inverted size-dependence of surface-enhanced Raman scattering on gold nanohole and nanodisk arrays,” *Nano Lett.*, vol. 8, no. 7, pp. 1923–1928, 2008.

[38] H. Im *et al.*, “Template-stripped smooth Ag nanohole arrays with silica shells for surface plasmon resonance biosensing,” *ACS Nano*, vol. 5, no. 8, pp. 6244–6253, 2011.

[39] B. R. M. A. S, “Impact of ordering of gold nanohole arrays on refractive index sensing,” vol. 35, no. 10, pp. 2501–2508, 2018.

[40] K. Nakamoto, “Development of a mass-producible on-chip plasmonic

nanohole array biosensor," *Nanoscale*, pp. 5067–5075, 2011.

[41] S. Wang, X. Sun, M. Ding, and G. Peng, "The investigation of an LSPR refractive index sensor based on periodic gold nanorings array," 2018.

[42] E. M. Hicks *et al.*, "Plasmonic Properties of Film over Nanowell Surfaces Fabricated by Nanosphere Lithography," no. Figure 1, pp. 22351–22358, 2005.

[43] X. Dou, Y. Lin, B. Choi, K. Wu, and P. Jiang, "Sensitive surface plasmon resonance enabled by templated periodic arrays of gold nanodonuts," 2016.

[44] Diego Sanchez Saldaña, "Fabrication and optimization of nanoplasmonic sensors using Electron Beam Lithography (EBL)," *NTNU*, no. December, 2018.

[45] G. A. Álvarez, "Fabrication of microchannels and an IDT using a Maskless Aligner," *NTNU*, no. February, 2019.

[46] L. F. Hoyt, "New Table of the Refractive Index of Pure Glycerol at 20° C," *Ind. Eng. Chem.*, vol. 26, no. 3, pp. 329–332, 1934.

[47] A. Sonato *et al.*, "A surface acoustic wave (SAW)-enhanced gratingcoupling phase-interrogation surface plasmon resonance (SPR) microfluidic biosensor," *Lab Chip*, vol. 16, pp. 1224–1233, 2016.

[48] A. Laboratories, "for Quantitative Test Results," no. 1, pp. 1–50, 2006.

[49] A. A. Yanik *et al.*, "An Optofluidic Nanoplasmonic Biosensor for Biological Media," *Nano Lett.*, pp. 4962–4969, 2010.

[50] B. Diameter, "Tutorial - Beam current and pitch," *NTNU*, pp. 4–5.

[51] Y. Ek and A. E. Cetin, "Optical Response of Plasmonic Nanohole Arrays : Comparison of Square and Hexagonal Lattices," pp. 851–856, 2016.

[52] T. Scientific, "INSTRUCTIONS for Methyl- and carboxy-thiol PEGylation reagents," vol. 0747, no. 815, pp. 26133–26135.

[53] L. Guo, J. A. Jackman, H. Yang, P. Chen, N. Cho, and D. Kim, "Strategies for enhancing the sensitivity of plasmonic nanosensors," *Nano Today*, vol. 10, no. 2, pp. 213–239, 2015.

[54] S. Engel, E. Fritz, B. J. Ravoo, and E. Fritz, "New trends in the functionalization of metallic gold : from organosulfur ligands to N-heterocyclic carbenes," pp. 2057–2075, 2017.

A. Recipes

Nanoplasmonic sensor. Produced by Jonas M. Ribe, validated by Diego Sánchez Saldaña and contribution done by testing different thicknesses of photoresist and different thicknesses of metal deposited analysing lift-off process.

1. Cleaning of glass substrate
    - Acetone, Isopropanol, N2
    - Plasma cleaner 5 min O_2/50/50
2. Soft baking dehydration
    - Type: Soft baking
    - Temp: 250°C
    - Time: 5 min
3. Evaporation of HMDS
    - Desiccator with HMDS overnight
4. Photoresist, spin coat for 400nm diameter and 800 nm pitch features
    - CSAR 6200.13
    - 1000 rpm – 6 sec - 1000 rpm/sec
    - 6000 rpm – 60 sec - 1000 rpm/sec

Photoresist, spin coat for 200nm diameter and 400 nm pitch features

- CSAR 6200.13
- 1000 rpm – 6 sec - 1000 rpm/sec
- 5750 rpm – 60 sec - 1000 rpm/sec

5. Soft baking for glass
    - Type: Soft baking
    - Temp: 150°C
    - Time: 1 min

Soft baking for LinbO3

- Type: Soft baking
- Temp: 90°C
- Time: 2 min

6. Conductive layer, spin coat
   - Protective Coating PMMA Electra 92 AR-PC 5090.02
   - 1000 rpm – 2 sec - 1000 rpm/sec
   - 2000 rpm – 60 sec - 1000 rpm/sec
7. Pre-exposure soft baking
   - Type: Soft baking
   - Temp: 90°C
   - Time: 2 min
8. EBL exposure
   - Parameters determined by the photoresist
   - Dose: 172.5 μc/cm^2 current: 2 nA
9. Development
   - DI water 60 sec
   - AR 6000-546 60 sec
   - MBIK/IPA 1:3 2-3 sec
   - Rinse in IPA and N_2
10. E-beam evaporator
    - Type: AJA
    - Metall: Ti/Au
    - Thickness: 5 nm / 200 nm
11. Lift-off

- Ultrasonic bath with Stripper 1.5 min
- Rinse in Acetone
- Rinse in IPA
- Dry with N_2

Interdigital transducer (IDT). Produced by Jonas M. Ribe, validated by Diego Sánchez Saldaña.

1. Cleaning of LinbO3 substrate
    - Acetone, Isopropanol, N2
    - Plasma cleaner 5 min O_2/50/50
2. Soft baking dehydration
    - Type: Soft baking
    - Temp: 100°C
    - Time: 5 min
3. Photoresist spin coating
    - AZ5214E
    - 4000 rpm – 46 sec - rampage 4000rpm (1.5 µm)
4. Soft baking for LinbO3
    - Type: Soft baking
    - Temp: 950°C
    - Time: 90 sec
5. Exposure MLA 405nm wavelength laser
    - Dose 27 mJ/cm^2
6. Image reversal bake
    - Temp: 113°C
    - Time: 2 min
7. Flood exposure MA6
    - Dose: 200 mJ/cm^2
8. Development
    - AZ726 MIF during 40 sec (last 10sec stirring) + DI + N2

9. E-beam evaporator
    - Type: AJA
    - Metall: Ti/Au
    - Thickness: 5 nm / 80 nm
10. Lift-off
    - Ultrasonic 2 baths with acetone 1 min at 50ºC
11. Wire bonding

Microfluidics. Produced by Jonas M. Ribe, validated by Diego Sánchez Saldaña.

1. Cleaning of silicon substrate
    - Acetone, Isopropanol, N2
    - Plasma cleaner 5 min O_2/50/50
2. Soft baking dehydration
    - Type: Soft baking
    - Temp: 250°C
    - Time: 5 min
3. Photoresist spin coating
    - SU-8 (desire thickness 50um)
    - Initial 500 rpm/sec with rampage 250 rpm/sec 12 sec
    - Final 3000 rpm/s 46 sec
4. Soft baking for silicon
    - Type: Soft baking
    - Temp: 90°C
    - Time: 15 min
5. Exposure MLA 375 nm wavelength laser
    - Dose 2000 mJ/cm^2
6. Post-exposure bake
    - Type: Soft baking
    - Temp: 65°C
    - Time: 1 min
    - Temp: 95°C
    - Time: 4 min
7. Development

- Mr-Dev 600 for 5 min
- Rinse in Acetone, IPA and N_2

8. Deposition of Tridecafluoru-silane (under pressure) sample on a petri dish
9. PDMS (1:10)
   - Oven 65 ºC for 2 hours
   - Pierce inlets
   - Bond microchannel to substrate, 30s O2 50% power 20%
   - Finish the crosslinking Oven 65ºC for 5 min

B. Surface functionalization instructions

INSTRUCTIONS

$MT(PEG)_4$
$CT(PEG)_{12}$

Methyl- and carboxy-thiol PEGylation reagents

26132 26133

2341.0

Number	Description
26132	**$MT(PEG)_4$,** 100mg Molecular Weight: 224.32 Spacer Arm Length: 15.8Å
26133	**$CT(PEG)_{12}$,** 100mg Molecular Weight: 634.77 Spacer Arm Length: 47.8Å

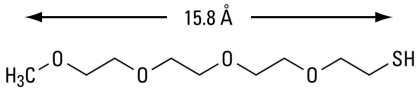

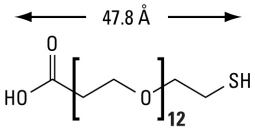

Storage: Upon receipt store at -20°C protected from moisture. Products shipped at ambient temperature.

Introduction

The Thermo Scientific $MT(PEG)_4$ (methyl-PEG_4-thiol) and $CT(PEG)_{12}$ (carboxy-PEG_{12}-thiol) are monodentate thiol-terminated polyethylene glycol (PEG)-containing reagents with either a methyl ether or carboxylic acid. These reagents have defined molecular weights and spacer lengths and are used for modifying surfaces such quantum dots, self-assembled monolayers and magnetic particles. Functionalization of solid surfaces with polyethylene glycol spacers significantly reduces nonspecific protein binding.[1-6]

The use of $MT(PEG)_4$ with $CT(PEG)_{12}$ in surface modification can form a hydrophilic "lawn" of methyl ether-terminated PEGs with periodic exposed carboxylic acid-containing PEGs. The exposed carboxylic acid groups can be coupled to affinity ligands using the carbodiimide coupling reaction with EDC and sulfo-NHS.

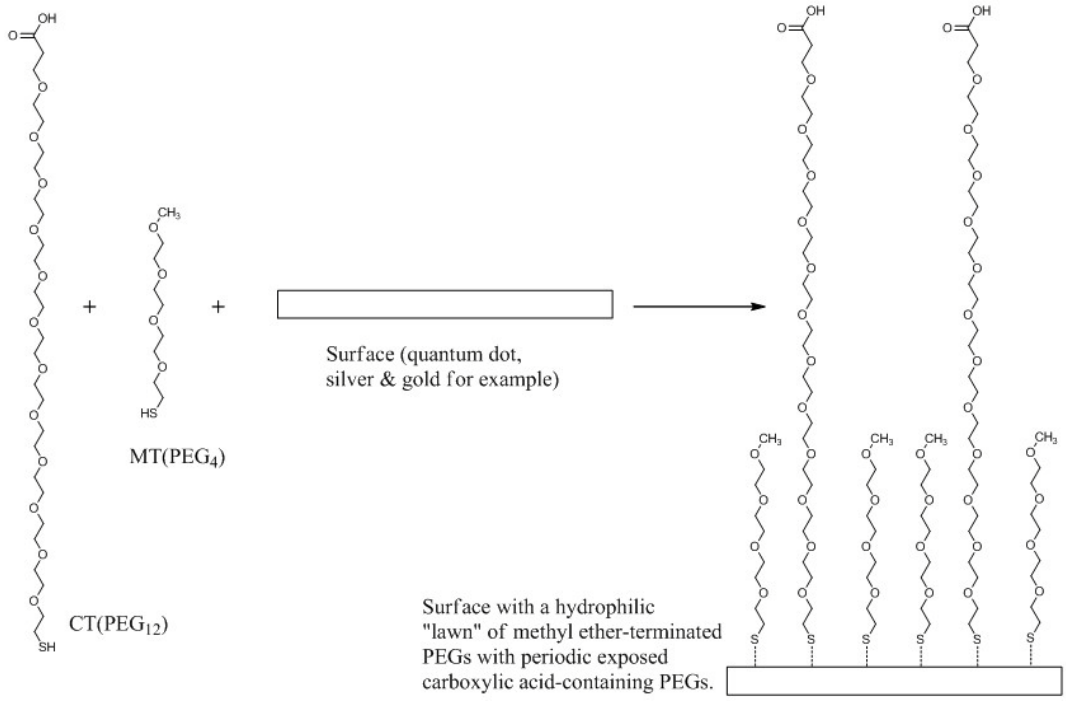

Figure 1. Surface modification with $MT(PEG)_4$ and $CT(PEG)_{12}$.

Pierce Biotechnology 3747 N. Meridian Road | PO Box 117 Rockford, IL 61105 USA | (815) 968-0747 (815) 968-7316 fax | www.thermoscientific.com/pierce

Important Product Information

- Use MT(PEG)$_4$ and CT(PEG)$_{12}$ in combination to modify surfaces and minimize nonspecific binding.
- The PEG-thiol reagents are low-melting solids that are difficult to weigh and dispense. To facilitate handling, make a stock solution by dissolving the reagent in dimethylsulfoxide (DMSO) or dimethylformamide (DMF).
- Store unused stock solution at -20°C. Equilibrate reagent vial to room temperature before opening to avoid moisture condensation. To minimize air exposure, keep the stock solution under an inert gas such as argon or nitrogen. Cap the stock solution with a septum and use a syringe to remove the solution.
- The ratio of MT(PEG)$_4$ to CT(PEG)$_{12}$ and the reagent mixture-to-surface ratio in the reaction affect the number of carboxylic acid residues available for further modification. Optimize these ratios to obtain the modification level needed for the specific application.
- Use non-amine-containing buffers at pH 7-9 such as PBS (20mM sodium phosphate, 150mM NaCl; pH 7.4) (Product No. 28372); 100mM carbonate/biocarbonate; or 50mM borate. Do not use buffers that contain primary amines, such as Tris or glycine, which compete with acylation.

Procedure for Surface Modification with MT(PEG)$_4$ and CT(PEG)$_{12}$

Materials Required

- Water-miscible organic solvent (molecular sieve-treated) such as DMSO or DMF
- Small-volume, non-coring syringes for dispensing the reagent stock solution while minimizing exposure to air
- Buffer A: Phosphate-buffered saline, PBS (20mM sodium phosphate, 0.15M NaCl; pH 7.2, Product No. 28372) or other non-amine, lone-pair sulfur-free buffers
- Buffer B: MES-buffered saline (0.1M MES, 0.5M NaCl; pH 6.0 or 0.1M MES, 0.9% NaCl; pH 4.7; Product No. 28390) or other non-amine, non-carboxy, lone-pair sulfur-free buffers
- EDC (Product No. 77149)
- NHS or Sulfo-NHS (Product No. 24500 and 24510, respectively)
- Hydroxylamine•HCl (Product No. 26103)

Procedure

1. Equilibrate the MT(PEG)$_4$ and CT(PEG)$_{12}$ reagents to room temperature before opening bottles.
2. Prepare stock solutions by dissolving 100mg of each reagent in the desired amount of DMF or DMSO. Cap, store and handle stock solutions as directed in the Important Product Information Section.
3. Prepare the appropriate amount of surface in Buffer A.
4. Prepare a mixture of MT(PEG)$_4$ and CT(PEG)$_{12}$ in Buffer A and add it to the surface. Incubate the reaction for 2 hours at room temperature.
5. Wash the surface with Buffer A to remove excess reagent.
6. The newly introduced carboxylic acid groups can be activated by adding appropriate amounts of EDC and NHS or sulfo-NHS to the modified surface in Buffer B and reacting for 15 minutes at room temperature. For best results, perform this reaction at pH 5-6.

   Note: The activation reaction with EDC and sulfo-NHS is most efficient at pH 4.5-7.2; however, the reaction of sulfo-NHS-activated molecules with primary amines is most efficient at pH 7-8.
7. Wash the surface with Buffer B to remove any remaining EDC and NHS.
8. Add the desired amine-containing substrate, prepared in Buffer A, to the activated surface and react for 2 hours at room temperature. For best results, raise the pH of the reaction solution to 7.2-7.5 with Buffer A immediately before adding the amine-containing substrate.
9. To quench the conjugation reaction, add hydroxylamine or another amine-containing buffer. Hydroxylamine hydrolyzes non-reacted NHS. Other quenching compounds include Tris, lysine, glycine or ethanolamine; however, these primary amine-containing compounds modify carboxylic acids.

Related Thermo Scientific Products

26134	**ML(PEG)$_4$** (methyl-PEG$_4$-lipoamide), 100mg
26135	**CL(PEG)$_{12}$** (carboxy-PEG$_{12}$-lipoamide), 100mg
28390	**BupH™ MES Buffered Saline,** 10 packs, makes 5L
28372	**BupH Phosphate Buffered Saline,** 40 packs, makes 20L
77149	**EDC,** 10mg
24500	**NHS (*N*-hydroxysuccinimide),** 25g
24510	**Sulfo-NHS (sulfo-*N*-hydroxysuccinimide),** 500mg
20290	**DTT,** 5g
20291	**DTT, No-Weigh™ Format,** 48 tubes × 7.7mg
26103	**Hydroxylamine,** 25g
26120	**CA(PEG)$_4$** (carboxy-PEG$_4$-amine), 100mg
26122	**CA(PEG)$_8$,** 100mg
26124	**CA(PEG)$_{12}$,** 100mg
26126	**CA(PEG)$_{24}$,** 100mg
26110	**MA(PEG)$_4$** (methyl-PEG$_4$-amine), 100mg
26112	**MA(PEG)$_8$,** 100mg
26114	**MA(PEG)$_{12}$,** 100mg
26116	**MA(PEG)$_{24}$,** 100mg

References

1. Prime, K.L. and Whitesides, G.M. (1991). Self-assembled organic monolayers: model systems for studying absorption of proteins at surfaces. *Science* **252:**1164.
2. Bentzen, E.L., *et al.* (2005). Surface modification to reduce non-specific binding of quantum dots in live cell assays. *Bioconjugate Chem* **16:**1488-94.
3. Lin, P-C., *et al.* (2006). Ethylene glycol-protected magnetic nanoparticles for a multiplexed immunoassay in human plasma. *Small* **2(4):**485-9.
4. Zheng, M., *et al.* (2003). Ethylene glycol monolayer protected nanoparticles for eliminating nonspecific binding with biological molecules. *J Am Chem Soc* **125:**7790-1.
5. Verma, A. and Rotello, V.M. (2005). Surface recognition of biomacromolecules using nanoparticle receptors. *Chem Commun* **3:**303-12.
6. Kidambi, S., *et al.* (2004). Selective depositions on polyelectrolyte multilayers: self-assembled monolayers of m-dPEG acid as molecular template. *J Am Chem Soc* **126:**4697-03.

Current product instructions are available at *www.thermoscientific.com/pierce*. For a faxed copy, call 800-874-3723 or contact your local distributor.

Pierce Biotechnology 3747 N. Meridian Road | PO Box 117 Rockford, IL 61105 USA | (815) 968-0747 (815) 968-7316 fax | www.thermoscientific.com/pierce